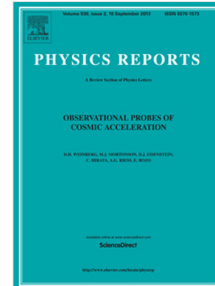


# Accepted Manuscript

Surrogate data for hypothesis testing of physical systems

Gemma Lancaster, Dmytro Iatsenko, Aleksandra Pidde, Valentina Ticcinelli,  
Aneta Stefanovska



PII: S0370-1573(18)30134-0

DOI: <https://doi.org/10.1016/j.physrep.2018.06.001>

Reference: PLREP 2010

To appear in: *Physics Reports*

Accepted date: 1 June 2018

Please cite this article as: G. Lancaster, D. Iatsenko, A. Pidde, V. Ticcinelli, A. Stefanovska, Surrogate data for hypothesis testing of physical systems, *Physics Reports* (2018),  
<https://doi.org/10.1016/j.physrep.2018.06.001>

This is a PDF file of an unedited manuscript that has been accepted for publication. As a service to our customers we are providing this early version of the manuscript. The manuscript will undergo copyediting, typesetting, and review of the resulting proof before it is published in its final form. Please note that during the production process errors may be discovered which could affect the content, and all legal disclaimers that apply to the journal pertain.

1  
2  
3           Surrogate data for hypothesis testing of physical systems  
4

5           Gemma Lancaster<sup>a</sup>, Dmytro Iatsenko<sup>b</sup>, Aleksandra Pidde<sup>a,c</sup>, Valentina Ticcinelli<sup>a</sup>, Aneta Stefanovska<sup>a,\*</sup>  
6

7                 <sup>a</sup>*Department of Physics, Lancaster University, UK*  
8                 <sup>b</sup>*Deutsche Bank, London, UK*

9                 <sup>c</sup>*Department of Information and Communication Technologies, Universitat Pompeu Fabra, Barcelona, Spain*

---

10           11           12           13           14           Abstract

15           The availability of time series of the evolution of the properties of physical systems is increasing, stimulating the  
16           development of many novel methods for the extraction of information about their behavior over time, including  
17           whether or not they arise from deterministic or stochastic dynamical systems. Surrogate data testing is an essential  
18           part of many of these methods, as it enables robust statistical evaluations to ensure that the results observed are  
19           not obtained by chance, but are a true characteristic of the underlying system.

20           The surrogate data technique is based on the comparison of a particular property of the data (a discriminating  
21           statistic) with the distribution of the same property calculated in a set of constructed signals (surrogates) which  
22           match the original data set but do not possess the property that is being tested. Fourier transform based surrogates  
23           remain the most popular, yet many more options have since been developed to test increasingly varied null hypothe-  
24           ses while characterizing the dynamics of complex systems, including uncorrelated and correlated noise, coupling  
25           between systems, and synchronization.

26           Here, we provide a detailed overview of a wide range of surrogate types, discuss their practical applications  
27           and demonstrate their use in both numerically simulated and real experimental systems. We also compare the  
28           performance of various surrogate types for the detection of nonlinearity, synchronization and coherence, coupling  
29           strength between systems, and the nature of coupling. A MatLab toolbox for many of the surrogate methods is  
30           provided.

31           *Keywords:* Surrogate data, dynamical systems, time series analysis, complex systems

32           *2010 MSC:* 00-01, 99-00

---

33           34           35           36           37           Contents

<b>1</b>	<b>Introduction</b>	<b>3</b>
40	1.1 Motivation . . . . .	3
41	1.2 Outline . . . . .	4
<b>2</b>	<b>Background</b>	<b>4</b>
44	2.1 What are surrogates and why do we need them? . . . . .	4
45	2.2 Typical vs. constrained realizations . . . . .	5
46	2.3 The null hypothesis . . . . .	5
47	2.4 Significance testing . . . . .	5
<b>3</b>	<b>Testing against noise</b>	<b>6</b>
50	3.1 Uncorrelated noise . . . . .	6
51	3.1.1 White noise surrogates . . . . .	6
52	3.1.2 Random permutation (RP) surrogates . . . . .	7
53	3.2 Correlated noise . . . . .	7
<b>4</b>	<b>Surrogates for nonlinearity testing</b>	<b>8</b>
57	4.1 Autoregressive moving average (ARMA) processes . . . . .	9
58	4.2 Nonstationarity . . . . .	9
59	4.3 Preprocessing . . . . .	10

---

61           \*Corresponding author

1		
2		
3	4.4 Autoregressive (AR) surrogates . . . . .	11
4	4.5 Fourier transform (FT) surrogates . . . . .	12
5	4.6 Amplitude adjusted Fourier transform (AAFT) surrogates . . . . .	14
6	4.7 Iterative amplitude adjusted Fourier transform (IAAFT) surrogates . . . . .	15
7	4.8 Iterative digitally filtered shuffled (IDFS) surrogates . . . . .	17
8	4.9 Comparing FT based surrogates . . . . .	19
9		
10	<b>5 Surrogates for specific nonlinearity testing</b>	19
11	5.1 Wavelet iterative amplitude adjusted Fourier transform (WIAAFT) surrogates . . . . .	19
12	5.2 Multifractal surrogates . . . . .	22
13	5.3 Cycle shuffled surrogates (CSS) . . . . .	22
14	5.4 Pseudo-periodic surrogates (PPS) . . . . .	23
15		
16	<b>6 Discriminating statistics for nonlinearity testing</b>	25
17	6.1 Correlation dimension . . . . .	25
18	6.2 Nonlinear prediction error . . . . .	26
19	6.3 Volterra polynomials . . . . .	26
20	6.4 Time-irreversibility . . . . .	27
21	6.5 Monte Carlo singular spectrum analysis (MCSSA) . . . . .	27
22	6.6 Lyapunov exponents . . . . .	28
23	6.7 Mutual information . . . . .	28
24	6.8 Identifying nonlinear oscillators by harmonic extraction . . . . .	28
25	6.9 Other statistics . . . . .	29
26		
27		
28	<b>7 Surrogates for independence testing</b>	29
29	7.1 Intersubject surrogates . . . . .	30
30	7.2 Cyclic phase permutation (CPP) surrogates . . . . .	31
31	7.3 Twin surrogates (TS) . . . . .	32
32	7.4 Time-shifted surrogates . . . . .	33
33		
34	<b>8 Discriminating statistics for interdependence testing</b>	35
35	8.1 Phase coherence . . . . .	35
36	8.2 Synchrogram . . . . .	35
37	8.3 Phase synchronization index . . . . .	36
38	8.4 Dynamical inference . . . . .	36
39	8.5 Mutual information . . . . .	37
40	8.6 Wavelet bispectrum analysis . . . . .	37
41		
42	<b>9 Applications to simulated and experimental data</b>	39
43	9.1 Nonlinearity testing . . . . .	39
44	9.1.1 Finding nonlinearity in data using the correlation dimension . . . . .	39
45	9.1.2 Finding nonlinearity using Volterra polynomials . . . . .	40
46	9.1.3 Finding oscillations in noisy data using MCSSA . . . . .	41
47	9.2 Synchronization of two coupled oscillators . . . . .	43
48	9.2.1 Simple oscillators . . . . .	44
49	9.2.2 Chaotic oscillators . . . . .	46
50	9.2.3 Phase coherence in real biological data . . . . .	48
51	9.3 Inferring the nature of coupling . . . . .	48
52	9.3.1 Coupling in simple phase oscillators . . . . .	49
53	9.3.2 Cardiorespiratory coupling . . . . .	51
54	9.3.3 Wavelet bispectrum . . . . .	52
55		
56	<b>10 Discussion</b>	54
57		
58		
59		
60		
61		
62		
63		
64		
65		

1	<b>A Further details</b>	<b>56</b>
2	A.1 MatLab toolbox . . . . .	56
3	A.2 Computational cost . . . . .	56
4	A.3 Phase extraction . . . . .	57
5	A.3.1 The Hilbert transform . . . . .	57
6	A.3.2 Phase vs. protophase . . . . .	58
7	A.3.3 Nonlinear mode decomposition . . . . .	58
8	A.4 Filtering . . . . .	58
9	A.5 Time-frequency analysis . . . . .	59
10	A.5.1 Windowed Fourier transform . . . . .	59
11	A.5.2 The continuous wavelet transform . . . . .	59
12	A.5.3 The discrete wavelet transform . . . . .	59
13	A.6 Embedding . . . . .	59
14	A.6.1 Estimation of time delay $\tau$ . . . . .	60
15	A.6.2 Estimation of embedding dimension $d$ . . . . .	60

## 1. Introduction

### 1.1. Motivation

The analysis of time series originating from dynamical systems often requires estimation of the value of some measure to characterise the behaviour of the underlying system. The natural variability of dynamical systems and the methods used to observe and analyse them means that without appropriate statistical testing, we cannot know the reliability of a single value obtained using these measures. Ideally, we would estimate the value of the same measure on a large number of realisations of the system dynamics, and obtain an accurate estimate from the distribution of values. The increasing availability of powerful computing facilities has made this possible for numerical simulations [1]. However, limited data availability in real experimental scenarios rules out this approach. When working with these limited data sets, confidence intervals can be estimated using the technique of bootstrapping [2], or specific hypotheses can be tested using another method known as surrogate data [3].

The method of surrogate data for hypothesis testing grew in popularity following the work of Theiler *et al.* [3], where it was presented as a test for nonlinearity. In this case, it involves creating multiple versions of an original time series with the same statistical properties, but which can only be described by a *linear* model, i.e. with any nonlinearities removed. When a nonlinear measure, or *discriminating statistic*, is applied to the original time series and the range of surrogates, if the result from the time series deviates significantly from the surrogate distribution, then we can conclude that the time series is unlikely to have a linear origin. The concept of surrogate data testing has now been expanded and used to test not only for nonlinearity [4], but more specifically for chaos [5], for synchronization between two or many systems [6], for coupling in nonlinear systems [7], and for oscillations in noisy signals [8], to name just a few of the wide range of applications.

Surrogate testing has formed the basis of new discoveries in many fields of research, including astrophysics [9, 10, 11], geophysics [12], applied mathematics [13], engineering [14], climate studies [15, 16], ecology [17, 18], finance [19, 20], digital signal processing [21], neuroscience [22, 23, 24] and biomedicine [25, 26, 27, 28]. The need for surrogate data testing arises from the increasing availability of time series from a wide variety of dynamical systems, i.e. systems for which their evolution in time can be described by a function, for example  $\dot{x} = f(x)$ . In order to understand the underlying dynamics of the systems from which we record these time series, we ideally need to somehow determine the function  $f$ , which will describe the physical principles of the system. There are two possible approaches. The first approach attempts to fit pre-existing models to the data, and checks how closely the data fit to the model. Another group of methods, the so-called inverse approach, seeks to learn from the data, with the observed characteristics then shaping the description of the dynamics [29, 30]. This approach involves the extraction of information about the properties of the time series, how they evolve in time, and how they interact with other systems. Surrogate testing is invaluable in the validation of the results obtained in both cases.

One area that surrogates have proven to be very useful is in biological systems. The application of time series analysis methods to physiological data sets is growing in popularity, as new theories and models to describe the dynamics of living systems are proposed. For example, the human body comprises a huge number of interacting dynamical systems [31, 32, 33, 23], all of which change their characteristics over time in order to meet energy demands and thrive in their environment [34]. Therefore, signals recorded from these systems can appear to be very complex, hard to characterise, and very difficult to repeat exactly. It can also be quite difficult in some of these systems to obtain sufficiently long recordings for the application of certain analysis methods. It is these

1  
2  
3 properties that make the application of surrogate hypothesis testing to biomedical data so appealing, ensuring that  
4 conclusions are sufficiently robust to provide new information about these systems, rather than discounting them  
5 as uninformative fluctuations or noise.

6 Biomedical data may take many forms. Electroencephalography (EEG) provides information about the electrical  
7 activity of the neurons in the brain. Electrocardiography (ECG) does the same for the pacemaker cells of the  
8 heart. The characteristics of the circulating blood, such as pressure, velocity and oxygenation can all be measured  
9 noninvasively, and can be seen to continuously fluctuate as they are influenced by adjacent dynamical systems.  
10 These are just a few of many possibilities; any parameter which can be measured from the systems of the body  
11 over time can provide insights into their functions. Simultaneously measured signals will provide yet further opportunities.  
12 The surrogate data approach has provided huge amounts of new information, for example on the nature  
13 of brain behaviour in health and disease [35, 22, 36, 37], cardiorespiratory interactions [38] and neurophysiological  
14 mechanisms of cardiovascular regulation [39].  
15

16 Although an essential tool for biomedical and neurological studies, surrogate data testing is just as applicable to  
17 any signal arising from any physical system. Surrogates aid in the robust characterisation of the physical laws and  
18 behaviours of these systems, to determine the function of any dynamical units that may make up the system, how  
19 they influence each other, and how they are affected by other systems, including higher-dimensional environments  
20 that may act as noise. They answer questions about the underlying system such as whether the data are nonlinear, or  
21 whether they contain significant oscillations, by providing examples of what the results of a particular analysis would  
22 look like if these properties were definitely not present. Answering these fundamental questions using surrogate data  
23 opens the door for further analysis on the origin of these observed effects. If more than one data set is available,  
24 we can also ask further questions, such as whether their underlying systems are synchronized, and, if so, what the  
25 nature of the coupling between them is. Considering the physics of these systems is the key to understanding their  
26 past and future evolution, and surrogate data testing is a crucial tool to ensure the reliability of the results.  
27

## 28 1.2. Outline 29

30 The development of many surrogate types over the years means that it may be difficult to know which is the optimal type to use when designing a study and analysing results. The aim of this paper is to provide a clear, up-to-date introduction to the topic and present scenarios in which surrogates have been used to great effect.  
31

32 The first part of the review describes in detail the most popular surrogates in use today, for testing for nonlinearity and testing for interdependence, and provides examples, algorithms and applications. Examples of some lesser known surrogates which may be promising for future applications are also discussed.  
33

34 The second part of the paper presents a comparison of the performance of different surrogate types for the detection of nonlinearity, the detection of synchronization in two coupled oscillators, both simple phase oscillators and chaotic oscillators, and detection of coupling in simulated oscillators and real experimental data using dynamical Bayesian inference.  
35

36 We also provide step-by-step algorithms and a MatLab toolbox for the implementation of many of the surrogates that are discussed.  
37

## 43 2. Background 44

### 45 2.1. What are surrogates and why do we need them? 46

47 Before we begin to describe the wide range of surrogates that have been developed, we will discuss a well known example in which their use is crucial. Consider a research study in which a time series has been recorded from a system, and we have no prior information about the underlying dynamics. The overall aim of the study is to determine whether the system in question is chaotic. Popular measures, or *discriminating statistics*, for whether a system is chaotic include the correlation dimension [40] and Lyapunov exponents [41], although the implementation of the latter can be difficult in finite noisy data sets. Applying both measures to the data will yield finite results, supposedly providing information on whether the system is chaotic or not, and we may reach a conclusion based on this analysis. However, when applying these techniques to data that appear complex, one implicitly assumes that the system dynamics comes from deterministic nonlinearity rather than stochasticity. It follows that if the system is in fact linear, the results of these tests are unlikely to be pointing to chaos in the system. It is clear that before nonlinear techniques can be applied, the presence of nonlinearity must first be established. This question is the focus of a large portion of the available surrogate methods.  
48

49 Hence, to proceed the question must be simplified: Do the data demonstrate evidence of nonlinearity? To answer, we formulate a *null hypothesis* to test against, i.e. the case that remains if the answer to our question is no, that the data can be fully described by a linear system. Once we have established the correct null hypothesis for our  
50  
51  
52  
53  
54  
55  
56  
57  
58  
59  
60  
61  
62  
63  
64  
65

purpose, the goal is then to create a large number of surrogate data sets which correspond to this null hypothesis. In this case, each surrogate should be a random copy of the system, with all linear properties maintained, but with any nonlinearity destroyed. The discriminating statistics can then be applied to the original data, and every surrogate data set. It is crucial in any surrogate application to treat the original data and each surrogate in *exactly the same way*, including any preprocessing, filtering or embedding, and to ensure that properties such as sampling frequency and data length are the same in the surrogates as in the original data. The results are then compared, and if the result in the original data is significantly different to the results obtained for the surrogates the null hypothesis can be rejected with a confidence level based on the statistical threshold chosen. A result that is not significantly different to the surrogate distribution means that we cannot consider the data as having a nonlinear origin, or the test used is insufficient to reveal any nonlinearity present in the system. As chaos is necessarily a nonlinear phenomenon, except in the special case of infinite dimensional systems where linear chaos can be observed, we cannot make any statistically significant conclusions about chaos in the system.

## 2.2. Typical vs. constrained realizations

Within the surrogate family, there are two approaches: typical realisations and constrained realisations. Typical realisations fit a model to the data, for example by estimating the coefficients of an autoregressive (AR) model and then producing Monte Carlo realisations of this model to compare with the data (see Section 4.4). This has the disadvantage that the user must know the model and its parameters beforehand.

In contrast, constrained realisations are calculated directly from the data, producing surrogates that match all properties of the original data other than the property being tested. The differences between these two approaches have been thoroughly discussed by Theiler & Prichard [42]. Constrained realisations are more widely used, as they can be used with almost all discriminating statistics, whilst the applicability of the typical realisation approach is dependent on whether the discriminating statistic is “pivotal”, i.e. whether its distribution is the same for all processes consistent with the null hypothesis [42]. Whilst the constrained realisation approach is more popular, being what is usually referred to as surrogate data, it should be noted that the constrained realisation approach is designed only for hypothesis testing, and thus, in contrast to typical realisations, cannot be used for the estimation of confidence intervals [42].

## 2.3. The null hypothesis

It is very important when using surrogate data to formulate the correct null hypothesis. When rejecting a null hypothesis, we can say that this underlying hypothesis is unlikely to describe the origin of the data [43]. On the contrary, failure to reject the null hypothesis does not necessarily mean that the null hypothesis is true. All surrogates test only, and exactly, the null hypothesis specified for them. Therefore, it is extremely important to choose the correct surrogate for the purpose. It is also important, if possible, to test generated surrogates before use to ensure that they are suitable, i.e. if they reject the null hypothesis only in expected scenarios, and not just as a result of the inaccuracy or inapplicability of the surrogates, or because there are not enough data available to reach a reliable conclusion about the dynamical property in question. For example, Paluš [44, 45] discusses the importance of identifying problems in surrogate data by using linear and nonlinear redundancies. If, when testing for nonlinearity, linear redundancy is rejected in the linear surrogates, then there is likely a problem in the surrogate data which may result in spurious nonlinear statistics.

## 2.4. Significance testing

In many applications of surrogates, it has been assumed that the distribution of the discriminating statistics calculated in a set of surrogates is Gaussian, and thus the significance level has been set as a number of standard deviations above or below the mean, usually two. However, the distribution of these surrogates is not always Gaussian, and so this assumption should be checked before taking this approach. Alternatively, and more robustly, the nonparametric rank-order test can be used, in which the significance level is determined as, for example, the 95<sup>th</sup> percentile of the surrogates [3, 4].

The number of surrogates required will depend on whether a one or two-sided test is to be performed. A one-sided test means that the null hypothesis can be rejected only if the distribution of the surrogate values of the discriminating statistic deviates from those calculated in the original data in one specified direction, i.e. it is only lower or only higher. For example, deterministic signals should have better predictability than noise, thus, constructed surrogates that are realizations of noise will indicate rejection only if the original data are more predictable than most of the surrogates, whilst no conclusion is drawn if they are less predictable. A two-sided test allows testing for the possibility of the discriminating statistic being either higher or lower in the surrogates than in the original data.

The number of surrogates required will also depend heavily on the characteristics of the data and the specific surrogates being used. A good starting point is to use 100 surrogates, and test how much the spread of values of the discriminating statistic varies with increasing numbers of surrogates. If the range of surrogate statistics is still increasing when reaching 100, then more will be required. For some applications, it may not be necessary to calculate 100 surrogates in order to calculate the significance level. If computational effort is a limiting factor, and the spread of the surrogate data is not too large, for a one sided test,  $M = K/\alpha - 1$  surrogates can be generated, where  $K$  is a positive integer and  $\alpha$  is the probability of false rejection corresponding to a level of significance  $(1 - \alpha) \times 100\%$ . For a two-sided test,  $M = 2K/\alpha - 1$  surrogates should be generated. Therefore, if  $K = 1$ , 19 or 39 surrogate time series are required for one- and two-sided tests, respectively, at a significance level of 95% [4]. In this case, the maximum/minimum of the surrogates should be taken as the significance level, rather than setting a percentile threshold. However, these assumptions should be carefully tested before use, and are unlikely to be sufficient in many applications.

If multiple statistical tests are performed, it becomes increasingly likely that significant results will be obtained by chance. Therefore, in these cases, the significance level must be updated accordingly to prevent false rejections of the null hypothesis (type 1 error). The Bonferroni correction can be used to compensate for this by altering the overall significance level to  $\alpha/m$  where  $\alpha$  is the overall significance level and  $m$  is the number of hypotheses. In the context of surrogates, this would alter the percentile above which the result is considered significant. The examples presented in the current work each include one test only, therefore this correction has not been applied.

### 3. Testing against noise

The very first question when embarking on the analysis of a signal, from what we suspect is a dynamical system, is usually whether the dynamics of the system results in purely random noise, or exhibits some deterministic features. This is a question which is not trivial, especially in real systems where we can regularly face a very low signal-to-noise ratio. Surrogate methods have been employed to provide answers to this question, but the assumptions made about the underlying null hypothesis are extremely important as they will significantly affect the outcome. If the background noise against which the data are tested is not estimated correctly, false rejections of the null hypothesis are likely to occur. At the same time, when testing against noise, it is important to remember that whilst rejection of the null hypothesis means that the data are unlikely to be the particular type of noise against which we are testing, a failure to reject does not mean that the data are definitely just noise. While this is a possibility, it is also possible that deterministic dynamics is present in the data, but cannot be observed with the applied methods, for example due to a low signal-to-noise ratio, or the use of an inappropriate discriminating statistic. Keeping this in mind, we discuss various methods with null hypotheses of either white (uncorrelated) or coloured (correlated) noise. The methods described here mostly take the *typical realization* approach, i.e. a model is estimated, and many realizations of this model are generated in order to test the deviation of the discriminating statistics calculated for the original data from the distribution of those calculated for the surrogates.

#### 3.1. Uncorrelated noise

When considering the complexity and time-variability of the signals arising from dynamical systems, it is clear that it is very unlikely that the data will be perfectly random noise, and it may be very easy to reject this null hypothesis. However, random surrogates can still be very useful for initial testing of whether a data set is suitable for further analysis.

##### 3.1.1. White noise surrogates

Arguably the simplest surrogate method, white Gaussian noise surrogates can be used to estimate significance levels when signal filtering is used. White Gaussian noise signals are generated with the same mean and standard deviation as the data to be analysed, and identical analysis is applied. They test the null hypothesis that the data are uncorrelated Gaussian noise by providing a threshold of discriminating statistics that would be obtained if the data were purely white Gaussian noise. Bandrivskyy *et al.* [46] used white Gaussian noise signals to demonstrate the low frequency bias in wavelet phase coherence calculations. Wavelet phase coherence was calculated between skin temperature and blood flow, revealing two frequency ranges apparently involved in temperature regulation. 30 pairs of uncorrelated white Gaussian noise signals were used to demonstrate the bias in wavelet phase coherence, resulting from the finite length of the data sets used, and to test the null hypothesis that there is no phase coherence between skin temperature and blood flow.

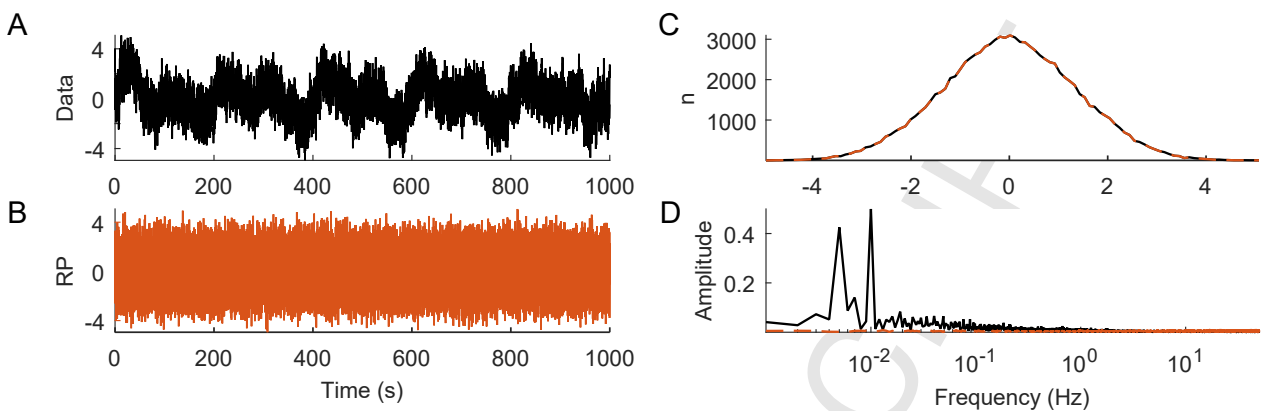


Figure 1: Comparison of a simulated signal ( $\sin(0.02\pi t) + \sin(0.01\pi t) + 1/f$  noise) (A) with a random permutation (RP) surrogate (B) obtained by randomly shuffling the time series in (A). Histograms of both signals demonstrate that the distribution of the time series is conserved, as seen in (C). (D) Fourier transforms of the signals, demonstrating that the power spectrum is destroyed in the RP surrogate. In all cases, black lines are from the original data and orange lines are from the surrogate.

### 3.1.2. Random permutation (RP) surrogates

To check the simple case of whether there is any temporal structure in the data, or the data are just uncorrelated noise, random permutation (RP) surrogates can be used. RP surrogates possess the same mean, variance, and histogram distribution as the original signal, but any temporal structure is destroyed [25]. These surrogates are also known as independent identically distributed (IID), scrambled or shuffled surrogates.

*Null hypothesis.* The observed data is fully described by independent and identically distributed (IID) random variables [3].

*Algorithm.* Randomly shuffle the original time series.

*Issues.* An example of a simulated oscillatory signal and its RP surrogate is shown in Figure 1. Rejection of the null hypothesis in this case means that the data possess temporal structure, which includes correlated noise. Any correlations present in the data will lead to this rejection. In this case, just by comparing the Fourier transforms, it is clear that the difference in power spectra between the original signal and the surrogate warrants the rejection of the null hypothesis, i.e. there is some temporal structure in the data. This is the only conclusion which can be made from this test, we cannot conclude anything further about the nature of this structure without further tests. Whilst in the majority of cases data can usually be verified as not being uncorrelated noise by visual inspection, RP surrogates can be very useful in the further calculation of discriminating statistics which are strongly affected by variations in parameters, for example to check if the length of a time series is too short, causing almost any signal to have the same value of a particular discriminating statistic.

*Applications.* RP surrogates are more widely applicable than white noise surrogates, as they allow for a non-Gaussian distribution. Lachaux *et al.* [47] presented for the first time a practical method for the quantification of frequency specific synchronization between two neuroelectric signals (phase locking statistics (PLS)). RP surrogates were used to validate synchrony values against background fluctuations [47]. Kenwright *et al.* [48] used RP surrogates to investigate the effect of low-frequency oscillations on cardiorespiratory synchronization during rest and exercise. 100 shuffled instantaneous cardiac and respiratory frequency surrogates were calculated for each subject in order to test them for cardiorespiratory synchronization. This revealed higher order, shorter duration cardiorespiratory synchronization during exercise than that found at rest [48].

### 3.2. Correlated noise

In many real world applications, it is highly unlikely that the background noise in recorded data is purely uncorrelated noise, and thus RP and white Gaussian noise surrogates cannot be expected to provide much new information. The study of geophysics [12] and climate [15, 16] are fields in which the null hypothesis of a red or Brownian noise (with power spectral density of the form  $1/f^2$ ) background is more appropriate. One example is the persistence of the weather, i.e. if one day is sunny and warm, the next day will have a high tendency of being similar, which results in a red noise background in the power spectra of long-time meteorological records [49]. Many real

1  
2  
3 biological systems are difficult to distinguish from Ornstein-Uhlenbeck processes [50], thus surrogates are crucial  
4 when searching for dynamics in observations resembling them [51].

5 While the form of the background spectra alone is an important property of the system, failure to take it into  
6 account may hinder the search for any other, less obvious dynamics in the data. The presence of strong background  
7 noise in data may lead to the conclusion that there are no interesting features within this data beyond its power  
8 spectrum, without full consideration of the possibility that less obvious dynamics may be buried.

9 It is very important to consider that the ‘noise’ itself may simply be a manifestation of one or more complex  
10 processes, for example multiple interacting dynamical systems, and should be fully understood before being con-  
11 sidered inherent to the system. Various manifestations of correlated noise can be studied in their own right using  
12 surrogates. If  $1/f$  type behaviour is observed, it can be tested to see if it represents a monofractal or multifractal  
13 process [52], demonstrating that the noise should not be completely dismissed. The properties of noise are also  
14 crucial in chronotoxic systems, which are dynamical systems that possess a moving point attractor [53, 54]. The  
15 presence of this point attractor can be identified in real data by characterising the phase fluctuations, or noise, in  
16 the system, with more uncorrelated fluctuations indicating stronger chronotoxicity [55, 56].

17 Once the background noise has been characterised and explained, the search can then widen to try to extract  
18 information about other dynamics that may be observed in the system.  
19

#### 20 21 4. Surrogates for nonlinearity testing

22 The surrogate method for testing for nonlinearity gained huge popularity following the work of Theiler *et al.* [3].  
23 The surrogates reviewed in this section were developed in response to the need to test for nonlinearity in data, once  
24 it was emphasized that *the application of nonlinear analysis methods must be justified by first finding nonlinearity*  
25 *in the time series* [57]. Calculation of discriminating statistics meant to infer information from nonlinear systems  
26 on a linear system may still provide a finite result, but it may not make much sense. As discussed above, white  
27 noise or RP surrogates present an inadequate test for any system with correlated variables, and thus new surrogates  
28 are required which maintain the same serial correlations, i.e. the same autocorrelation function as the original data,  
29 but the nonlinearity is removed, providing the null hypothesis of a linear system. It has been shown to be more  
30 useful to test for a specific nonlinear property, than to test for nonlinearity generally [45], though the presence or  
31 absence of nonlinearity already provides valuable information about the underlying system.  
32

33 The following surrogate types (with the exception of autoregressive surrogates) are designed to test the null  
34 hypothesis that the data were generated by a noisy linear process, and can be fully characterized by linear charac-  
35 teristics, namely mean, standard deviation, and autocorrelation for all lags. The Wiener-Khinchin theorem ([58],  
36 explained in detail in [14]) demonstrates that autocorrelation can be preserved by preserving the power spectrum,  
37 which is implemented in the majority of the surrogates in this section. Preserving the power spectrum while  
38 randomizing the Fourier phases of the data provides a surrogate in which any nonlinear structure is destroyed.  
39

40 Here, we describe the most commonly used surrogate types for testing for nonlinearity in data: Fourier transform  
41 (FT), amplitude adjusted Fourier transform (AAFT) and iterative amplitude adjusted Fourier transform (IAAFT)  
42 surrogates. FT, AAFT and IAAFT have been extensively studied and used in a wide range of applications [3, 59,  
43 60, 61, 4]. Therefore, they are relatively safe to use, as all of their pitfalls have been studied in detail. The reader is  
44 encouraged to consult [4] for an excellent review. Although these surrogates are very well known and widely used,  
45 it is still extremely important to choose the correct surrogate depending on the application.

46 We also consider another Fourier based surrogate method introduced by Dolan *et al.* [62, 63] named iterative  
47 digitally filtered surrogates (IDFS), which deliberately do not preserve the power spectrum exactly for all surrogate  
48 realisations, in order to allow for the naturally expected variation in a system. Wavelet based surrogates for  
49 nonlinearity testing are also discussed.

50 One area where these surrogates for nonlinearity testing have been of great importance is neuroscience, where  
51 they have been used to scrutinise some previous conclusions of nonlinearity and chaos in brain signals [64]. Soon  
52 after the introduction of the concept of chaos, it became extremely popular as a possible explanation for previously  
53 seemingly unexplainable behaviour. For the first time, it provided a solution in which a system can be completely  
54 deterministic, yet appear random, due to its extremely sensitive dependence on initial conditions. It was a partic-  
55 ularly popular concept in the analysis of EEG data, which was concluded to be chaotic in many studies, usually  
56 using correlation dimension and Lyapunov exponents as discriminating statistics. Further investigation and in-  
57 creased scrutiny using newly developed surrogate data testing [65] revealed that these conclusions may have been  
58 premature [66], with researchers struggling in some cases to consistently find even nonlinearity in normal EEG time  
59 series. However, nonlinear time series analysis methods were shown to be crucial in the identification of the focal  
60 hemisphere in epilepsy patients, with a much greater accuracy achieved with nonlinear methods combined with sur-  
61 rogates, than in either the application of linear methods, or the application of nonlinear methods without surrogates  
62  
63

[67]. This was also shown to be the case for bivariate analysis techniques for the investigation of interdependence [36].

Whilst chaos cannot be directly proven in a time series [68], nonlinear dynamics can. In the vast majority of cases, the absence of nonlinear dynamics means that chaos can be excluded. However, it is more difficult to look specifically for chaos in a time series which has been shown to be nonlinear using surrogate data. An irregular time series arising from a nonlinear deterministic system is likely in most cases to be either chaotic or pseudo-periodic (defined as a representative of a periodic orbit perturbed by dynamical noise, contaminated with observational noise, or a combination of both, with states within one cycle being largely independent of those within previous cycles (see Section 5.4)) [69]. Thus being able to exclude the possibility that the time series is pseudo-periodic would mean that the time series is more likely to be chaotic, or vice versa. As it is generally difficult to distinguish between the two scenarios, various surrogate data tests with null hypotheses beyond nonlinearity alone have been developed for this purpose [69].

#### 4.1. Autoregressive moving average (ARMA) processes

Rejection of the null hypothesis using the surrogates in this section and some nonlinearity measure suggests that the data possess nonlinear structure. If the null hypothesis cannot be rejected, the data are either linear, i.e. generated by a linear set of equations driven by noise, or the chosen test parameter is not sufficient to reveal the nonlinearity in the data. This could be because the nonlinearity is weak, or the discriminating statistic is testing for the wrong type of nonlinearity. For the discussed FT based surrogates (FT, AAFT and IAAFT) the underlying process is assumed to be “stationary linear Gaussian”. Considering each word separately, it is clear that this test for nonlinearity, whilst rejecting the null hypothesis for a nonlinear signal, would also reject the null hypothesis if the underlying process was linear Gaussian but nonstationary or nonautonomous, linear but non-Gaussian, or any combination of these. Failure to reject the null hypothesis does not necessarily mean that the underlying process is stationary linear Gaussian. This highlights the importance of also considering the effects of nonstationarity and time-variability in the data before assuming nonlinearity. It should also be kept in mind that underlying dynamics can be masked by noise or the use of incorrect discriminating statistics, or the time series may not fully represent the system being studied.

When considering how strict these conditions are, the most important question is: what is a stationary linear Gaussian process? The fundamental question when using these surrogates is whether the system demonstrates nonlinear phenomena or not, i.e. must it be described by nonlinear equations, or can it also be described by linear equations with additive noise? This is what we want to test for.

In discrete time, the most general stationary Gaussian model with finite correlation time is the autoregressive moving average (ARMA(M,N)) model [70]:

$$s_n = \sum_{i=1}^M a_i s_{n-i} + \sum_{i=0}^N b_i \eta_{n-i}, \quad (1)$$

where  $\eta_i$  are independent Gaussian increments with zero mean and unit variance, and  $a_i, b_i$  are coefficients. It should be noted that the ARMA model does not include all possibilities of linear equations, and as a result the corresponding surrogate tests may reject the null hypothesis for linear processes of the form (1) but with:

1. Time dependent parameters (nonautonomous systems). However, this can be regarded as nonlinearity.
2. Any (including Gaussian) multiplicative noise in parameters.
3. Types of noise which cannot be represented as uncorrelated Gaussian or correlated noise with a fixed timescale.

#### 4.2. Nonstationarity

Surrogates that test against the null hypothesis of a linear, Gaussian, stationary stochastic process may not only provide a rejection in the case of a nonlinear system, but also if the system is linear but nonstationary. This was demonstrated by Timmer [71] using the correlation dimension and Fourier transform surrogates. It is therefore very important to ensure that the data are indeed stationary, i.e. their statistical properties are invariant, before applying any surrogate technique with this assumption in their null hypothesis. Borgnat and Flandrin [72] discuss in detail how to utilise the stationarization which is a natural property of Fourier transform surrogates, and how to test for nonstationarity using surrogates.

Another approach to the problem is to update the null hypothesis and the surrogate algorithm to match any nonstationarity in the data so that it cannot be the source of significant differences in the result. The method proposed by Lucio *et al.* [73] achieves this by detrending and retrending the data and applying a technique

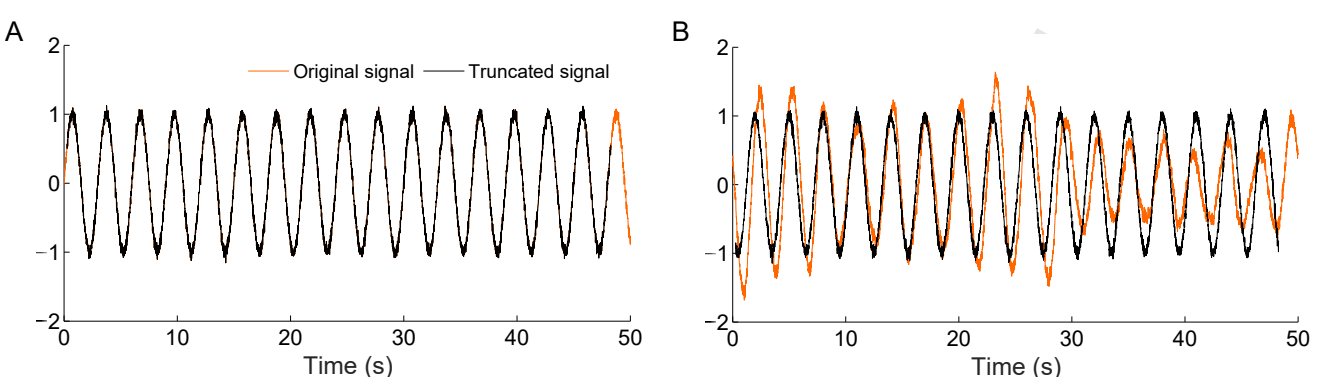


Figure 2: (A) Example of a noisy sine wave before and after preprocessing by matching the ends and first derivatives. (B) Fourier transform (FT) surrogates of the original and truncated signal. A ‘beating’ phenomena can be observed in the non-preprocessed case (orange lines).

introduced in by Nakamura *et al.* in [74]. The authors presented a method for investigating nonlinearity in irregular fluctuations, or the short-term variability of time series even if the data exhibit long-term trends [74]. The method presented, named the truncated Fourier transform surrogate (TFTS) method, is an extension of FT surrogates in which a frequency threshold is determined, above which the phases of the original signal are randomized and below which they remain the same. This randomizes the short-term variability in a time series whilst preserving long-term trends. As a surrogate method based on the Fourier transform, the accuracy of this method will suffer with the presence of end-to-end mismatch of the data (see Section 4.3), so the authors propose to symmetrize the data to correct this before applying the algorithm, resulting in symmetrized TFTS (STFTS) [74]. It should be noted that the method discussed in [73] is only applicable when it can be assumed that the nonlinearity in the static transformation in AAFT and IAAFT is weak, as it is very difficult to separate simultaneously occurring nonstationarity and nonlinearity.

Wavelet based surrogates, which preserve the local mean and variance of the data, were introduced by Keylock [75, 76]. The fact that wavelet analysis does not assume stationarity makes it particularly useful in the study of ecological time series [17]. Wavelet surrogates have since been used directly to test for stationarity [77]. Wavelet surrogates are discussed further in Section 5.1.

It is emphasised that windowing is usually preferable when dealing with nonstationary time series. Surrogate tests can be performed for different windows of data, and nonlinearity could even be tested at different scales to find out exactly at which times and scales nonlinearity can be found. In contrast, for stationary signals as long a signal as possible is optimal, to ensure transient interactions are not missed [78].

#### 4.3. Preprocessing

Once possible nonstationarity in the data has been addressed, the data should be preprocessed to avoid spurious results introduced solely by the surrogate generation method. The preprocessing should be performed in the following order:

1. Remove any trends in the data which are not important or relevant to the results, so that they are not incorporated into the surrogates.
2. Correct any mismatch between start and end points and corresponding first derivatives. This is very important and must not be overlooked, and arises from the assumptions made when calculating any of the Fourier transform based surrogates.
3. Subtract the mean to ensure that results are not affected by significantly different mean values.

The goal of most FT-based surrogates is to preserve the autocorrelation of the signal, and preserving the Fourier spectrum provides a way to achieve this easily. The Wiener-Khinchin theorem states that there is one-to-one correspondence between Fourier amplitudes and *periodic* autocorrelation. As the latter suggests, this correspondence is only exact when the data can be considered as containing an integer number of periods of oscillation. If this is not the case, then the assumption of correspondence breaks down, and autocorrelation is no longer preserved. If there is a finite mismatch between the beginning and end of the data, spurious results will be obtained [4], especially in periodic signals. Figure 2 demonstrates this using a sine wave and its Fourier transform surrogate. A ‘beating’ phenomenon can be seen in the surrogate calculated from the non-preprocessed signal. This is a purely numerical artifact and is due to the separation of the dominant frequency peak into other frequency bins. This demonstrates

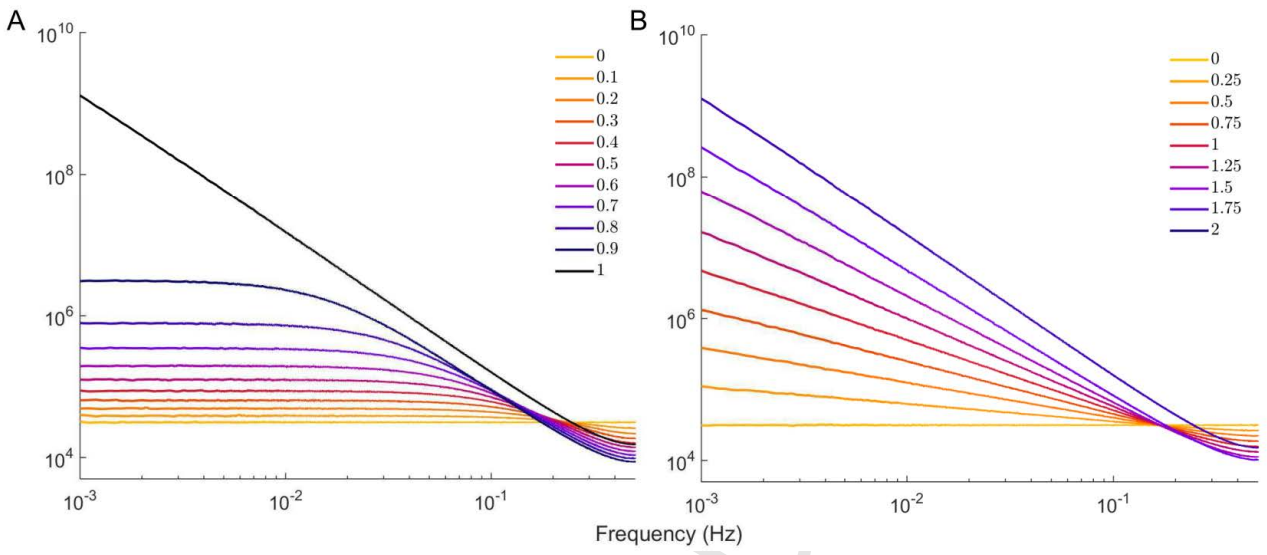


Figure 3: (A) Fourier spectra of first order autoregressive noise as calculated in Eq. 3 with varying values of  $\rho$ . For each value there is a point at which the spectrum saturates. This must be taken into account when selecting the noise model for the null hypothesis for the data to be studied. (B) Fourier spectra of  $1/f^\alpha$  noise with varying values of  $\alpha$ . In all cases, signals were 10,000 points, sampling frequency 1 Hz and the mean of 10,000 realisations for each value is shown.

the importance of preprocessing, as it is highly likely that this behaviour would cause the rejection of the null hypothesis of a linear process.

To prevent problems arising from the issues described above, the start and end points of the data should be matched as closely as possible. The first derivatives should also be matched, to ensure that non-integer number of cycles are not permitted, which would alter the power spectrum and again cause the system to appear as nonlinear. The matching of start and end points can be achieved by choosing the closest pair of values from the first  $K_1$  and last  $K_2$  points, and truncating data before and after these points, respectively. For a periodic signal, matching the first derivatives is also important, and can be achieved by not only matching points, but minimizing the mismatch between consecutive points at the beginning and the end of the signal as follows:

$$\{k_{start}, k_{end}\} = \operatorname{argmin}_{k_1, k_2} \sum_n^p (s_{k_1+n} - s_{k_2+n})^2, \quad (2)$$

where  $k_1 = 1 \dots K_1$ ,  $k_2 = L - K_2 - p \dots L - p$  are indices of points at the beginning and end. Then truncate the time series up to  $k_{start}$  at the beginning and from  $k_{end}$  to the end, so the new “processed” time series will be  $s_{n=k_{start} \dots k_{end}}$ . The variable  $p$  determines smoothing, and should be greater for noisy systems. Stam *et al.* [68] reported that  $p = 10$  is appropriate in most cases. However, this value will depend on the signal, including its shape, the period of oscillations, the sampling frequency, and the presence of noise. It is recommended that  $p$  be chosen as a portion of the period of the oscillation, from  $T/10$  to  $T/2$ , depending on the data. The latter case would be used for example if one had a square wave, as a smaller value may mean matching at any point along a flat part of the signal.

This truncation process and the surrogates that it generates have been considered as surrogates in their own right, as so-called length-adjusted discrete Fourier transform (LA-DFT) surrogates [68], but preprocessing should be considered an essential step for all FT based surrogates, and also time-shifted surrogates (see Section 7.4). One interesting case in which the effects of not preprocessing are obvious is a sine wave. If the ends of a sine wave are not matched, surrogate testing coupled with a discriminating statistic may consider it as nonlinear, whilst if preprocessing is performed correctly it will be regarded as linear.

#### 4.4. Autoregressive (AR) surrogates

Autoregressive surrogates are used to estimate the background noise spectrum of the observed data, and are an example of *typical* realisation surrogates. An autoregressive process is a discrete representation of a random

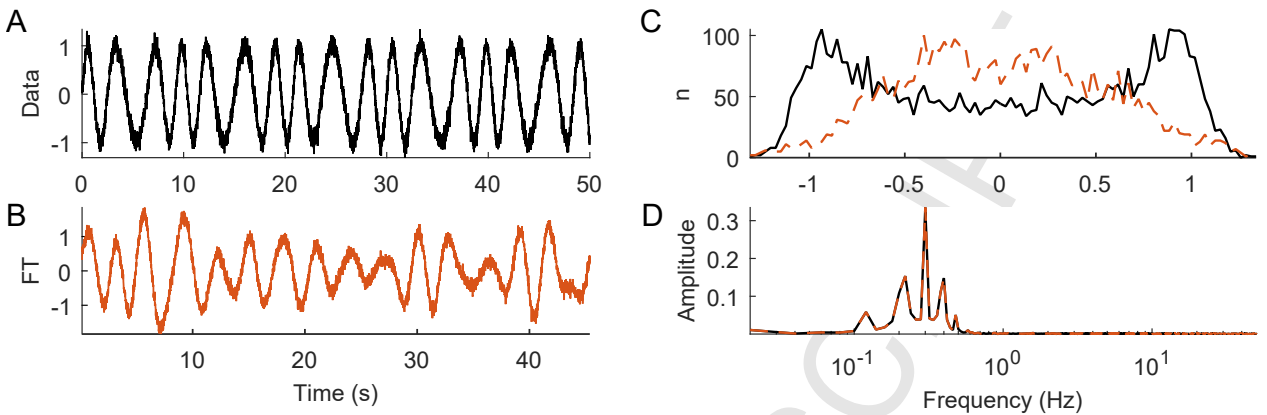


Figure 4: (A) 50 s noisy sinusoid with time-varying period  $\sin(2\pi(t + 0.5 \sin(2\pi t/10))/3)$ , with sampling frequency 100 Hz, preprocessed as discussed in Section 4.3. (B) Example Fourier transform (FT) surrogate calculated from the signal in (A). The amplitude distribution (C) is not preserved. The power spectrum (D) is perfectly preserved. In all panels, black lines represent the original signal and orange lines represent the surrogate.

process. It assumes that a variable depends linearly on its previous values and a stochastic term,

$$x_t = c + \sum_{n=1}^p \rho_n x_{t-n} + \sigma \varepsilon_t, \quad (3)$$

where  $x_t$  is the variable,  $\rho_i$  are parameters of the model,  $c$  is a constant (assumed to be zero for simplicity),  $\varepsilon_t$  is a random variable from a Gaussian distribution with zero mean and unit variance, and  $\sigma$  is the standard deviation of the Gaussian distribution. Higher-order AR processes can actually support oscillations themselves, thus great care must be taken when selecting a null hypothesis and during parameter estimation.

*Null hypothesis.* The observed data can be fully described by an autoregressive noise model.

*Algorithm.* In the case of the assumption of AR(1) noise, surrogates can be simulated by estimating the correlation coefficient  $\rho$  from the time series using lag-0 and lag-1 covariances. The model (3) is then simulated with this estimated value for each surrogate.

*Issues.* As with any surrogate method, to obtain meaningful results, the null hypothesis must be carefully considered. As previously discussed, it has been shown that a large proportion of climate data has a red noise (Brownian noise,  $1/f^2$ ) background. Red noise can be perfectly described by the AR(1) model with  $\rho = 1$ . A comparison of frequency spectra for different values of  $\rho$  is given in Figure 3(A). It becomes clear that although red noise can be well represented by this model, it may be more difficult to estimate the spectrum of signals for which a value of  $\rho$  other than 1 or 0 is estimated from the data. How well the AR(1) model matches the background noise of the signal may depend upon the number of points in the signal, with a plateau appearing in the spectra at lower frequencies (see Figure 3(A)).

One example of background noise which cannot be estimated using the AR(1) model is pink noise ( $1/f$ ), with energy that is inversely proportional to the frequency of the signal. Pink noise-like spectra have been observed in many physical and biological systems [79], and may be considered when searching for dynamics in noisy data arising from nature. More generally, the noise spectrum may be described by  $1/f^\alpha$  where  $\alpha = 1$  for pink noise, 2 for red noise and 0 for white noise. Figure 3(B) shows the  $1/f^\alpha$  spectra for different values of  $\alpha$ . Surrogates can also be generated from this model, if this better fits the characteristics of the data. When using this model for the underlying surrogates, the parameter  $\alpha$  will need to be estimated from the data [80]. Examples of the use of AR and  $1/f$  surrogates are shown in Section 9.1.3.

#### 4.5. Fourier transform (FT) surrogates

Fourier transform (FT) surrogates use a phase randomization process to test for nonlinear structure in a time series. Despite some drawbacks, discussed below, they are widely used, and computationally very cheap.

1  
2  
3 *Null hypothesis.* The data were generated by a stationary linear Gaussian process. Equivalently, the null hypothesis  
4 can be formulated as that the data do not contain any nonlinear structure. The surrogates satisfy the null hypothesis  
5 if they have the same power spectrum as the original data.  
6

7 *Algorithm.* This procedure is known as phase randomization, and serves to preserve linear behaviour, i.e. the power  
8 spectrum/autocorrelation, but destroy any nonlinear behaviour.  
9

- 10 1. Calculate the Fourier transform  $ft_x$  of the original signal  $x_n$ .
- 11 2. Generate a vector of random phases (i.e. a random sequence of values in the range  $[0 \ 2\pi]$ )  $\varphi_r$ , with length  
12  $L/2$ , where  $L$  is the length of the time series.
- 13 3. As the Fourier transform is symmetrical, to create the new phase randomized vector  $ft_r$ , multiply the first  
14 half of  $ft_x$  (i.e. the half corresponding to the positive frequencies) by  $\exp(i\varphi_r)$  to create the first half of  $ft_r$ .  
15 The remainder of  $ft_r$  is then the horizontally flipped complex conjugate of the first half.
- 16 4. Finally, the inverse Fourier transform of  $ft_r$  gives the FT surrogate.  
17

18 An example FT surrogate of a noisy sinusoid is shown in Figure 4.  
19

20 *Issues.* As with all surrogates, it should be noted that if the data do not meet the criteria of the whole null  
21 hypothesis, it will be rejected. For example, in the case of FT surrogates, the null hypothesis, in addition to being  
22 rejected if the data are indeed nonlinear, will also be rejected if the data are linear but cannot be described by an  
23 ARMA process, i.e. the process is linear but nonstationary/nonautonomous, the data are linear but non-Gaussian,  
24 or are linear but contain any multiplicative noise.  
25

26 As discussed in Section 4.3, the restraints of the Wiener-Khinchin theorem requires that data is truncated to  
27 only include an integer number of periods before application of the FT algorithm. This also applies to the amplitude  
28 adjusted Fourier transform (AAFT) and iterative amplitude adjusted Fourier transform (IAAFT) surrogates  
29 discussed below. It should also be noted that FT surrogates tend to indicate nonlinearity for linear time series with  
30 long coherence times, which is thoroughly discussed in [59].  
31

32 *Applications.* Contrary to studies that have failed to find significant nonlinearity in the electroencephalogram  
33 (EEG), Stam *et al.* [35] found evidence for nonlinearity in normal and abnormal EEG during the awake/eyes closed  
34 state, and conclude that it is the spatial structure in the EEG that exhibits much of the nonlinear structure. The  
35 nonlinear EEG measures presented show more or less specific patterns of dysfunction in dementia and Parkinson's  
36 disease. The surrogates used in this case were FT surrogates with linear correlations maintained [35] (see below for  
37 further discussion on multivariate surrogates). The null hypothesis for the surrogates used was that all structures  
38 in the EEG, in the time and in the spatial domain, can be adequately described by a linear model.  
39

40 Using FT surrogates with linear redundancy, Paluš [22] found that there is nonlinearity in vigilant and sleep  
41 EEG recordings, but that it was not consistent with the hypothesis of low-dimensional chaos, as assumed many  
42 times previously before the use of surrogate data. Faes *et al.* [25] compared surrogate types, including IID, FT  
43 and AR, using simulations and real cardiovascular data, and found that when testing coherence significance levels,  
44 surrogates which preserve the autocorrelation in the data (FT and AR) are superior to those which only preserve  
45 the amplitude distribution (IID). FT surrogates have also been used in synchronization analysis between HRV and  
46 EEG in epilepsy [81]. Yamamoto *et al.* [82] found evidence of deterministic chaos in HRV at extreme altitude based  
47 on surrogate testing for nonlinearity with correlation dimension and FT surrogates.  
48

49 *Multivariate FT surrogates.* Fourier transform surrogates, and any other surrogate type in which the phases are  
50 randomized (i.e. AAFT, IAAFT), can be used for the investigation of discriminating statistics and nonlinear  
51 dependencies in multivariate data by preserving the cross spectrum between signals in addition to preserving their  
52 power spectrum [60]. This is achieved by adding the same random phases to each FT surrogate. The corresponding  
53 null hypothesis would then be that all signals are stationary linear Gaussian processes, with only linear dependence  
54 between them. Equivalently, the null hypothesis is that the data are a realization of a multivariate Gaussian process.  
55 Rombouts *et al.* [83] used multivariate surrogates to investigate nonlinearity in EEG signals. Breakspear and Terry  
56 [84] combined AAFT and multivariate surrogate data techniques to search for nonlinear interdependence in EEG  
57 data.  
58

59 Multivariate surrogates have been used to test for nonlinear dependence between signals, but care must be taken,  
60 as the null hypothesis requires that the signals are linear. Therefore, a test with these surrogates may reject the  
61 null hypothesis in the case of linearly coupled nonlinear systems, providing a misleading result. This means that  
62 these surrogates are not suitable for testing the nature of coupling, where no prior information is available.  
63  
64

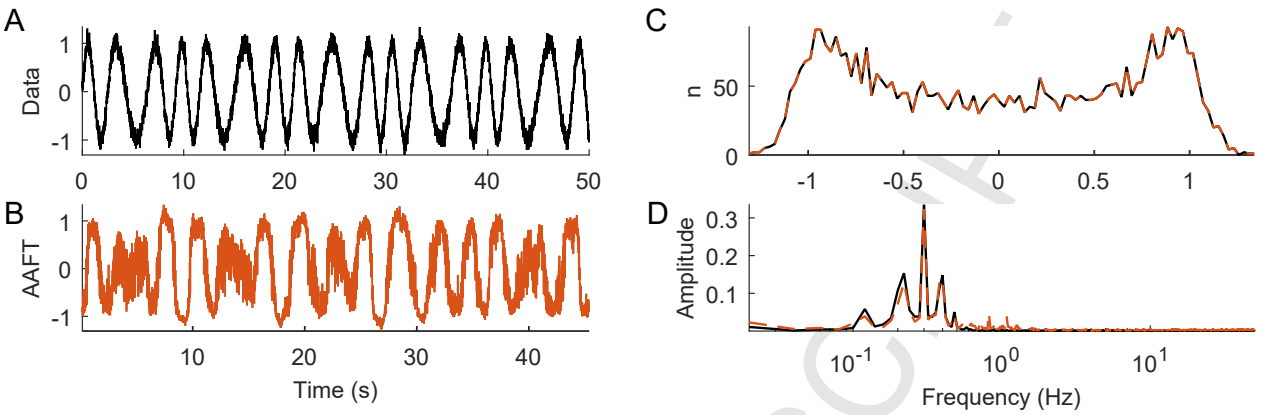


Figure 5: (A) 50 s noisy sinusoid with time-varying period  $\sin(2\pi(t + 0.5 \sin(2\pi t/10))/3)$ , with sampling frequency 100 Hz, preprocessed as discussed in Section 4.3. (B) Example amplitude adjusted Fourier transform (AAFT) surrogate calculated from the signal in (A). The amplitude distribution (C) is perfectly preserved. The power spectrum (D) is slightly distorted. In all panels, black lines represent the original signal and orange lines represent the surrogate.

#### 4.6. Amplitude adjusted Fourier transform (AAFT) surrogates

FT surrogates usually have a Gaussian distribution of values, which is often not the case in real data, which can then lead to false rejections of the null hypothesis purely based on differences in amplitude distribution. Care must be taken to ensure that a conclusion of nonlinearity does not arise through the presence of a static nonlinearity, i.e. introduced into the system during measurement and therefore not a result of the underlying dynamics of the system [6]. To counter this, a histogram transformation can be applied, e.g. to transform the data into a Gaussian distribution [85, 44], or the distribution of the surrogates can be adjusted to match the original time series, as in the amplitude adjusted Fourier transform surrogates described below [3]. These surrogates are also known as histogram adjusted isospectral (HAFT) surrogates [86].

*Null hypothesis.* The data represent a rescaled linear Gaussian process, which means that the data were generated by a stationary linear Gaussian process, measured by an invertible time-independent instantaneous (i.e. no time delays) measurement function  $s(\cdot)$ :

$$s_n = h(x_n), x_n = \sum_{i=1}^M a_i x_{n-i} + \sum_{i=0}^N b_i \eta_{n-i}, \quad (4)$$

where the restriction that  $h(\cdot)$  is invertible (i.e.  $x_n = h^{-1}(s_n)$ ), time-independent (stationary/autonomous) and instantaneous is very severe and essential [4].

*Algorithm.* In AAFT surrogates, as well as trying to preserve the power spectrum as in FT surrogates, the amplitude distribution is also preserved. First we should find the possible underlying process  $x_n$  from the measured data  $s_n$ , phase randomize it, and transform back to recover the original distribution of  $s_n$ . Since the underlying linear process  $x_n$  should have a Gaussian distribution of values, to find it one should rescale the original values  $s_n$  to conform with a Gaussian distribution. This is usually done by rank ordering, which attempts to empirically invert the measurement function. The procedure for AAFT surrogates is as follows [3]:

1. Sort the original time series  $s$  in ascending order, and rank the original location of the values from 1 to  $L$ , where  $L$  is the length of the time series. For example, if  $s_n$  is the fifth smallest element among all  $s$ ,  $ranks_n$  will be 5.
2. Generate a Gaussian noise signal with the same length as the original time series, and sort in ascending order to give  $G_s$ .
3. Reorder  $G_s$  to match the ranks of the original time series to create a new vector  $x$ . If  $s_n$  is the  $n$ th smallest of all  $s$ , then  $x_n$  will be the  $n$ th smallest of all  $G_s$ . Therefore,  $x_{n=1,\dots,L} = G_s^{ranks(1,\dots,L)}$ .
4. Calculate the FT surrogate of  $x$  (as described in Section 4.5), denoted  $xs$ .
5. Sort  $xs$  in ascending order, and again assign a rank to these values in a new vector  $ranks2$ .
6. Reorder the sorted values of the original signal according to  $ranks2$  to obtain the surrogate.

An example AAFT surrogate of a noisy sinusoid is shown in Figure 5.

1  
2  
3 *Issues.* Kugiumtzis [87] highlighted the importance of ensuring that surrogate data are suitable for the application  
4 before use, by demonstrating some problems with the AAFT algorithm. It is stressed that AAFT surrogates are only  
5 applicable if the static transform  $h$  is invertible. The invertibility, i.e. a clear one-to-one correspondence between the  
6 underlying process  $x_n$  and the observed data  $s_n$ , is especially crucial. This restricts the types of possible rescalings  
7 which can be tested by AAFT surrogates. An example of the performance of AAFT surrogates when the data are  
8 subject to an invertible  $((s_n)^3)$  vs. a non-invertible  $((s_n)^2)$  transformation is given in Section 9.1.1.  
9

10 AAFT surrogates do not perfectly preserve all specified constraints, as the amplitude adjustment part of the  
11 algorithm introduces some changes in the power spectrum. Consequently, the surrogates no longer perfectly match  
12 the original time series. This is shown in Figures 5 and 9(A), where there is strange behaviour in the surrogate  
13 time series and the spectrum clearly does not match that of the original signal, with spurious harmonics being  
14 introduced. This is due to the fact that AAFT surrogates assume Gaussian distribution of the underlying process,  
15 whilst the sinusoids have highly non-Gaussian distributions. Thus, AAFT surrogates will regard sinusoids as  
16 a nonlinear process using most discriminating statistics. The corruption of the power spectrum makes AAFT  
17 surrogates inappropriate for testing any type of background frequency content introduced by the calculation of  
18 a discriminating statistic. Even when all requirements are met, AAFT surrogates still have a ‘whitened’ power  
19 spectrum when compared to the original time series due to the finite number of samples.  
20

21 *Applications.* AAFT surrogates have been used in many applications. Paluš & Novotná [86] investigated amplitude  
22 frequency correlations (AFC) in sunspot index data using 150,000 FT and AAFT surrogates leading to evidence of  
23 a nonlinear oscillator underlying the dynamics of the sunspot cycle. Bernjak *et al.* [88] used wavelet phase coherence  
24 combined with AAFT surrogates to investigate common fluctuations between simultaneously recorded microvascular  
25 blood flow and blood oxygen saturation signals, finding significant coherence between these parameters in shallow  
26 skin recording locations but not in deeper recordings. The same methods were also used to investigate recordings  
27 of sympathetic nerve activity with two needles inserted into nerve tracts supplying skin and muscles, showing  
28 continuously varying and coherently coupled human skin and muscle sympathetic nerve oscillations over time [89].  
29

30 Musizza *et al.* [90] investigated EEG signals in rats during deep and shallow anaesthesia. By combining the  
31 method of conditional mutual information [91] and AAFT surrogates, they found that the power of individual  
32 brain waves, as well as brain connectivity, clearly differs between deep and shallow anaesthesia, and between  
33 different types of anaesthetic. Stankovski *et al.* [39] combined time-frequency methods and voluntary ramped-  
34 frequency breathing to explore human neurophysiological mechanisms by calculating wavelet phase coherence and  
35 directionality of coupling, testing their significance with AAFT surrogates.  
36

37 Kvandal *et al.* [92] also applied wavelet phase coherence analysis to intracranial pressure (ICP) and arterial  
38 blood pressure (ABP) signals with significance levels determined by AAFT surrogates. They found that a phase  
39 shift between the ICP and ABP signals in the interval 0.07-0.14 Hz indicates normal cerebrovascular activity, while  
40 a phase shift in the interval 0.006-0.07 Hz indicates an altered cerebrovascular reactivity. Sheppard *et al.* [93]  
41 also used AAFT surrogates in the analysis on ICP and also tested for time-localized coherence. Ehlers *et al.* [94]  
42 investigated the effects of ethanol on the brain using AAFT and nonlinearity measures.  
43

#### 4.7. Iterative amplitude adjusted Fourier transform (IAAFT) surrogates

44 Iterative amplitude adjusted Fourier transform (IAAFT) surrogates were introduced by Schreiber & Schmitz  
45 [61] to overcome the flatness bias observed in the power spectrum of AAFT surrogates. They are constructed by  
46 iterative replacement of Fourier amplitudes with the correct values and rescaling the distribution to achieve a closer  
47 match between both the distribution and the power spectrum in the original data and the surrogates.  
48

49 *Null hypothesis.* The data represent a stationary linear Gaussian process, measured through an invertible, time-  
50 independent instantaneous measurement function.  
51

52 *Algorithm.* The power spectrum and the amplitude distribution of the original time series should be preserved  
53 in the surrogates. The iterative nature of the algorithm for IAAFT surrogates increases the computation time  
54 depending on the number of iterations required for convergence.  
55

- 56 1. Generate a random shuffle of the data,  $y_n^{(0)}$ .  
57
- 58 2. Fourier transform the current iteration  $y_n^{(i)}$ , replace Fourier amplitudes (but not phases) with those from the  
59 original signal and inverse Fourier transform. This generates a signal,  $z_n^{(i)}$  which has the same power spectrum  
60 as the original time series but a slightly different distribution of values.  
61
- 62 3. Rescale  $z_n^{(i)}$  to the original distribution of  $s_n$  to produce the next iteration  $y_n^{(i+1)} = s_{rank(z_n^{(i)})}$ .  
63
- 64
- 65

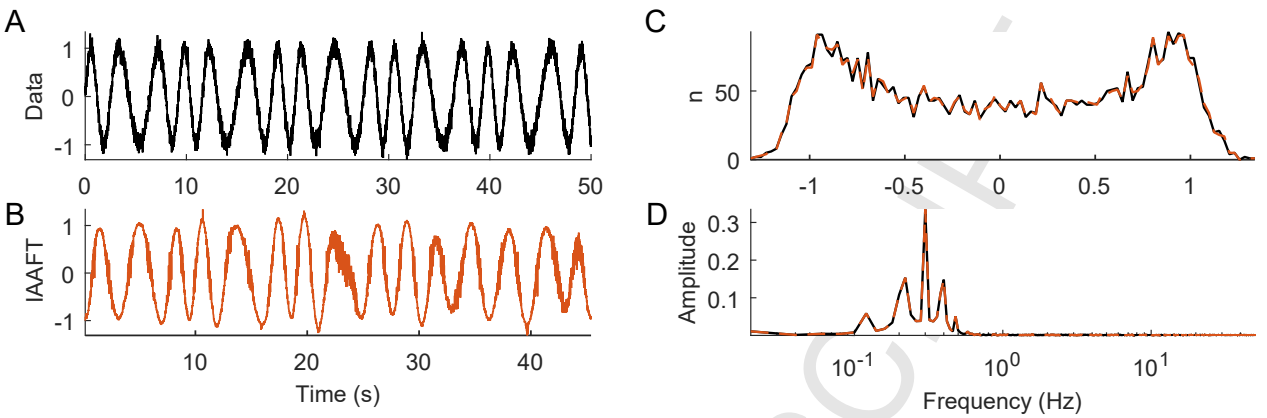


Figure 6: (A) 50 s noisy sinusoid with time-varying period  $\sin(2\pi(t + 0.5 \sin(2\pi t/10))/3)$ , with sampling frequency 100 Hz, preprocessed as discussed in Section 4.3. (B) Example iterative amplitude adjusted Fourier transform (IAAFT) surrogate calculated from the signal in (A). The amplitude distribution (C) is not perfectly preserved. The power spectrum (D) is perfectly preserved. In IAAFT-1 surrogates (not shown), the amplitude distribution is extremely close to the original and can be regarded statistically the same, but the power spectrum may differ slightly. In all panels, black lines represent the original signal and orange lines represent the surrogate.

4. Repeat steps 2-3 until the exact reordering in step 3 is repeated, i.e.  $\text{rank}(z_n^{(i+1)}) = \text{rank}(z_n^{(i)})$  for all  $n$ . This indicates that the procedure has converged, and that the power spectrum and distribution are as close to the original data as possible.
5. As the final surrogate signal, either take the last  $z_n$  of step 2 to exactly preserve the power spectrum (IAAFT-2), or the last iteration of step 3 to exactly preserve the amplitude distribution (IAAFT-1).

An example IAAFT-2 surrogate of a noisy sinusoid is shown in Figure 6.

*Issues.* The iteration involved in the IAAFT algorithm cannot preserve both the amplitude distribution and the power spectrum exactly. Therefore, the user must decide which is most important for the application. IAAFT surrogates in which the amplitude distribution is preserved exactly are known as IAAFT-1 surrogates, whilst those in which the power spectrum is perfectly preserved are known as IAAFT-2. The latter are recommended in cases where specific features of the amplitude distribution are not being studied, due to false rejections which may occur as a result of autocorrelation not being preserved [87]. Typically, IAAFT-2 surrogates are used due to the fact that most discriminating statistics for nonlinearity depend on the spectrum. Therefore, in all further discussions we will use IAAFT-2 surrogates, and refer to them only as IAAFT.

IAAFT surrogates have a very small spread of values due to the very accurate preservation of the specified constraints, which should be carefully considered during testing as very small deviations may affect the outcome of the test. This leads to a slightly lower power of the test when compared to AAFT, which means it may more often fail to reject the null hypothesis when it is false, but the number of false rejections of the null hypothesis is much smaller than for AAFT [61, 87], which is a great advantage. The small spread also has the advantage that less surrogates are required to determine significance levels.

The lower power of the test has also been attributed to possible phase correlations introduced during the adjustment and iteration process. The original creators of the IAAFT algorithm warn that the constraints introduced mean that “it cannot be excluded that the iterative scheme is able to converge only by also adjusting the phases of the Fourier transform in a nontrivial way” [61]. Indeed, Räth *et al.* have since clearly shown phase correlations in both AAFT and IAAFT surrogates when there should be none [95]. An example of these phase correlations is shown in Figure 7. This introduction of nonlinearity by the algorithm could lead to an incorrect failure to reject the null hypothesis of a linear Gaussian process in data from a nonlinear system, purely because both the data and the surrogates contain nonlinearities. This important issue should be kept in mind when deciding which surrogates are optimal.

It should be noted that IAAFT surrogates often perform well even in the case when  $h(\cdot)$  is noninvertible, whereas AAFT completely fail in this case [87]. This is a huge advantage over AAFT, as in real data there is no way to distinguish between invertible and noninvertible transformations.

*Applications.* IAAFT surrogates were used with a nonlinear prediction statistic to investigate the dynamics of the human alpha rhythm [96]. Nonlinearity was detected in only 1.25% of alpha rhythm time series. The authors highlight the variations in results of previous studies when looking for nonlinearity in EEG.

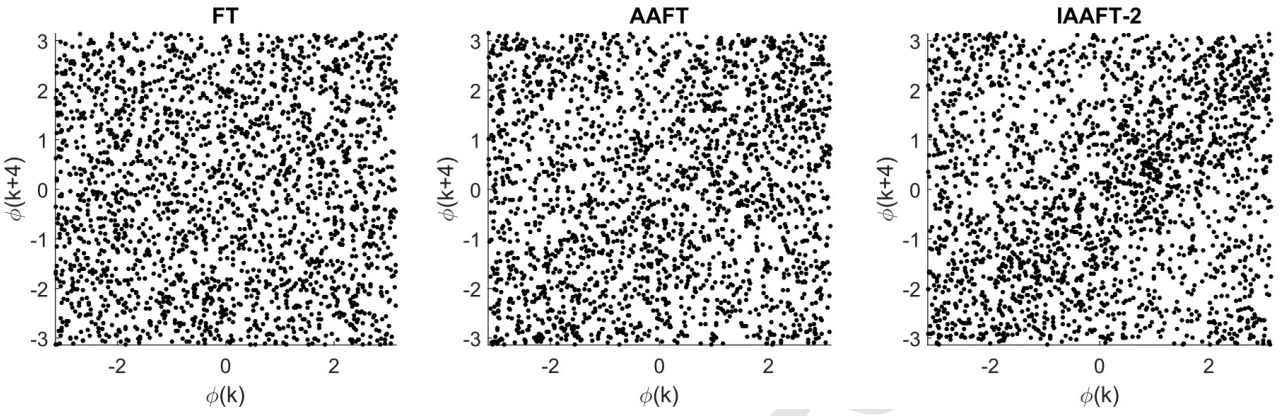


Figure 7: 2D phase plots for different surrogate types for the example signal shown in Figure 4. The Fourier transform phases were plotted against their delayed versions, as detailed in [95], in this case with a delay of 4. It is clearly shown that rather than having no phase correlations and being completely random, as in the FT surrogate, the AAFT and IAAFT surrogates contain some correlations in phase, thus indicating the presence of nonlinearity.

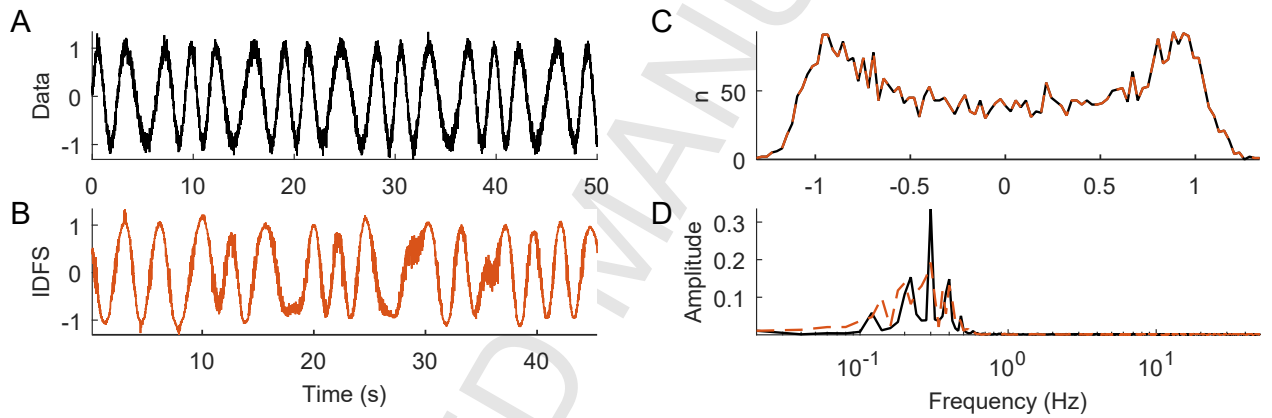


Figure 8: (A) 50 s noisy sinusoid with time-varying period  $\sin(2\pi(t + 0.5 \sin(2\pi t/10))/3)$ , with sampling frequency 100 Hz, preprocessed as discussed in Section 4.3. (B) Example iterative digitally filtered shuffled (IDFS) surrogate calculated from the signal in (A). The amplitude distribution (C) is perfectly preserved. The power spectrum (D) is slightly different for each surrogate realisation. In all panels, black lines represent the original signal and orange lines represent the surrogate.

Andrzejak *et al.* [97] combined the nonlinear prediction error and an estimate of an effective correlation dimension with the method of IAAFT surrogates to compare dynamical properties of brain activity from different recording regions and from different physiological and pathological brain states. The strongest indications of nonlinear deterministic dynamics were found during seizure activity.

In astrophysics, Gan *et al.* [10] tested solar radiation time series for nonlinearity using kurtosis of the residuals following analysis of deviations from the best linear approximation of the time series and IAAFT surrogates. They found that the 5-min, hourly and daily global solar radiation time series exhibit nonlinearity while the monthly time series does not. IAAFT surrogates have also been used in the study of self-similar processes [13].

#### 4.8. Iterative digitally filtered shuffled (IDFS) surrogates

The problem with FT and IAAFT surrogates is that they exactly preserve the power spectrum of the original signal by design. Therefore, the null hypothesis must be considered very carefully. If the particular statistic used is sensitive to variations in the power spectrum, then clearly any surrogate that does not allow for variations in the power spectrum is unsuitable, as the variance of the statistic would be much smaller for the surrogates than in true repetitions of the original measured process.

Iterative digitally filtered shuffled (IDFS) surrogates stand out as a possible improvement to IAAFT, due to the constraint that IAAFT surrogates preserve the spectrum of a single realization of the process exactly. This can lead to a very small spread of values of discriminating statistics. In reality we would expect some variation in the power spectra of repeated processes [62, 63]. AAFT surrogates naturally have some variation in their power spectrum, but this variation can be unpredictable, and thus cannot be considered as being equivalent to the variations that

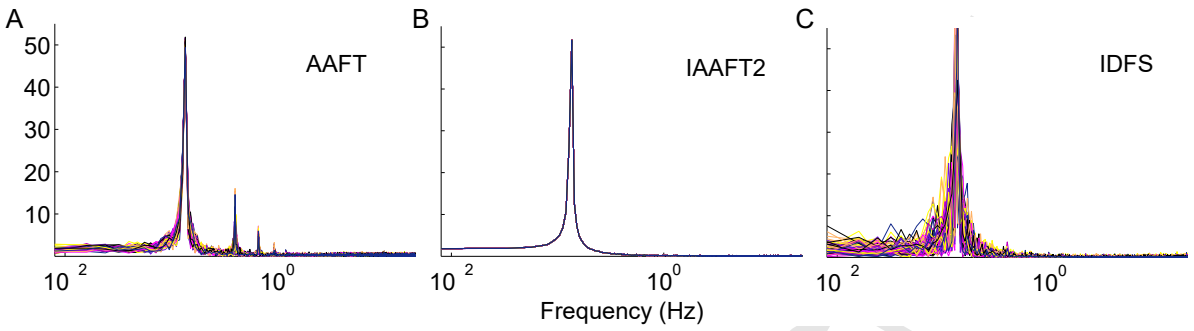


Figure 9: Comparison of the power spectra of 100 surrogates of different types for a 50 s noisy sinusoid  $\sin(2\pi t/3)$ , with sampling frequency 100 Hz. (A) AAFT surrogates show variations in the power spectrum, but also inaccuracies in the form of extra peaks. (B) IAAFT-2 surrogates by construction retain an identical power spectrum to the original signal, which results in no variations between surrogates. This may be undesirable in some applications. (C) IDFS surrogates result in variations in the power spectrum of the original signal, consistent with the null hypothesis of statistically independent realizations of a nonlinear static transformation of a linear stochastic process.

would be seen for independent realisations of the system. The IDFS method introduces a controlled variation into the power spectrum by creating each surrogate from statistically independent permutations of the original data filtered with a response function to maintain spectral properties. The power spectra of 100 AAFT, IAAFT and IDFS surrogates are compared in Figure 9.

*Null hypothesis.* The data are the result of a linear stochastic process, possibly influenced by a nonlinear measurement transformation.

*Algorithm.* The aim of IDFS is to produce surrogates with the same amplitude distribution as the original data but with a variance in the spectra of the surrogate population consistent with independent realisations of the underlying process.

1. Using overlapping windowed Fourier transforms (see Appendix A.5.1), estimate the power spectrum of the original time series  $x_n$  and find the average power spectrum  $S(f)$ .
2. Calculate the inverse Fourier transform of the square root of the power spectrum  $\sqrt{(S(f))}$  to give a response function  $R(f)$ .
3. Create a random permutation of the data  $x_n$  (i.e. a RP surrogate, see Section 3.1.2), denoted  $y_n$ .
4. Convolve the random permutation  $y_n$  with the response function  $R(f)$ . According to the convolution theorem,

$$g * h \Leftrightarrow G(f)H(f), \quad (5)$$

the Fourier transform of the convolution is equal to the product of the individual Fourier transforms [98]. Thus to calculate the convolution  $C_n$ , first calculate the Fourier transforms of  $R(f)$  and  $y_n$ , then calculate the inverse Fourier transform of their product.

5. Rescale  $C_n$  back to the original data distribution (in the same way as in the AAFT surrogate algorithm), to produce a signal  $z_n$  with the same distribution as the original time series  $x_n$  but a slightly different power spectrum.
6. To correct the power spectrum, Fourier transform  $z_n$ , replace Fourier amplitudes (but not phases) with those from the Fourier transform of  $C_n$  and inverse Fourier transform to obtain a signal with the same power spectrum as  $C_n$ .
7. Similar to the IAAFT procedure, iterate steps 5 & 6 until the power spectrum and distribution are as close as possible to those of  $C_n$  and  $x_n$ , respectively.

*Issues.* The rescaling in step 5 introduces a whitening of the spectrum, as also seen in AAFT surrogates. Therefore, these surrogates are iterated to bring the distribution closer to the correct values, similar to the procedure used in IAAFT surrogates. In the case of IDFS surrogates, the Fourier amplitudes should be repeatedly adjusted and rescaled. Note that, the Fourier amplitudes to adjust to are not those of the original data, but of the surrogate just before the first rescaling [62]. The IDFS algorithm has a computational cost and complexity similar to that of IAAFT surrogates.

1  
2  
3 *Applications.* The non-iterated version of these surrogates (DFS) were compared with IAAFT in [14] for the assessment of structural damage combined with the discriminating statistics of nonlinear prediction error (NPE),  
4 mutual information and bicoherence. Similar results were observed when comparing DFS, IAAFT-1 and IAAFT-2  
5 for NPE and bicoherence, but for mutual information all surrogates performed poorly, with IAAFT-1 being the  
6 most successful of the three [14].  
7

8 **4.9. Comparing FT based surrogates**

9 The first surrogates to be discussed, random permutation (RP), Fourier transform (FT) and amplitude adjusted  
10 Fourier transform (AAFT) are also known as algorithms 0, 1 and 2, respectively. There are many reviews that  
11 go into further detail, discussing and comparing these ‘traditional’ surrogate types [3, 99, 4, 100, 101, 45, 102].  
12 Generally, it is concluded that IAAFT are superior to AAFT for most applications [61, 103], due to the lack of  
13 conservation of the autocorrelation in the latter, but it should be emphasised that no surrogate method should be  
14 blindly applied without careful consideration of the system being studied and the assumed null hypothesis [85].  
15 Attention should also be paid to differences in methodology in these comparisons. When considering the various  
16 investigations have been done to compare AAFT and IAAFT, care must be taken in their interpretation. If IAAFT  
17 with exact distribution rather than exact spectrum were used, or the data were not preprocessed, this may lead to  
18 completely different results (see discussion in Section 4.3).  
19

20 There have been many other variations on FT surrogates than those discussed here. Statistically transformed  
21 autoregressive process (STAP) surrogates aim to tackle the problem of possible noninvertibility of the measurement  
22 function. They were first introduced by Kugiumtzis as corrected AAFT (CAAFT) surrogates in [104] and then  
23 generalized and renamed to STAP [100]. Comparisons with AAFT, IAAFT and STAP are presented in [105].  
24 The author concludes that STAP surrogates, being a typical realisation approach, have less power, i.e. may be  
25 more conservative, than the constrained realisation approaches of AAFT and IAAFT when not using a pivotal test  
26 statistic [105]. However, this difference in methods gets smaller as the time series length increases.  
27

28 **5. Surrogates for specific nonlinearity testing**

29 Fourier transform based surrogates are still the most widely used for the detection of nonlinearity in a time  
30 series. However, in cases in which their null hypotheses (i.e. nonlinearly scaled linearly filtered noise) can be easily  
31 rejected, we may wish to make the null hypothesis more specific. We can then begin to ask questions about the  
32 nature of these oscillations themselves, such as whether the individual cycles are correlated, i.e. whether there is  
33 any long term determinism, or whether there is any correlation between different frequency scales.  
34

35 **5.1. Wavelet iterative amplitude adjusted Fourier transform (WIAAFT) surrogates**

36 The wavelet transform is a time-frequency domain analysis method that is ideal for characterising systems which  
37 have time-varying properties. Wavelet surrogates rely on the use of the inverse wavelet transform following some  
38 manipulation of the wavelet transform coefficients.  
39

40 Most of the existing wavelet surrogates are based on the discrete wavelet transform (DWT). The DWT is  
41 a method which decomposes a signal into coefficients at different scales. The advantage of the DWT for this  
42 application is that the original signal can be reconstructed exactly from the resultant wavelet coefficients [106].  
43 However, the DWT usually downsamples the data by a factor of 2 for each scale, thus the maximum overlap  
44 discrete wavelet transform (MODWT) is used, which ensures that each scale is represented by the same number  
45 of coefficients. A comprehensive introduction to the discrete wavelet transform and the MODWT used in many of  
46 these techniques is provided in [107], and is accompanied by a MatLab toolbox.  
47

48 Breakspear *et al.* [108] introduced an alternative technique to randomizing phases in the Fourier domain to  
49 create surrogates, which exploits the fact that wavelets can better represent spatio-temporal patterns than Fourier  
50 modes. The technique is based on the resampling of wavelet coefficients, and exploits correlations between scales  
51 that exist within nonlinear data but which are absent or weak in stochastic data. The performance is comparable  
52 to phase randomisation in terms of the preservation of linear properties, removal of nonlinear structure, and,  
53 importantly, computational demands. Three different coefficient resampling techniques were considered: 1) shuffling  
54 of wavelet coefficients within each scale, 2) cyclic rotation of coefficients within each scale (time-shifting), and 3)  
55 block resampling of wavelet coefficients within each scale, in which blocks of coefficients are shuffled in time. The  
56 latter two were introduced in [108] for the first time, whilst the first was used in [109].  
57

58 However, Keylock [75] argues that the randomization of the coefficients on the time axis employed in the previous  
59 method [108] provides no clear advantage over IAAFT for univariate time series. This problem was addressed by  
60 applying the IAAFT to each level of MODWT coefficients, to ensure that their power spectrum and amplitude  
61

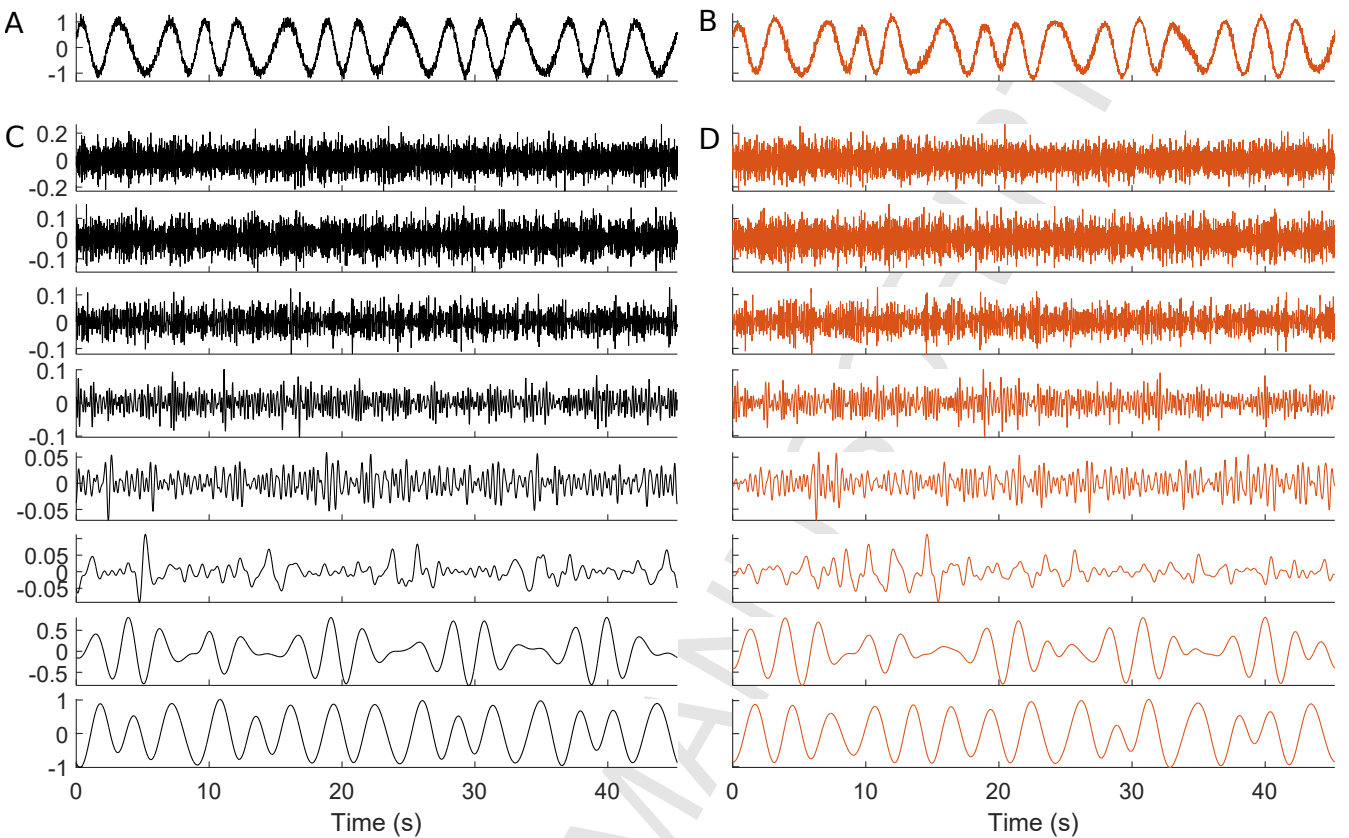


Figure 10: Calculation of a wavelet iterative amplitude adjusted Fourier transform (WIAAFT) surrogate using the method described in [75]. The first step is decomposition of the preprocessed time-varying noisy sinusoid  $\sin(2\pi(t + 0.5 \sin(2\pi t/10))/3)$  shown in (A) using the maximal overlap discrete wavelet transform (MODWT). The decomposed scales are shown in (C). An IAAFT surrogate is calculated for the coefficients at each scale, and then the surrogate or its mirror image is matched as closely as possible to the original coefficients. The resulting coefficients are shown in (D). Finally, the inverse wavelet transform is calculated on the new coefficients and the original scaling function (not shown), giving the WIAAFT surrogate shown in (B).

distribution are retained. This method was named the wavelet iterative amplitude adjusted Fourier transform (WIAAFT) method [75], and is described below.

*Null hypothesis.* The data were generated by a linear Gaussian stochastic process, possibly with a nonlinear measurement transformation. Stationarity is not assumed.

#### Algorithm.

1. Calculate the maximal overlap discrete wavelet transform (MODWT) of the time series  $x_n$ . This will separate  $x_n$  into multiple times series of coefficients (as shown in Figure 10(C)).
2. For each scale, calculate an IAAFT surrogate of the wavelet coefficients.
3. Take the IAAFT surrogate produced at each level, and compute its mirror image. Compare both the IAAFT surrogate and the mirror image with the original coefficients, and ascertain which version most closely matches the original coefficients using a least squares algorithm. The most closely matching time series becomes the surrogate coefficients for the current scale. An example of the resulting surrogate coefficients is shown in Figure 10(D).
4. Calculate the inverse MODWT of the matched surrogate coefficients. This will reconstruct a surrogate time series (see Figure 10) from the new coefficients.
5. Repeat steps 2–4 for each surrogate required.

Once the inverse MODWT is calculated from these surrogate coefficients, a signal is produced that ‘looks like’ the original data in terms of its temporal evolution. However, like other surrogate methods, this process alters the distribution of the values in the resulting time series when compared to the original data. Thus, an amplitude adjustment step, identical to that used in AAFT surrogates, is required. In turn, this then degrades the power

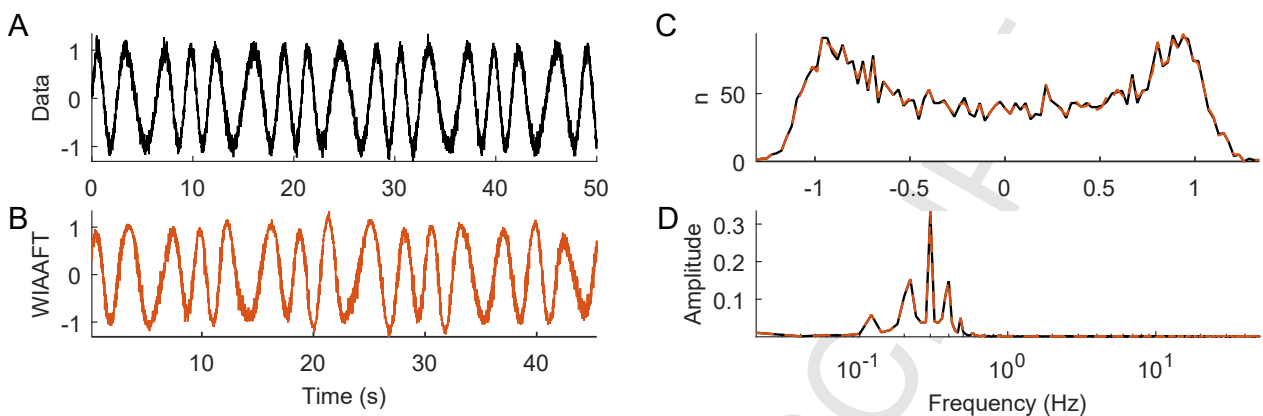


Figure 11: (A) 50 s noisy sinusoid with time-varying period  $\sin(2\pi(t+0.5 \sin(2\pi t/10))/3)$ , with sampling frequency 100 Hz, preprocessed as discussed in Section 4.3. (B) Example wavelet iterative amplitude adjusted Fourier transform (WIAAFT) surrogate calculated from the signal in (A). The amplitude distribution (C) is preserved. The power spectrum (D) is perfectly preserved. In all panels, black lines represent the original signal and orange lines represent the surrogate.

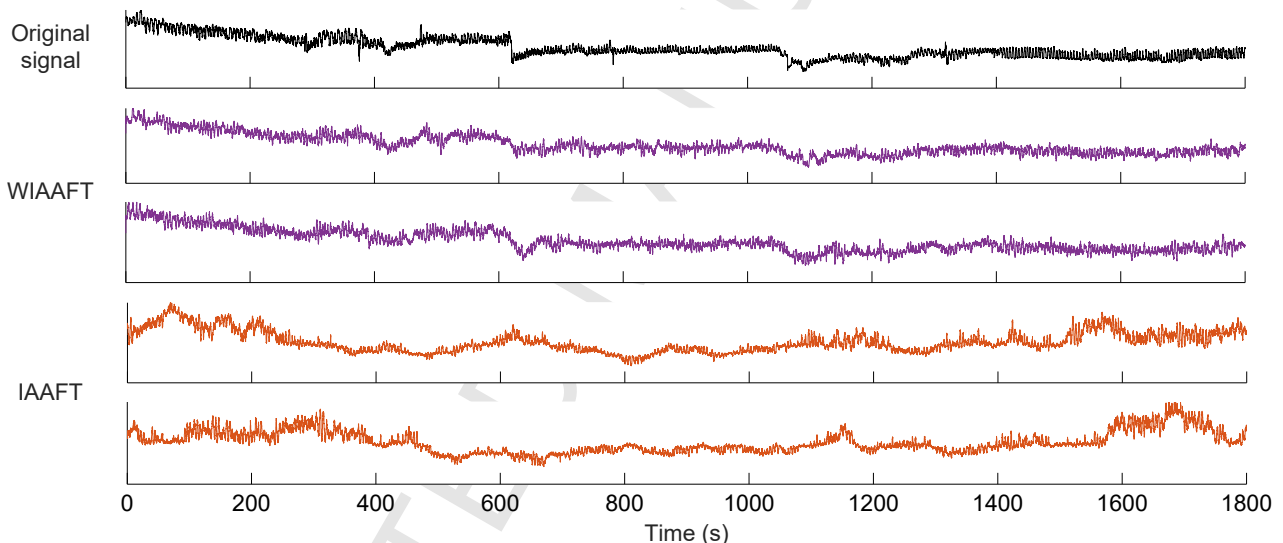


Figure 12: Comparison between surrogates generated from a respiration signal using the WIAAFT and IAAFT methods. WIAAFT surrogates maintain the shape of the original data whilst the IAAFT surrogates do not.

spectrum, and thus the final iterative part of the IAAFT algorithm is applied to recover the correct values. An example WIAAFT surrogate is shown in Figure 11. WIAAFT surrogates are compared to IAAFT surrogates in Figure 12.

**Issues.** For long data sets, the WIAAFT algorithm is much more computationally expensive than Breakspear’s shuffling technique, and also than IAAFT alone, as it has to be performed multiple times per surrogate. The most computationally intensive step is the matching of the surrogate coefficients to the original data in step 3. However, WIAAFT surrogates do provide an advantage in any application in which the nonstationarity in the data is required to be preserved, while the nonlinear aspects of the signal are randomized. In an extension to this work [75], Keylock introduced further constraints into the WIAAFT method [76], providing further discussion about difficulties with the IAAFT method when dealing with pseudo-periodic data, and the nonstationarity that is introduced, as discussed in [19]. Keylock suggests that pseudo-periodic surrogates (PPS) (see Section 5.4) are not fully constrained, and introduces Pinned Wavelet Iterative Amplitude Adjusted Fourier Transform (PWIAAFT) surrogates to address this [76]. Rather than using the optimal matching procedure in [75], this method introduces a threshold for the wavelet coefficients, above which they are “pinned” in place during the generation of the surrogate data. This results in the surrogates being approximately aligned with the data, and should significantly reduce computation time. Using this method reduces the number of possible surrogate realisations, to a degree which depends on the threshold, the choice of which is discussed in [76]. In the examples presented in this paper, we use WIAAFT surrogates rather

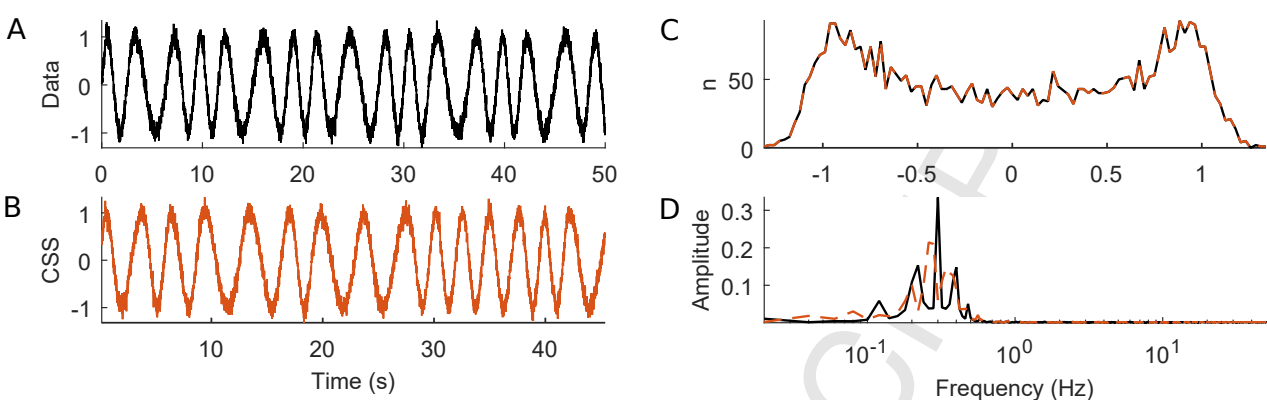


Figure 13: (A) 50 s noisy sinusoid with time-varying period  $\sin(2\pi(t+0.5\sin(2\pi t/10))/3)$ , with sampling frequency 100 Hz, preprocessed as discussed in Section 4.3. (B) Example cycle shuffled surrogate (CSS) calculated from the signal in (A). The amplitude distribution (C) is perfectly preserved. The power spectrum (D) is not preserved due to slight mismatch between the beginning and end of shuffled cycles. In all panels, black lines represent the original signal and orange lines represent the surrogate.

than PWIAAFT to avoid the issues introduced by the choice of this threshold.

*Applications.* WIAAFT can be used to test hypotheses which cannot be addressed with standard IAAFT. The example given in [75] is the changing Hurst exponent of fractional Brownian motion, and it is suggested to be useful in any application in which one is concerned with changes in the properties of a signal through time. These methods also form the basis of the gradual wavelet reconstruction (GWR) technique, also introduced by Keylock [110, 111], which allows systematic generation of surrogates with an increasing proportion of the properties of the original signal.

*Other wavelet surrogates.* Gur *et al.* [112] recently introduced a wavelet based surrogate generation method comprising wavelet transforms and sampling statistically equivalent realisations, and applied it to the simulation of chemical reactions. Wavelet surrogates based on the continuous wavelet transform have also been used to test for stationarity in data [77]. The use of the CWT is possible in this case because inverse transformation is not required [106]. The performance of wavelet surrogates in the identification of coupling in wavelet bispectrum analysis is investigated in Section 9.3.3.

### 5.2. Multifractal surrogates

The discrete wavelet transform has also been used as the basis of multifractal surrogates, which aim to enable testing of nonlinear interdependence within, with, between or among time series obtained from multifractal processes [113]. Multifractal surrogates preserve the multifractal properties of input data, i.e. interactions among scales and nonlinear dependence structures [113]. This approach was developed further by Keylock [114] and named iterated amplitude adjusted wavelet transform (IAAWT) surrogates. IAAWT surrogates are designed to preserve both, the multifractal characteristics of the time series and also the distribution of values in the time series using the iterative approach used in IAAFT surrogates. Multifractal surrogates have been used to test cross-scale interactions in atmospheric dynamics [115].

### 5.3. Cycle shuffled surrogates (CSS)

Since the introduction of surrogate data testing, surrogates have been used in many studies to test conclusions on the presence of chaos. Theiler [65] introduced cycle shuffled surrogates as a means to guide the judgement required in the search of chaos. Unlike many previously discussed surrogates, this is not a test for nonlinearity in the time series, so this should be established beforehand if unknown.

*Null hypothesis.* The signal is generated by a periodic oscillator with no dynamical correlation between cycles, i.e. the evolution of cycles is not deterministic.

#### Algorithm.

1. Use regular peaks or troughs in the data to separate each cycle in the time series.
2. Create a new time series by randomly shuffling these data segments.

Example cycle shuffled surrogates are shown in Figures 13 & 14.

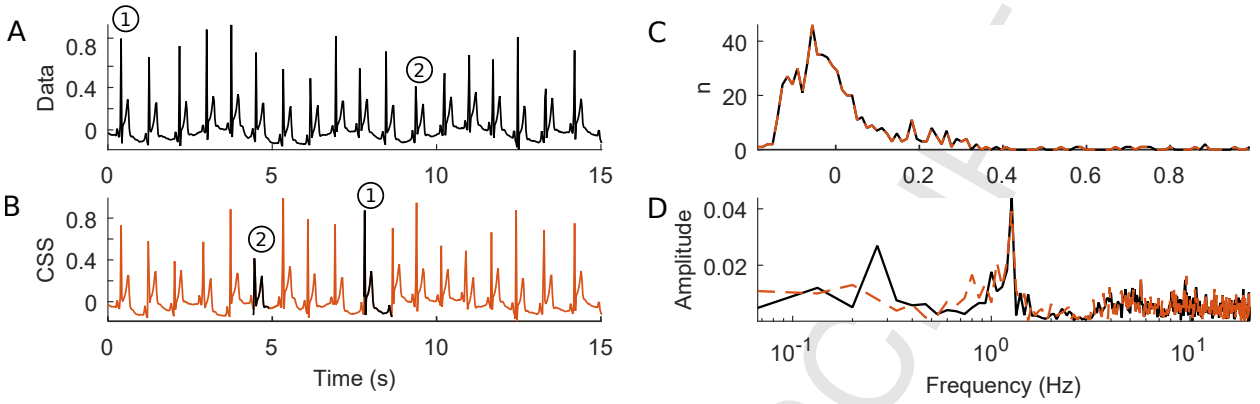


Figure 14: (A) 15 second portion of an ECG signal, with sampling frequency 40 Hz. (B) Example cycle shuffled surrogate (CSS) calculated from the signal in (A). As an example, two individual cycles are numbered in the original signal, and their eventual location in the surrogate shown in (B). In all cases, black lines are from the original data and orange lines are from the surrogate.

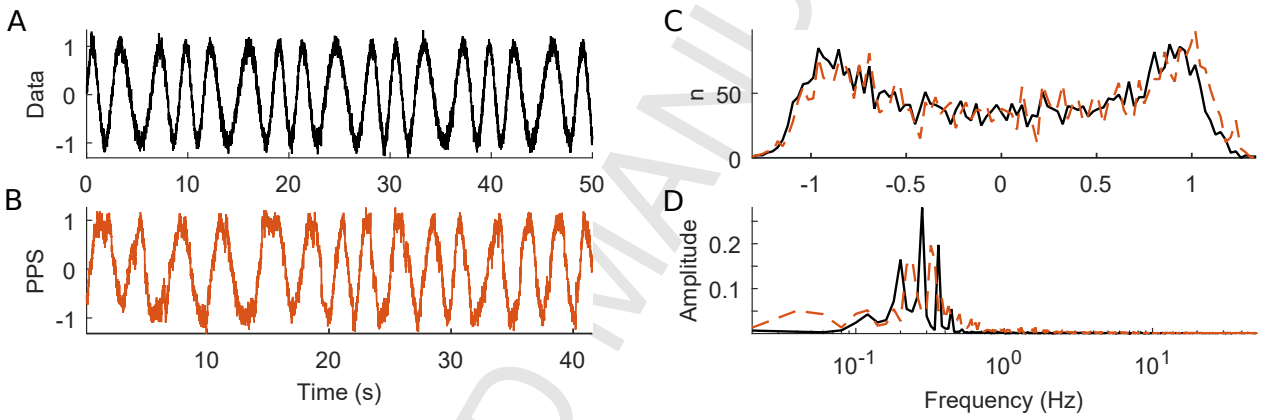


Figure 15: (A) 50 s noisy sinusoid with time-varying period  $\sin(2\pi(t+0.5\sin(2\pi t/10))/3)$ , with sampling frequency 100 Hz, preprocessed as discussed in Section 4.3. (B) Example pseudo-periodic surrogate (PPS) calculated from the signal in (A). The amplitude distribution (C) is not conserved. The power spectrum (D) is also not preserved. In all panels, black lines represent the original signal and orange lines represent the surrogate.

**Issues.** The cycle-shuffled method has the disadvantage that if the peaks and troughs of each cycle do not always occur at the same amplitude, aligning them vertically may introduce nonstationarity and jumps into the surrogate data which are not present in the original data [43], therefore increasing the risk of incorrectly rejecting the null hypothesis. The algorithm also requires that the individual cycles of oscillation can clearly be distinguished, for example with clear, regular events such as an R-peak in an ECG (see Figure 14), or the firing of a neuron in a membrane potential recording.

**Applications.** Theiler [65] introduced and applied this method to a nearly periodic EEG time series recorded from a patient undergoing an epileptic seizure. Although it had previously been reported to be chaotic [116], the author was not able to draw the same conclusion when using these surrogates coupled with the calculation of the Lyapunov exponents and correlation dimension [65]. Ivanov *et al.* [117] found a loss of multifractality in heartbeat dynamics with congestive heart failure using cycle shuffled surrogates. Also applying CSS to cardiac dynamics, Musizza *et al.* [23] investigated interactions between cardiac, respiratory and EEG oscillations in rats. CSS were also used to analyse X-ray light curves, where evidence of chaos could not be concluded using these methods [11].

#### 5.4. Pseudo-periodic surrogates (PPS)

Introduced by Small *et al.* in [5], and further developed in [19], pseudo-periodic surrogates (PPS) test the null hypothesis that the system dynamics can be reduced to a periodic orbit with uncorrelated noise, or in other words that there is no determinism other than the periodic behaviour in the observed data. PPS combined with the correlation dimension were shown to be able to distinguish between chaotic and periodic behaviour in the Rössler system [5]. The surrogates can also distinguish between periodic systems driven by white and coloured noise [5].

1  
2  
3 demonstrating that the null hypothesis includes only *uncorrelated noise* in the intercycle dynamics. If coloured  
4 noise is to be part of the null hypothesis, the updated algorithm discussed in [69] should be used.  
5

6 *Null hypothesis.* Data are a realization of a periodic orbit with uncorrelated noise, i.e. no determinism is present in  
7 the system other than the periodic behaviour.  
8

9 *Algorithm.* The basic idea of PPS is the addition of uncorrelated noise into the system in the form of small random  
10 shifts to nearby points in the phase space to investigate how this affects the dynamics. If there is a stable periodic  
11 cycle, all points will still approach it, and the observed dynamics will remain almost unchanged. However, if the  
12 dynamics is more complicated, for example in a chaotic system, then the dynamics will change, but the shape of  
13 the signal will be preserved, providing an advantage over cycle-shuffled surrogates.  
14

- 15 1. Reconstruct the original time series  $\vec{x}$  in phase space, using time delay embedding (see Appendix A.6).
- 16 2. Find the index  $q$  of the first nearest neighbour from the first half of the embedded signal to its last value  
 $\vec{x}_L : \|\vec{x}_q - \vec{x}_L\| = \min, q \in [1, L/2]$ . This applies periodic boundary conditions to avoid cycling near the last  
value, for example when the nearest value to the last value is the previous one and the noise level is small.
- 17 3. Choose the noise level, which is the free parameter  $\rho$ .
- 18 4. As the first value of the generated surrogate, choose  $\vec{x}_i$  for random  $i$ , equivalent to a random time shift.
- 19 5. Add an  $m$ -dimensional vector of random Gaussian noise with variance  $\rho$  to the current surrogate value to  
produce perturbed values.
- 20 6. Find the location  $j$  of the nearest point of the original phase space trajectory to the perturbed value. If  $j$  is  
the last index, i.e.  $j = L$  set  $j = q$ .
- 21 7. Set the next surrogate point as  $\vec{x}_{j+1}$ .
- 22 8. Repeat steps 4-6 to generate a surrogate of the desired length, and choose its first component as the scalar  
surrogate signal. To generate multiple surrogates, repeat only steps 4-8.

23 An example PPS surrogate is shown in Figure 15.  
24  
25

26 *Parameters.* PPS requires an estimation of the embedding dimension [118]. It also requires selection of the free  
27 parameter  $\rho$ . No general formula has been proposed for this noise level. When  $\rho \rightarrow 0$  the surrogates will recover the  
28 original signal, whereas if  $\rho$  is very large, then the surrogates will resemble random permutation surrogates. It was  
29 suggested by Small *et al.* [5] that the optimal  $\rho$  should maximise the expected number of short segments (of length  
30 2) that are the same for the original time series and the surrogate. However, this approach is computationally  
31 expensive. Here, we propose that the choice of the noise level  $\rho$  be based on the average distance between nearest  
32 neighbours in the reconstructed phase space:  
33

$$\rho = 0.7 < \min_j \|\vec{x}_i - \vec{x}_j\| >, \quad (6)$$

34 where  $< \dots >$  denotes averaging over  $i$ . While this choice depends on distribution, it will usually establish a large  
35 number of short segments and many jumps at the same time, since the probability of white noise with variance  
36  $\rho$  to outreach  $0.7\rho$  is  $\approx 52\%$ . Note that this applies for maximum distance choice, and thus stays valid for any  
37 embedding dimension.  
38

39 *Issues.* PPS are sensitive to the addition of observational noise, and can even amplify it, so care must be taken in  
40 very noisy systems. Unlike the similar surrogates suggested by Small and Judd [119], PPS have a more intuitive  
41 method for the specification of the noise parameter. The computational cost of PPS is very high.  
42

43 The PPS algorithm in [5, 19] works well even with very large amounts of dynamical noise, but may incorrectly  
44 reject the null hypothesis if the intercycles of the pseudo-periodic orbit have a linear stochastic dependence induced  
45 by *coloured* additive observational noise. The updated algorithms introduced in [69, 120] for pseudo-periodic  
46 surrogates also allow the rejection of the coloured noise case, without the requirement for embedding. This null  
47 hypothesis covers a wider scope and its rejection would mean that the time series was even more likely to be chaotic.  
48 However, some problems with Luo's method have been highlighted by Shiro *et al.* [121], who introduced the idea of  
49 using Poincaré sections combined with random shuffle surrogates to search for chaos. More recently, neural networks  
50 have been used to increase the accuracy of the distinction between pseudoperiodic and chaotic time series [122].  
51 These multiple approaches to the problem of identifying chaos in data demonstrate that it is not a trivial task,  
52 especially in the presence of noise. While introducing twin surrogates (see below) Thiel *et al.* [123] state that PPS  
53 are not appropriate to test for phase synchronization because they are not capable of mimicking chaotic oscillators.  
54 Keylock discusses the similarities of this approach with the work of Moeckel & Murray [124, 125].  
55  
56

1  
2  
3 Applications. Small & Tse [19] combined PPS and AAFT surrogates in the analysis of financial data sets and found  
4 that the AAFT surrogates were clearly rejected, yet the PPS surrogates were not, suggesting that the financial data  
5 exhibits short term nonlinear deterministic dynamics, but no long term determinism. Luo *et al.* [69] applied a  
6 modified PPS surrogate algorithm to an ECG recording and found no evidence that it was chaotic.  
7  
8

## 9 6. Discriminating statistics for nonlinearity testing

10 The surrogates discussed above are usually used in combination with one or more discriminating statistics. Many  
11 statistics have been proposed for the detection of nonlinearity. Here we review the most widely used. A variety  
12 of discriminating statistics are also reviewed in [126] and software for their calculation is provided by the authors.  
13 Some of the following statistics and surrogates for nonlinearity testing require time-delay embedding (see Appendix  
14 A.6), which attempts to recover the true multi-dimensional dynamics of the underlying system from a univariate  
15 time series.  
16

### 17 6.1. Correlation dimension

18 Since its introduction by Grassberger and Procaccia in 1983 [40], the correlation dimension,  $\nu$ , has become  
19 very popular since, among other uses, it provides the possibility of distinguishing between deterministic behaviour  
20 such as chaos, and random behaviour. The correlation dimension aims to measure the actual dimension of fractal  
21 objects. In the original paper the correlation dimension of different objects is compared to other measures of fractal  
22 dimension and demonstrated to be closely related [40]. Calculation of the correlation dimension requires embedding  
23 (see Appendix A.6) and is based on the correlation integral  
24

$$25 \quad C(\epsilon, L) = \frac{1}{L(L-1)} \sum_{i,j,i \neq j} H(\epsilon - r_{ij}), \quad (7)$$

26 where  $r_{ij} = \|\vec{x}_i - \vec{x}_j\|$  is the maximum (recommended) or Euclidian distance between  $\vec{x}_{i,j}$ ,  $\vec{x}_i$  is the embedded  
27 signal, and  $L$  is the length of the embedded signal. The correlation integral is in fact the fraction of intervector  
28 distances less than  $\epsilon$ , and ranges from 0 to 1. The correlation dimension  $\nu$  is then given as  
29

$$30 \quad \nu = \lim_{\epsilon \rightarrow 0} \lim_{L \rightarrow \infty} \frac{\log C(\epsilon, L)}{\log \epsilon}. \quad (8)$$

31 It is clear that in real situations and computations we are not able to take such limits. Usually the graph of  
32  $\log C(\epsilon, L)$  vs.  $\log \epsilon$  is constructed, regular linear areas are identified and from them the correlation dimension is  
33 calculated. However, the graph needs to be plotted and analysed each time, which can be inconvenient. Thus, the  
34 most popular estimation of correlation dimension is given by the so-called Taken's best estimate [127, 128]:  
35

$$36 \quad \nu \approx \frac{C(\epsilon_{max}, L)}{\int_0^{\epsilon_{max}} (C(\epsilon, L)/\epsilon) d\epsilon}, \quad (9)$$

37 where  $\epsilon_{max}$  is some upper cutoff on  $\epsilon$  in (7), which should be neither too large nor too small. Alternatively, Taken's  
38 best estimate (9) [127, 129] can be rewritten in the form  
39

$$40 \quad \nu \approx -1/\eta, \quad \eta \equiv \langle \log(r_{ij}/\epsilon_{max}) \rangle_{r_{ij} < \epsilon_{max}} = \frac{1}{N_{r_{ij} < \epsilon_{max}}} \sum_{i,j,i>j:r_{ij} < \epsilon_{max}} \log(r_{ij}/\epsilon_{max}), \quad (10)$$

41 which is more convenient for numerical implementation. In (10) the sum is taken over all unique pairs  $i, j$  for which  
42  $\|\vec{x}_i - \vec{x}_j\| < \epsilon_{max}$ , and  $N_{r_{ij} < \epsilon_{max}}$  is the number of such pairs.  
43

44 One can of course try to simply find  $\nu$  as the average slope of  $\log C(\epsilon, L)$  over  $\log \epsilon$ , but we found this estimation  
45 to be much more unstable than (9) and (10), especially when the embedding dimension is not known and needs to  
46 be estimated, for example by the false nearest neighbors method. Direct use of the correlation integral  $C(\epsilon, L)$  has  
47 also been suggested as a discriminating statistic [3].

48 In the course of our investigations, we found that in general, the use of the maximum distance in (7) appears  
49 superior to the use of Euclidian distance. However, we have not found any better choice of  $\epsilon$  than 1/4 of the root  
50 mean square of the signal, as originally used in [3]. This choice performs well even when the embedding dimension is  
51 highly overestimated. However, the performance of such choice is still not perfect in many cases, and the correlation  
52 dimension is quite often underestimated and sometimes overestimated. Thus, in all further investigations, we use  
53

maximum distance in (7) and  $\epsilon = \sigma/4$  in (9), where  $\sigma$  is the root mean square of the signal (before embedding or first component after embedding)  $\sigma = \sqrt{\frac{1}{N} \sum_i s_n^2}$ .

There are some possible modifications to the calculation of the correlation integral (7) and, subsequently, the correlation dimension, as discussed in [42]. However, their effect is considerable only for small data lengths. If calculated straightforwardly, i.e. by calculating distances between each pair of points, the computational cost of estimating the correlation dimension is  $O(N^2)$ , but there are alternative algorithms which make this faster. We employed the modification of the algorithm suggested in [129] with computational cost usually between  $O(N \log N)$  and  $O(N^{3/2})$ . Examples of the use of the correlation dimension and different surrogate types to demonstrate nonlinearity in time series can be found in Section 9.1.1.

### 6.2. Nonlinear prediction error

Nonlinear prediction error characterizes the predictability of the system based on its reconstructed phase space trajectory. Deterministic systems should be much more predictable (lower prediction error) than stochastic ones. The most popular prediction error is of the form [4, 130]:

$$\gamma(\epsilon) = \left( \frac{1}{N - (d-1)\tau - 1} \sum_{n=1}^{N-(d-1)\tau-1} [s_{n+1} - F(\vec{x}_n, \epsilon)]^2 \right)^{1/2}, \quad (11)$$

where  $s_n$  are values of the scalar time series,  $\vec{x}_n = \{s_n, s_{n+\tau}, \dots, s_{n+(d-1)\tau}\}$  is its phase space embedding, while  $d$  and  $\tau$  are embedding dimension and time-delay, respectively. Nonlinear predictor  $F(\vec{x}_n, \epsilon)$  tries to predict the next value  $s_{n+1}$  (in fact first component of  $\vec{x}_{n+1}$ ) based on the previous point in the phase space  $\vec{x}_n$ . It is given by averaging over the future values of all neighboring delay vectors closer than  $\epsilon$  in  $d$  dimensions:

$$F(\vec{x}_n, \epsilon) = \frac{1}{N_\epsilon} \sum_{i=1}^{N_\epsilon} s_{n+1}^{(i,\epsilon)}, \quad (12)$$

where  $s_n^{(i,\epsilon)}$  denote first component of  $i$ th nearest neighbor  $\vec{x}_{n+1}^{(i,\epsilon)}$  to  $\vec{x}_n$  (including itself) in terms of  $\epsilon$ :  $\|\vec{x}_n - \vec{x}_{n+1}^{(i,\epsilon)}\| < \epsilon$ , and  $N_\epsilon$  is the number of such neighbors.

There are also other choices of both the form of the prediction error (11) and the nonlinear predictor (12). They include prediction over a few time steps, and prediction based both on the past and future values etc. However, the form (11,12) is the most popular.

### 6.3. Volterra polynomials

Barahona & Poon [131] first proposed the use of Volterra polynomials for the detection of nonlinearity. This approach was then successfully used to investigate the performance of different surrogate types, revealing some important issues with AAFT and IAAFT [87]. Volterra polynomials  $p_n^{(m)}(x_i, x_{i-2}, \dots, x_{i-(m-1)})$  of degree  $D$  and memory  $m$  have number of terms  $n = (m+D)!/(m!D!)$  and the form:

$$p_n^{(m)}(x_i, x_{i-1}, \dots, x_{i-(m-1)}) = a_0 + a_1 x_i + a_2 x_{i-1} + \dots + a_m x_{i-(m-1)} + a_{m+1} x_i^2 + a_{m+2} x_i x_{i-1} + \dots + a_{n-1} x_{i-(m-1)}^D. \quad (13)$$

One can fit a polynomial to the data, expressing  $x_{i+1} = p_n^{(m)}(x_i, x_{i-2}, \dots, x_{i-(m-1)})$  and choosing coefficients  $a_k$  to minimize mean squared error  $\sum_{i=m}^N (x_{i+1} - p_n^{(m)}(x_i, x_{i-2}, \dots, x_{i-(m-1)}))^2$ . Nonlinear systems should be better fitted by nonlinear polynomials, while for linear systems there are only the linear terms in (13). Thus, one can fit a signal and its surrogates to polynomials (13) and observe how the goodness of fit increases for the signal and its surrogates with the appearance of nonlinear terms in the fitting polynomials. Goodness of fit  $K_n^{(m)}$  can be calculated as

$$K[p_n^{(m)}] = 1 - \frac{\sum_{i=m}^N (x_{i+1} - p_n^{(m)}(x_i, x_{i-2}, \dots, x_{i-(m-1)}))^2}{\sum_{i=m+1}^N (x_i - \bar{x})^2}, \quad (14)$$

where  $\bar{x} = \sum_{i=m+1}^N x_{i+1}$  is the mean value of the signal. Since the standard deviation of the signal  $\sum_{i=m+1}^N (x_i - \bar{x})^2$  represents the worst possible fit, goodness of fit  $K_n^{(m)}$  ranges from zero to unity.

If with the addition of nonlinear terms the goodness of fit for the signal increases considerably more than for the surrogates, this indicates nonlinearity.

Ideally, one would have discriminating statistics as single numbers. Thus, the difference of the goodness of fit with linear and nonlinear polynomials  $f_{\text{linear}}(x_i, \dots, x_{i-9}) = a_0 + a_1 x_i + a_2 x_{i-1} + \dots + a_{10} x_{i-9}$  and  $f_{\text{nonlinear}}(x_i, \dots, x_{i-9}) = f_{\text{linear}}(x_i, \dots, x_{i-9}) + a_{11} x_i^2 + a_{12} x_i x_{i-1} + a_{13} x_i^3$  can be used. Although usually it is enough to observe increase in goodness of fit with addition of first nonlinear term (e.g.  $x_i^2$ ), this is not always the case (see e.g. Fig.7 in [87]).

For nonlinear signals,

$$\rho = K[p_m^{(m+k)}] - K[p_m^m] \quad (15)$$

has to be larger than for linear signals (e.g. surrogates), so it should be used as a one sided test. It is simple and fast, does not require embedding and yields good results (especially for discrete signals). There may be some nonlinear signals for which goodness of fit will considerably increase only with addition of more higher terms, but they are extremely rare. One should be very careful when applying this technique for continuous systems, since goodness of fit greatly increases for such systems with addition of linear terms even when the system is highly nonlinear. Care should be taken in the implementation of this technique, as the results also vary with sampling frequency. Section 9.1.2 presents an example of the use of Volterra polynomials and various surrogate types to search for nonlinearity in data.

#### 6.4. Time-irreversibility

The measure

$$\alpha = \frac{1}{N} \sum (s_{n+1} - s_n)^3 \quad (16)$$

is called time-irreversibility and, as suggested by its name, characterizes invariance of the signal with respect to inversion of time. It is a very powerful statistic, as was shown in [130], while also being computationally very cheap and does not require embedding. As all linear systems are time-reversible, time-irreversibility indicates nonlinearity. It can achieve both positive and negative values, while for time-reversible signals it should be near zero. Thus, contrary to the previous statistics, it is used as a two-sided test: the surrogate test rejects the null hypothesis if either (16) for the original signal is higher or lower than for its surrogates.

It should be emphasized that time-irreversibility is a sufficient condition for nonlinearity, but not necessary. Thus, many nonlinear systems are time-invariant, and in this quite large extent of cases time-irreversibility (16) used as discriminative statistic has zero power. For example, with this statistic one is not able to distinguish nonlinearity in the Lorenz system [130]. Thus, any conclusions should be made only if the null hypothesis of time-reversibility is rejected and nonlinearity is indicated, while otherwise it just indicates that the system is possibly time reversible.

Time-irreversibility, also known as temporal asymmetry, was used in [22] to demonstrate the presence of temporal asymmetry in EEG data.

#### 6.5. Monte Carlo singular spectrum analysis (MCSSA)

Allen & Smith [8] introduced a statistical test which combines singular spectrum analysis (SSA) with surrogate data testing in order to test for oscillations against an arbitrary ‘coloured noise’ hypothesis, but largely focused on noise which can be described by an autoregressive (AR) model. This method, known as Monte Carlo SSA (MCSSA), tests for the presence of modulated oscillations against an arbitrary null hypothesis [8]. To date, the technique has largely been applied to first order autoregressive (AR(1)) noise [8, 132], in particular to climate data with red noise backgrounds, but the generalization to higher order AR and moving average (MA) processes is straightforward [8]. Paluš and Novotná [133] extended the method to test the dynamical properties of significant modes and demonstrated significant oscillations in historical European temperature records [132]. Vejmelka *et al.* [134, 135] further extended this approach to higher orders using the chaotic nonlinear Lorenz system with additive 5<sup>th</sup> order autoregressive noise, and found evidence of nonlinear oscillations only in the specific frequency band where the Lorenz oscillations manifested. The same authors also applied this method to EEG data and found nonlinearity during sleep stage 2, in which spindle-like oscillatory phenomena in the sigma band (11 - 17 Hz) are observed [134, 135].

Here we consider the first order autoregressive (AR(1)) model (assuming  $c = 0$ ),

$$x_t = \rho x_{t-i} + \sigma \varepsilon_t. \quad (17)$$

MCSSA is implemented as follows:

1. Decide on the null hypothesis, i.e. which noise model is to be tested against (as discussed in Section 4.4).

- 1  
2  
3 2. Embed the time series [136, 127] using a window of length  $L$ , to obtain a set of vectors which are delayed  
4 versions of the original time series  $(x_1, \dots, x_N)$  of length  $N$ ,

$$\mathbf{X} = \begin{bmatrix} x_1 & \cdots & x_L \\ x_2 & \cdots & x_{L+1} \\ \vdots & & \vdots \\ x_K & \cdots & x_T \end{bmatrix}$$

11 where  $K = N - L + 1$ .

- 12 3. Calculate the time lag-covariance of the time series,

$$\mathbf{C} \equiv \eta \mathbf{X}^T \mathbf{X} \quad \eta = 1/K. \quad (18)$$

- 16 4. Diagonalise  $\mathbf{C}$ :

$$\mathbf{\Lambda} = \mathbf{E}^T \mathbf{C} \mathbf{E}, \quad (19)$$

19 where  $\mathbf{\Lambda}$  is the diagonal matrix and the columns of  $\mathbf{E}$  correspond to consecutive eigenvectors  $(e_1, e_2, \dots, e_L)$ .

- 20 5. Sort eigenvalues  $\mathbf{\Lambda}$  into decreasing order and thus obtain the eigenspectrum.

- 21 6. Apply the same procedure to surrogate data, using the eigenvectors from the original data, and compare  
22 the eigenspectra for the time series and the distribution of surrogates. Oscillations will be represented as an  
23 almost equal pair of eigenvalues above the surrogate threshold, which will also have almost equal associated  
24 frequencies, as determined from the power spectrum of the eigenvectors.

26 The method used here to decompose a single time series into a matrix and obtain its eigenvalues and eigenvectors  
27 is known as Karhunen-Loèv expansion or principle value decomposition [137, 138, 29], discussed in [139], and has  
28 some parameters which need to be chosen: the time delay and the embedding dimension. Time delay embedding,  
29 and the choice of these parameters, is discussed in Appendix A.6.

30 If evidence of oscillations is found in the time series based on the discovery of significant eigenvectors, they can  
31 be reconstructed using diagonal averaging of these eigenvectors.

33 The length of the signal will affect the results obtained using MCSSA. The longer the signal, the less fluctuations  
34 in the autocorrelation, and the smaller the width of the distribution of eigenvalues, ultimately leading to more precise  
35 results. It should be noted that this method assumes that the oscillations are stationary, so too much time-variation  
36 may lead to an artificially large number of modes being required to reconstruct the time series.

37 In Section 9.1.3, we test the performance of MCSSA on data containing simulated oscillations with additive  
38 autoregressive noise and real experimental EEG data.

#### 40 6.6. Lyapunov exponents

41 Lyapunov exponents quantify the rate of separation of infinitesimally close trajectories. The largest Lyapunov  
42 exponent is a very useful quantity to calculate, since if it is positive it indicates not simply nonlinearity, but chaos  
43 [140, 141, 142]. However, there is also the issue that the other Lyapunov exponents are only meaningful if there is  
44 a positive exponent, and if chaos is not present in the system, there is a greater amount of statistical error in the  
45 calculation as the difference between the trajectories in phase space is relatively small. Apart from difficulties in its  
46 estimation when the equations of motion are unknown, which is usually the case in reality, its accurate calculation  
47 may also be difficult in the presence of noise [3].

#### 49 6.7. Mutual information

51 Multidimensional mutual information (or redundancies) of time series and their delayed versions has been used  
52 to identify nonlinearity in data, in combination with surrogates [143, 44]. The authors showed that the functional of  
53 the series probability distribution densities can reflect nonlinearities in the data, whilst the series covariance matrix  
54 is sensitive to linear relationships only [143]. This approach has also been extended to multivariate time series [144].  
55 Mutual information can also be used to test for coupling, see Section 8.5.

#### 57 6.8. Identifying nonlinear oscillators by harmonic extraction

59 Many oscillations arising from real systems are not strictly periodic, and may contain many linear and nonlinear  
60 components. Nonlinearities often manifest as higher harmonics within a signal, and investigation into the properties  
61 of these harmonics can provide valuable information about the underlying dynamics of the system. However, the  
62 identification and separation of these components can be difficult. Combining mutual information, surrogate testing,  
63

1  
2  
3 and the wavelet transform, Sheppard *et al.* extracted multiple harmonics from human skin blood flow data and  
4 reconstructed the nonlinear oscillations [145]. More recently, a method known as nonlinear mode decomposition  
5 has been developed, which also utilises surrogate testing and time-frequency analysis to extract and reconstruct  
6 time-varying nonlinear modes from time series [21].  
7

#### 8 6.9. Other statistics

9 Using the discussed methods to estimate background noise, the significance of regions of interest in the wavelet  
10 transform can also be found using Monte Carlo methods. This can be quite computationally expensive, with the  
11 wavelet transform of all surrogate realizations required to be in memory at once in order to calculate significance  
12 levels. An alternative would be to calculate the mean and second moments for each wavelet coefficient, which can  
13 be quickly updated and discarded once a new wavelet transform is calculated, and apply a Gaussian approximation,  
14 which would be less accurate, but more memory efficient. Grinsted *et al.* [12] applied the cross wavelet transform  
15 and wavelet coherence to the analysis of geophysical time series. Monte Carlo methods were used to assess the  
16 statistical significance against red noise backgrounds using surrogate data set pairs with the same AR(1) coefficients  
17 as the original data, and their wavelet coherence calculated. A similar approach is also used in [146] to confirm  
18 associations in ecological time series.  
19

20 Many other discriminating statistics are available for the investigation of nonlinearity. However, they are not as  
21 popular as those discussed above. Some other statistics, for example higher order autocovariance, were also shown  
22 to be less useful than those discussed [4]. For more examples of nonlinear discriminating statistics, we refer the  
23 reader to [130, 4].  
24

## 25 7. Surrogates for independence testing

26 In addition to being extremely useful in the search for underlying dynamics in univariate time series, surrogates  
27 can also be crucial in the investigation of interactions between systems, when given two or more time series.  
28 Although equally applicable to networks, here we mainly consider the bivariate case, i.e. how to infer from two  
29 given data sets whether their underlying systems are interacting, the nature of these interactions, if present, and  
30 whether their coupling is sufficient to lead to synchronization.  
31

32 The FT based surrogates discussed so far for nonlinearity testing have also been used in the search for dependence  
33 between systems, by ensuring that the same phase randomization is applied in all surrogate realizations.  
34 Stam *et al.* [147] proposed a novel measure for generalized synchronization in multivariate data sets to overcome  
35 the bias depending on degrees of freedom. Pereda *et al.* [148] review multivariate analysis specifically for neuro-  
36 physiological time series, and include an in-depth discussion of surrogates in this context. They illustrate the use  
37 of multivariate surrogate data testing for the assessment of the strength and the type of interdependence between  
38 neurophysiological signals. In an application to ecology, Sheppard *et al.* [18] investigated spatial synchrony in aphid  
39 pests. Spatial coherence was tested for significance using Fourier transform surrogates with their cross-spectrum  
40 and cross-correlation conserved [18].  
41

42 There are many types of surrogates other than the FT based ones already discussed, and the most useful for  
43 the purpose of testing for independence between signals are discussed in this section. Some of these surrogates  
44 require some extra steps before they can be used. Cyclic phase permutation (CPP) surrogates require extraction  
45 of the phase of the oscillations in a time series, whilst twin surrogates (TS) require time-delay embedding as  
46 previously discussed for pseudo-periodic surrogates (see Section 5.4). The onset of phase synchronization between  
47 two interacting oscillators with increasing coupling strength has been shown to precede the appearance of amplitude  
48 covariations [149], and thus can be detected at weaker coupling strengths and in noisy systems by only considering  
49 phase dynamics. Therefore, here we discuss the surrogate methods which have been used to investigate phase  
50 synchronization only.  
51

52 Surrogates can be used to test for phase synchronization and coupling between oscillators using various dis-  
53 criminating statistics, including phase coherence, the phase synchronization index (PSI) [150], mutual information  
54 [151], dynamical Bayesian inference [152] and synchronization likelihood [147] among many others (some of these  
55 measures are discussed in Section 8). However, great care is required in their application. Many methods used for  
56 this purpose rely on various representations and quantifications of the phase difference between two oscillators. It is  
57 very important to remember that a constant phase difference alone, whilst a requirement for phase synchronization,  
58 is not sufficient [153].  
59

60 We previously discussed Fourier transform based surrogates for testing for nonlinearity in the time series, but  
61 they have also been used successfully in bivariate data to search for phase synchronization. Paluš & Hoyer [6]  
62 demonstrated the use of FT surrogates for the investigation of cardiorespiratory synchronization in newborn piglets.  
63

1  
2  
3 They showed that the null hypotheses of random permutation surrogates, with and without their cross-dependence  
4 maintained, are not sufficient to provide an answer to whether the system is synchronized. Instead they showed,  
5 using mutual information as a discriminating statistic, that FT surrogates can be used to test for significant phase  
6 synchronization, and FT surrogates with the cross-spectrum of the original data maintained, as detailed in [60],  
7 can be used to test whether it is nonlinear [6]. Using these methods, the authors showed significant nonlinearity  
8 and phase synchronization between the respiratory movements and the heart rate fluctuations of the piglets.  
9

10 Schäfer *et al.* [31] highlight some problems with the approach of using surrogates for the detection of synchronization,  
11 arguing that Fourier phase randomization alone may be inappropriate, because of the mixing of phase and  
12 amplitude information. Hurtado *et al.* [78] developed a variant on the FT surrogate which works only with phase  
13 and preserves the power spectrum of the instantaneous frequency rather than that of the original data.

14 Sun *et al.* [154] also compared surrogate tests for phase synchronization in order to ascertain which surrogate  
15 method is most appropriate for phase synchronization analysis. Two widely used phase synchronization indices,  
16 mean phase coherence and entropy based, were compared and combined with five surrogate types. In contrast to  
17 [78], the authors conclude that RP and FT surrogates of the instantaneous frequency are not suitable for phase  
18 synchronization analysis in EEG signals, as the thresholds derived from them correlate highly with the original  
19 phase synchronization index (PSI) values. It was also shown that PS index based on mean phase coherence was  
20 less affected by the sampling rate of the data when compared to the entropy based PSI, suggesting that the former  
21 is more widely applicable in real data.

22 This study concluded that FT surrogates of the original time series provide the closest result to the true result  
23 provided by intersubject surrogates (which were used as the standard against which the performance of all other  
24 tests were measured), and are thus recommended in the absence of the latter [154]. However, this study only  
25 included RP and FT surrogates, so it is possible that other surrogates could offer improvements on these results.  
26 Intersubject surrogates are discussed further in Section 7.1.

27 Mezeiova & Paluš [155] concluded that phase synchronization analysis is not superior to coherence analysis,  
28 stating that both techniques lead to similar results. However, this was using mean phase coherence as a measure of  
29 synchronization, which may demonstrate the need for measures which focus more on the interactions between the  
30 systems over time rather than their averaged coherence, such as dynamical Bayesian inference.  
31

32 It is clear from these mixed results that Fourier based surrogate tests for synchronization have their disadvantages.  
33 To counter this, other surrogate types have since been presented in attempts to address these problems  
34 [78, 123, 156] and are discussed in the following sections.

### 35 7.1. Intersubject surrogates

36 Intersubject surrogates [27], also known as mismatched [157], or natural [123] surrogates, are truly independent  
37 realizations of a system being studied. This technique was introduced by Toledo *et al.* [158] for the investigation  
38 of cardiorespiratory synchronization, and has since been used to investigate maternal and foetal heart rates [159],  
39 ageing [27, 160], and brain-heart-lung interactions under general anaesthesia [161].  
40

41 As an example, consider the scenario in which the interactions between the breathing and the heart rate are  
42 being studied in a large group of subjects. There will be data available for each subject, measured on different days  
43 and at different times, and it is clear that if it is mismatched, i.e. the breathing of subject one is compared to the  
44 heart rate of subject two, we should not expect any dependence at all as there can be no causal relations. This  
45 method has been used as a standard against which other surrogates are tested in the search for synchronization  
46 [154].  
47

48 *Null hypothesis.* There is no dependence between the two systems.  
49

50 *Algorithm.* Create surrogate pairs by finding all possible mismatched pairs available in the data set.  
51

52 *Issues.* There are some drawbacks in the use of these surrogates. It is possible that the dynamics of the underlying  
53 systems may be different, for example the natural frequency may be slightly different [123], leading to surrogate  
54 realisations which are not fully constrained. Subject-specific features of the signals (like particular frequencies or  
55 waveforms) could lead to higher variability in the results. In some systems, it is also possible that enough data  
56 collection to provide sufficient natural mismatched pairs may be too expensive both in time and cost.  
57

58 *Applications.* Sheppard *et al.* [157] applied wavelet-based time-localized phase coherence and intersubject surrogates  
59 to investigate the relationship between blood flow and skin temperature, and blood flow and instantaneous heart rate  
60 (IHR) during vasoconstriction and vasodilation provoked by local cooling or heating of the skin. The distribution of  
61

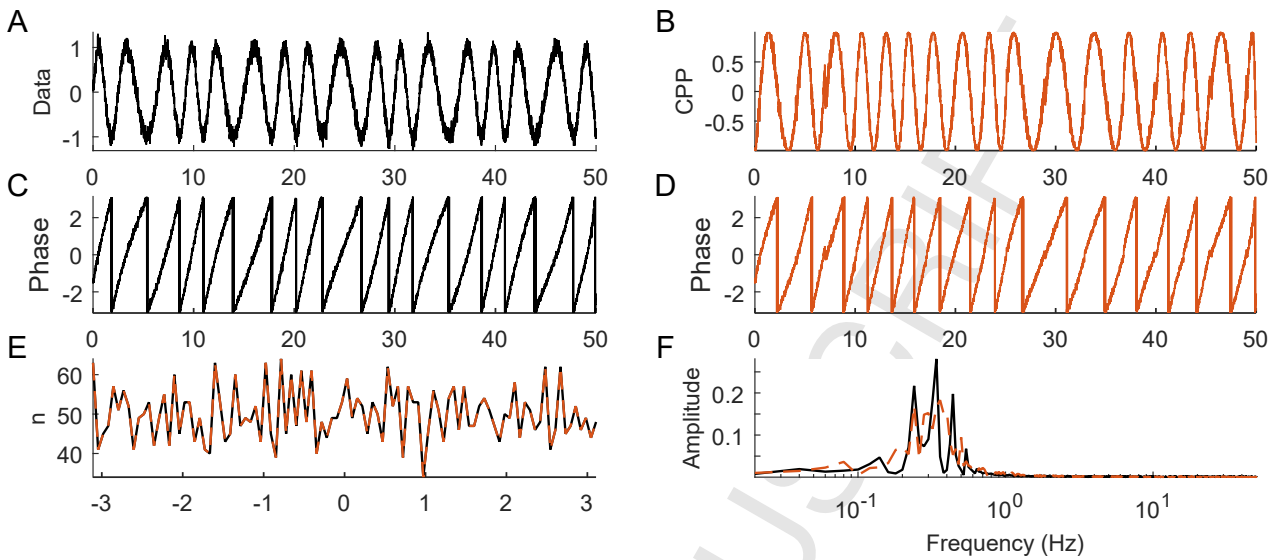


Figure 16: (A) 50 s noisy sinusoid with time-varying period  $\sin(2\pi(t+0.5\sin(2\pi t/10))/3)$ , with sampling frequency 100 Hz, preprocessed as discussed in Section 4.3. (B) Example cyclic phase permutation (CPP) surrogate (B). The phase of the signal in (A) was extracted using the Hilbert transform and is shown in (C). These phase cycles are then rearranged to create the phase surrogate, shown in (D) (the signal in (B) is obtained by  $\sin(\phi)$ ). Histograms of the phases in both signals demonstrate that the phase distribution of the time series exactly conserved, as seen in (E). (F) shows the Fourier spectra of the sinusoidal signals. In all cases, black lines are from the original data and orange lines are from the surrogate.

actual phase coherence values at each frequency was compared with the surrogate distribution using the Kolmogorov-Smirnov test.

Intersubject surrogates were also used by Iatsenko *et al.* [27] with the synchrosqueezed wavelet transform and Bayesian inference to investigate the cardiorespiratory coupling in terms of synchronization, coupling functions and contributions of different mechanisms. The authors found that intersubject and IAAFT surrogates gave the same significance threshold for wavelet phase coherence.

Donner & Thiel [162] used historic solar activity data with similar dynamics as data from the past 130 years as surrogates for their tests on sun-spot activity between hemispheres.

### 7.2. Cyclic phase permutation (CPP) surrogates

Cyclic phase permutation surrogates are phase surrogates. They are similar to cycle shuffled surrogates (see Section 5.3), but do not possess their drawbacks as they work directly with the phase of the signal. These surrogates are designed to test for interdependence between systems and are constructed by rearranging the cycles within the extracted phase. If the phase dynamics of two systems are not independent, then phase evolution over time of one system will be dependent on the phase evolution of the other system. Rearranging the cycles destroys this dependence, whilst preserving the general form of the phase dynamics of each system. This simple approach is very powerful for testing significance levels of measures which are expressed through the phases of systems.

*Null hypothesis.* Two systems have independent phase dynamics.

*Algorithm.*

1. Extract the instantaneous phase from the time series using either the Hilbert transform or extraction from the wavelet transform (see Appendix A.3 for more details).
2. If the extracted phase is unwrapped (not bounded), wrap the phases between 0 and  $2\pi$ .
3. Find individual cycles in the signal and divide it into cycles by selecting points of discontinuity, i.e. places in the wrapped phase signal in which the phase suddenly drops a large amount.
4. At the beginning and end of the time series there will be incomplete cycles, these should remain in place for all surrogates.
5. Reconstruct a new phase series with these beginning and end points, and randomly permute all other phase cycles between them.
6. Repeat for each surrogate.

The calculation of CPP surrogates is very fast. An example CPP surrogate is shown in Figure 16.

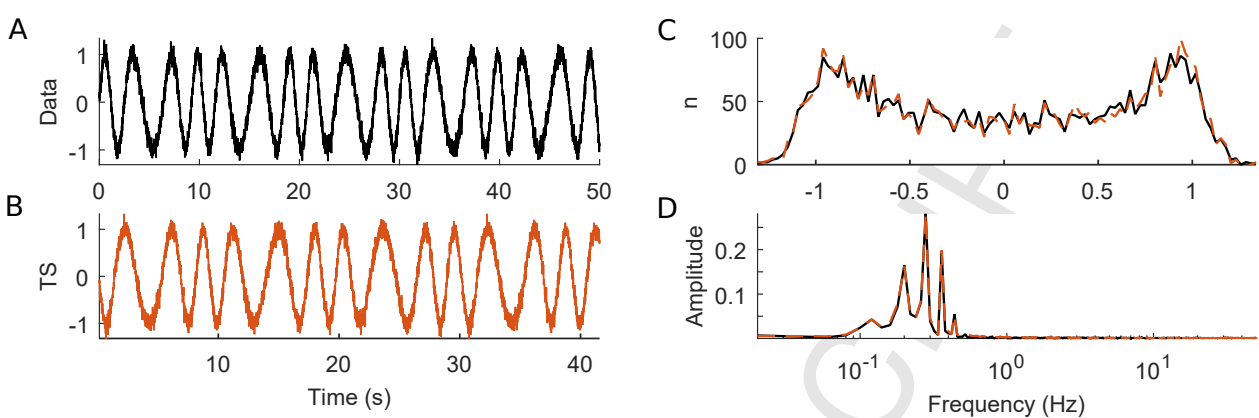


Figure 17: (A) 50 s noisy sinusoid with time-varying period  $\sin(2\pi(t+0.5\sin(2\pi t/10))/3)$ , with sampling frequency 100 Hz, preprocessed as discussed in Section 4.3. (B) Example twin surrogate (TS) calculated from the signal in (A). Histograms of both signals demonstrate that the distribution of the time series is not exactly conserved, as seen in (C). (D) shows the Fourier spectra of the signals. In all cases, black lines are from the original data and orange lines are from the surrogate.

**Issues.** CPP are capable of testing whether the phase dynamics of periodic signals is really synchronized or whether they just have the same rhythm, i.e. can distinguish between coherence and synchronization. This is because they seek more sophisticated expressions of synchronization than just coincidence of rhythms, such as the adjustability of cycle periods between two systems. However, it might be that, for example, both phase dynamics and frequency modulation are independent, but coincide, in which case this test will reject the null hypothesis. In real systems this is very unlikely. The null hypothesis will also be rejected if the noise in one system is correlated with the noise in the other, which can still be regarded as dependence, since in real systems noise can be just a complicated realization of high dimensional phase dynamics, and thus such systems are indirectly coupled through other elements.

**Applications.** Jamšek *et al.* [7] combined conditional mutual information and cyclic phase permutation (CPP) surrogates in the investigation of the nature, strength, and direction of coupling between two or more time-varying oscillators. CPP surrogates are used in [163] with different methods of conditional mutual information estimation to investigate the problem of inferring direction of coupling from time series, but it is shown that any current surrogate method may introduce bias into the results. CPP surrogates are also used in [155] in the comparison of coherence and phase synchronization analysis.

### 7.3. Twin surrogates (TS)

Unlike PPS, which by definition cannot mimic chaotic oscillators, twin surrogates were developed to test for complex synchronization by Thiel *et al.* [123] and further developed in [164, 156]. They are based on the popular recurrence plot analysis discussed in [165]. Twin surrogates mimic the dynamical behaviour of the system, reproducing both linear and nonlinear properties. They correspond to a trajectory of the underlying system, but starting at different random initial conditions.

**Null hypothesis.** Two systems are independent.

**Algorithm.** Twin surrogates, like PPS, require embedding before calculation.

- 50 1. Embed original time series and produce a  $d$ -dimensional representation  $\vec{x}$ .
- 51 2. Find the index  $q$  of the first nearest neighbour from the first half of the embedded signal to its last value  
 $\vec{x}_L : \|\vec{x}_q - \vec{x}_L\| = \min, q \in [1, L/2]$ . This is so that periodic boundary conditions can be applied to avoid cycling near the last value, for example when the last value has no twins and the nearest value to it is the previous one.
- 52 3. Choose parameter  $\delta$ . (See below)
- 53 4. Calculate recurrence matrix  $R_{ij}$ :

$$R_{ij} \equiv H(\delta - \|\vec{x}_i - \vec{x}_j\|), \quad (20)$$

54 where  $H(x > 0) = 1, H(x < 0) = 0$  is a Heaviside function. We recommend the use of maximum norm  
 $\|\vec{x}_i - \vec{x}_j\| = \max(x_i - x_j)$ .

- 1  
2  
3 5. For each  $i$ , find the set of  $j$ 's corresponding to similar columns in the recurrence matrix:  $R_{ik} = R_{jk}$  for any  
4  $k$ . Points  $\vec{x}_j$  then have the same neighbourhood as  $\vec{x}_i$  and are called twins. Denote these sets  $S[i]$  and include  
5 in this set trivial  $i$  so that it will always contain at least one element. It should be noted that almost always  
6 and for any  $\delta$  there are similar columns in the recurrence matrix.  
7 6. As a first value of the surrogate signal, set  $\vec{S}_1 = \vec{x}_i$  for random  $i = 1 \dots L$ .  
8 7. Given the value of the current iteration  $\vec{S}_i = \vec{x}_k$ , randomly select index  $j$  from the set of twins  $\vec{x}_k : j =$   
9  $rand(S[k])$ . If  $j$  is the last index  $j = L$ , set  $j = q$ . Set next iteration value as next value for chosen twin  
10  $\vec{S}_{i+1} = \vec{x}_{j+1}$ .  
11 8. Repeat steps 5–6 to generate  $\vec{S}$  of length  $L$  and choose its first component as the scalar surrogate signal. To  
12 generate more surrogates, repeat steps 6–8.

13 An example TS surrogate is shown in Figure 17.

14  
15 Parameters. The only parameter, aside from those for the initial embedding, is  $\delta$ , and it was shown that the results  
16 are not hugely influenced by its value in reasonable limits [156]. However, each interval  $\delta$  should include at least  
17 one point [166]. It is stated in [123] that the appropriate choice of  $\delta$  should correspond to 5–20% of unit entries in  
18 the recurrence matrix  $R_{ij}$ .

19 To find  $\delta$  which will give proportion  $\alpha$  unities in  $R_{ij}$  (so there are overall  $\alpha N^2$  unities), one should first calculate  
20 distances between points in phase space and then set  $\delta$  to the  $\alpha N^2$ th smallest distance. So the procedure is as  
21 follows:

22 1) Choose the desired proportion  $\alpha$  of unities in the recurrence matrix. According to [123], an appropriate choice  
23 is  $\alpha \in [0.05; 0.2]$ . In our algorithms we use  $\alpha = 0.1$  (as the authors in [123] also usually do).

24 2) Calculate matrix of distances

$$D_{ij} = \|\vec{x}_i - \vec{x}_j\|. \quad (21)$$

25 3) Sort  $D_{ij}$  in ascending order and set  $\delta$  to its  $\alpha N^2$ th smallest value:  $\delta = sort(D_{ij})_{\alpha N^2}$ .

26 This choice will give proportion of  $\alpha$  unit entries in  $R_{ij}$ . This is done in step 3 of the algorithm. To not slow  
27 down computations, the calculated  $D_{ij}$  (21) is then substituted into (20) in step 4 to calculate the recurrence matrix  
28  $R_{ij} = H(\delta - D_{ij})$ . Other choices also exist ([165] pp.11–12), but in general the one discussed here is sufficient.  
29 It was also shown that the performance of twin surrogates does not depend strongly on the choice of embedding  
30 parameters [156].

31 Issues. The computational cost for TS is extremely high. The most computationally expensive procedure is the  
32 seeking of twins, since for each  $i = 1, \dots, L$  it needs to compare  $L - 1$  columns in the recurrence matrix with  $L$   
33 elements each. Next, the recurrence matrix of  $L^2$  elements needs to be saved in the memory, which may slow down  
34 computation or be impossible for very large data sets. Once twins have been found, which only needs to be done  
35 once, surrogates can be calculated very fast, making the computational speed almost independent of the number of  
36 surrogates, which can be seen in Figure 34(B).

37 Applications. Thiel *et al.* [164] applied twin surrogates to study eye movements, and found that the fixational  
38 movements of the left and right eye are synchronized. Twin surrogates are also used in a climate context in [167],  
39 where they were used to help uncover novel pathways of global energy and dynamical information flow in the climate  
40 system, and were shown to have a higher test power than shuffled time series or Fourier surrogates for this purpose.  
41 Romano *et al.* [168] proposed indices for the detection of asymmetry of coupling between interacting systems, and  
42 used twin surrogates to generate significance levels. TS were used in [169] to investigate synchronization between  
43 maternal and foetal heart rates with paced maternal breathing.

#### 51 7.4. Time-shifted surrogates

52 It was first proposed in [170] to generate surrogates by time-shifting the original data. This approach was then  
53 further developed in [171]. Time-shifted surrogates will have the same state space trajectory, and thus fully preserve  
54 all of the properties of the original signal. They test the null hypothesis of two processes with arbitrary linear or  
55 nonlinear structure but without nonlinear interdependence and without significant linear cross-correlation. Two  
56 variants have been proposed. The first is to shift the time series using periodic boundary conditions, i.e. wrapping  
57 around the end of a shifted time series to the beginning of the new time series. The second approach is to cut a  
58 window of samples from one signal and using as time shifted windows from the second signal as surrogates. The  
59 latter was shown to be safer due to the fact that using periodic boundary conditions can introduce a phase slip  
60 [171]. However, this problem is solved by preprocessing the data as discussed in Section 4.3. Thus, we propose  
61 [171].

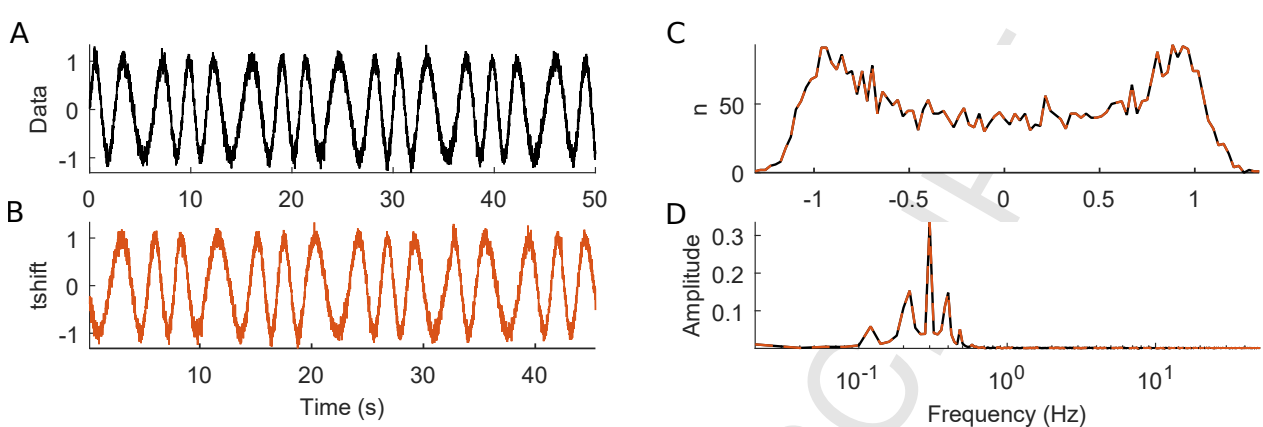


Figure 18: (A) 50 s noisy sinusoid with time-varying period  $\sin(2\pi(t + 0.5 \sin(2\pi t/10))/3)$ , with sampling frequency 100 Hz (A), preprocessed as discussed in Section 4.3. (B) Example time-shifted surrogate calculated from the signal in (A). Histograms of both signals demonstrate that the distribution of the time series is exactly conserved, as seen in (C). (D) shows that the Fourier spectra of the signals are identical, as expected. In all cases, black lines are from the original data and orange lines are from the surrogate.

the use of the former with preprocessing, to avoid unnecessary data loss, which is less than ideal when studying dynamical systems for which limited data is available.

It should be emphasised that in [170, 171] time-shifted surrogates are not used as surrogates in the usual sense, but by plotting the dependence of some nonlinear measure on the relative time shift between two time series, i.e. between one signal and a time-shifted surrogate of the other. If there is a clear peak at zero shift (which represents the original signal) in this dependence, it indicates rejection of the null hypothesis, since time-shifting decreases the interdependence. Observing a peak at a different time-shift may also indicate rejection of the null hypothesis, but it is unclear if this is always the case, and may depend on the discrimination statistic used. It was shown in [171] that this technique is useful for indicating nonlinear interdependence. These surrogates have also been used in a direct way using random time delays, and are discussed in the applications section below.

*Null hypothesis.* Two processes do not have any nonlinear interdependence or significant linear cross-correlation. The self structure of each signal can be arbitrary.

### Algorithm.

1. Preprocess the signal according to Section 4.3. Preprocessing is crucial here, as a mismatch at the beginning and end of the signal may lead to discontinuities.
2. Choose a random time shift independently for each surrogate.
3. Shift the signal in time, wrapping its end to the beginning.

Time-shifted surrogates are very fast to generate. Only one signal needs to be shifted, it does not matter which one. An example time-shifted surrogate is shown in Figure 18.

*Issues.* Time-shifted surrogates can be viewed as an independent copy of the system which preserve not only intracycle behaviour, but also intercycle behaviour (except for the first and last cycles). This makes them more constrained than TS, PPS and CPP surrogates. Time-shifting changes the cross-moments between two systems, but they may not be randomized completely, i.e. the full set of possible realizations consistent with the null hypothesis may not be realised. A larger number of time-shifted surrogates will generally be required than IAAFT, for example. The spectrum and the distribution are preserved exactly.

*Applications.* Canolty *et al.* [172] used time-shifting to demonstrate that an observed coupling strength between theta and high gamma oscillations in the human brain falls to much lower levels at large time lags, proving that this coupling was a significant observation. Petrock *et al.* [173] calculated cross wavelet transforms between cardiac and respiratory rhythms to identify any correlations between the signals. The significance level was found using time shifted surrogates, which in this case were also reversed in time following the time shift. The newly introduced method of nonlinear mode decomposition (NMD), a decomposition method for extracting oscillatory modes from time series [21], uses time-shifted surrogates to determine whether the harmonics of an oscillation in a time-frequency representation of the signal are significant based on the null hypothesis of independence between the first harmonic

1  
2  
3 and the extracted harmonic candidate. Netoff & Schiff [174] investigated synchrony in neural networks using  
4 time-shifted surrogates and mutual information.

5 As discussed previously, time-shifting as a method for generating surrogates has also been used as part of wavelet  
6 surrogate generation algorithms, in which the wavelet coefficients obtained from the discrete wavelet transform are  
7 time-shifted at each scale [108]. Time-shifted surrogates have also proven useful in the assessment of the performance  
8 of coupling measures [175, 176].  
9

## 10 8. Discriminating statistics for interdependence testing

11 Although surrogates were originally introduced to test for nonlinearity, they were soon also employed to search  
12 for interdependence between dynamical systems. As for nonlinearity, there are many discriminating statistics that  
13 can be used for this purpose, in bivariate and multivariate data, but here we focus mainly on synchronization and  
14 coupling between two systems.  
15

16 The dynamical systems found in nature are rarely isolated. Instead, they constantly interact with each other.  
17 The investigation of coupling has developed into a very active and rapidly evolving field [177]. However, the question  
18 of the nature of coupling between interacting systems still remains highly non-trivial to answer.  
19

### 20 8.1. Phase coherence

21 Phase coherence provides a measure of how stable the phase difference between oscillators is over time, and is  
22 the main measure of synchronization used in this paper. Phase coherence is defined as [157, 29],  
23

$$24 \quad \Pi(\omega) = \frac{1}{L} \left| \sum_{n=1}^L e^{i(\phi_1(\omega, t_n) - \phi_2(\omega, t_n))} \right|, \quad (22)$$

25 where  $\phi_1(\omega, t_n) - \phi_2(\omega, t_n)$  is the phase difference between the oscillatory components of the same frequency from  
26 the two time series at time  $t_j$ . In an ideal scenario, a value of 1 would be returned for perfect synchronization, and a  
27 value of zero for complete independence. It is highly unlikely in real systems to obtain these values. Synchronization  
28 measures, coupled with existing phase extraction measures, may not always indicate true synchronization in systems,  
29 due to the effects of finite data length, similar power spectra, or other factors. Therefore, in order to ascertain  
30 whether an obtained synchronization measure value indicates significance, we need to compare it against the same  
31 measure calculated in a case in which we know that there is no synchronization. This is where surrogates become  
32 essential.  
33

34 It should be noted that the notions of phase coherence and phase synchronization are not interchangeable.  
35 Consider two sinusoids with perfectly matching frequencies. Calculation of the phase coherence of these two signals  
36 will yield a value of one, i.e. they will be perfectly phase coherent. But how do we know if they are synchronized?  
37 Unfortunately, if there is no time-variability in the phase dynamics of the two signals, we cannot know if they are synchronized.  
38 Or whether they are coherent by chance, because we cannot observe how each oscillator may adjust  
39 the dynamics of the other over time. It is important to note that, assuming correct preprocessing as discussed  
40 in Section 4.3, FT-based surrogates of a perfect sine wave (which is an edge case of a linear process) can only  
41 be random in the relative phase shift, so all surrogate realisations will also be perfect sine waves, resulting in the  
42 acceptance of the corresponding null hypothesis. When testing for synchronization, it is crucial to remember that  
43 synchronization is not a state, but a process of adjustment of rhythms due to interaction [31] and thus we must  
44 also consider the evolution of the system and its parameters over time.  
45

46 Phase synchronization is usually defined as the locking of phases  $\phi_{1,2}$ :  
47

$$48 \quad n\phi_1 - m\phi_2 = \text{const}, \quad (23)$$

49 for integers  $n$  and  $m$ . Rosenblum *et al.* [178] described phase synchronization in coupled chaotic systems, for which  
50 the phase locking is relaxed as:  
51

$$52 \quad |n\phi_1 - m\phi_2| < \text{const}. \quad (24)$$

53 In both cases, the amplitudes can be completely independent.  
54

### 55 8.2. Synchrogram

56 A synchrogram is a visual representation of synchronization [29] between two oscillators in which marked events  
57 of one oscillator are compared to the wrapped (bounded between 0 and  $2\pi$ ) continuous phase of the other. Recording  
58 the phase of oscillator 2 each time an event, such as a peak, occurs in oscillator 1 and plotting this phase over time  
59

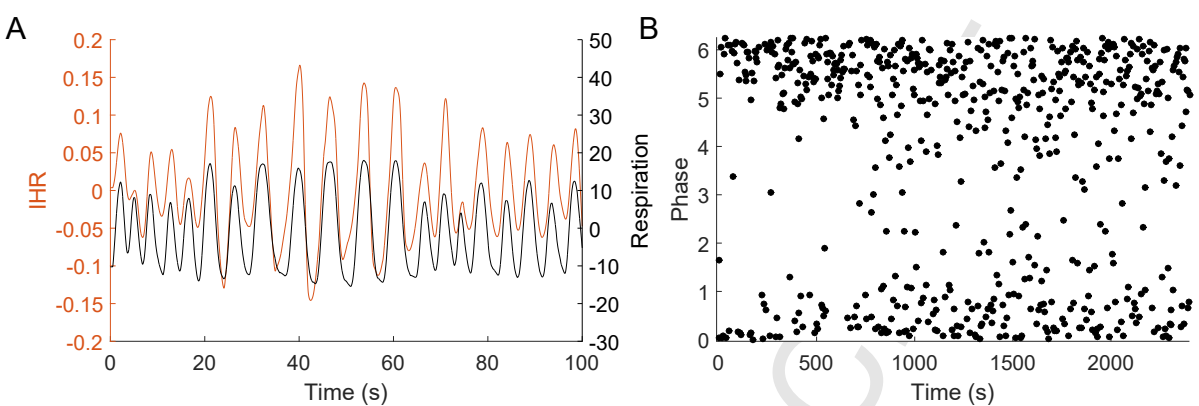


Figure 19: It is well known that the instantaneous heart rate and the breathing are coupled. This behaviour is called respiratory sinus arrhythmia (RSA), and can be seen in panel (A). An example synchrogram presents the phase of one oscillator relative to the other over time, and if perfect phase synchronization is present, horizontal lines will be observed. A clustering towards a preferred value can be seen here, but it is difficult to say whether this signifies synchronization from the synchrogram alone.

provides information about the phase difference over time. If the oscillators are synchronized, the marked events will occur at the same point within the cycle of the second oscillator over many cycles, and horizontal lines will emerge. The number of horizontal lines determines the type of synchronization, for example for 1:1 synchronization there would be one horizontal line, for 2:1 two horizontal lines. If the oscillators are not synchronized, a random scattering of phases will be observed. If there is a preferred phase difference in the system, horizontal lines will become visible as shown in Figure 19(B). If anything more than 1:1 synchronization is present in the data, the cycles over which the phase is wrapped needs to be increased, but this has to be done manually, making this method cumbersome for complex synchronization. In addition, it is very difficult to quantify synchronization using only the synchrogram, so other measures have been introduced.

### 8.3. Phase synchronization index

Introduced by Tass *et al.* [150], the phase synchronization index (PSI) involves dividing the cycle of one oscillator into  $N$  bins and integrating the complex phase of the other oscillator over each bin [29], in order to assess whether the section of the phase of each oscillator coincides within each division of the cycle. The average over bins then gives the PSI. The PSI suffers from the same problem as the synchrogram, that anything other than 1:1 synchronization has to be found by trying different combinations of  $n$  and  $m$  to eventually find  $n : m$  synchronization. For perfect synchronization, the PSI would be 1, but in practice this is very rare, and surrogates are required to investigate whether the observed PSI is significant. It should be noted that PSI values strongly depend on length of signals, especially if the synchronization is intermittent or variable. Sun *et al.* [154] suggest 3-16 or 5-12 wave cycles is optimal for PSI, at least in EEG.

### 8.4. Dynamical inference

A number of methods that have been proposed for the study of interactions perform dynamical inference, i.e. they reconstruct a model of differential equations from the interacting data. These methods inevitably require surrogate testing. The reconstruction within these methods is based on a variety of inference techniques, e.g. least squares and kernel smoothing fits [153, 179], dynamical Bayesian inference [180], maximum likelihood (multipleshooting) methods [181] and phase resetting [182, 183].

An example of such methods is Dynamical Bayesian inference (DBI), which can detect time-varying synchronization, directionality of coupling and time-evolving coupling functions simultaneously from the phase evolution of multiple oscillators [180, 184]. Following the extraction of the phases of two time series, or two oscillations within the same time series, their dynamics is assumed to be described by [180, 184, 55],

$$\dot{\varphi}_i = \omega_i + f_i(\varphi_i) + g_j(\varphi_i, \varphi_j) + \xi(t), \quad (25)$$

where  $\omega_i$  is the natural frequency of the oscillation of each oscillator,  $f_i(\varphi_i)$  are the self-dynamics of the phase,  $g_j(\varphi_i, \varphi_j)$  are the cross couplings, and  $\xi(t)$  is a two-dimensional white Gaussian noise  $\langle \xi_i(t) \xi_j(\tau) \rangle = \delta(t - \tau) E_{ij}$ , included to represent a process in a real system.

1  
2  
3 The inference of parameters utilises Bayes' theorem [185],  
4  
5

$$p_{\mathcal{X}}(\mathcal{M}|\mathcal{X}) = \frac{\ell(\mathcal{X}|\mathcal{M})p_{prior}(\mathcal{M})}{\int \ell(\mathcal{X}|\mathcal{M})p_{prior}(\mathcal{M})d\mathcal{M}}, \quad (26)$$

6 where  $p_{\mathcal{X}}(\mathcal{M}|\mathcal{X})$  is the posterior probability distribution and  $\ell(\mathcal{X}|\mathcal{M})$  is the likelihood function for the values of  
7 the model parameters  $\mathcal{M}$  given the data  $\mathcal{X}$ , and  $p_{prior}(\mathcal{M})$  is a prior distribution.  
8  
9

10 The inferred parameters of the coupling functions [177] can be used to determine whether the system is syn-  
11 chronized. The coupling strength obtained from this method should be verified by using surrogates in which there  
12 is definitely no coupling to provide a statistical threshold for significance. See [186] for further details and an in  
13 depth tutorial on dynamical Bayesian inference and its implementation.  
14  
15

### 16 8.5. Mutual information

17 Mutual information, also known as the redundancy, is a measure of how much information is common to two  
18 time series  $x_i$  and  $x_j$ , and can be used to detect coupling [29]. Using *conditional* mutual information (CMI),  
19 which characterizes the net dependence between two discrete random variables, Paluš [45] studied unidirectionally  
20 coupled Rössler and Lorenz systems, and also unidirectionally coupled Hénon maps. It should be noted that the  
21 direction of coupling can only be inferred from experimental data when the studied systems are coupled but not  
22 yet synchronized.  
23

24 All asymmetric measures, including CMI, will suffer from some bias when estimated from noisy, nonstationary  
25 experimental data, which may result in non-zero values even in the uncoupled direction of a unidirectionally coupled  
26 system. Thus, surrogates can be used to find the level of this bias in the case of no true coupling, or the “statistical  
27 zero”. For this purpose FT surrogates are used, as CMI is independent of the distribution of the data [45].  
28 Surrogates prevent the false detection of causality. However, a relatively large number of surrogates are required,  
29 and this number will increase if the frequencies of the two systems are different and if the system is noisy. If large  
30 amounts of noise are present, the applicability of the test is limited.  
31

32 Surrogates for inferring the direction of coupling were also discussed in [187, 163], and more recently by Jelfs  
33 and Chan [188] who demonstrated the importance of using surrogates when calculating directionality indices, by  
34 applying them to both CMI and evolution map approach methods.  
35

### 36 8.6. Wavelet bispectrum analysis

37 Bispectral analysis belongs to a group of techniques based on high-order statistics [189, 190]. It can be applied  
38 to detect Gaussianity [191], but more importantly may be used to study couplings between interacting oscillatory  
39 processes or investigate phase relations [192]. Unlike synchronization methods, which are unable to provide any  
40 information about the characteristics of couplings, bispectrum analysis is especially powerful for the investigation  
41 of the nature of interactions between coupled oscillators, while making no assumptions about the data under  
42 investigation.  
43

44 First introduced by Hasselmann [193] to study ocean waves, bispectral analysis has since been applied in  
45 oceanography [194], and has also gained popularity in biomedical sciences, for example in the analysis of EEG  
46 [195, 196, 197, 198, 199, 200], cardio-respiratory interactions [201] and abnormalities in respiration [202]. Bispec-  
47 trum analysis has also proven useful in geophysics [203], turbulence analysis [204, 205, 206], astrophysics [191],  
48 plasma physics [207], machine engineering [208], economics [209] and seismology [210].  
49

50 Early work on bispectrum analysis followed a traditional stationary approach, and took time into account only  
51 by partitioning signals in regions of interest. Van Millingen *et al.* [211, 205] introduced the *wavelet bispectrum*  
52 and the normalized version, *wavelet bicoherence*, and applied them to nonlinear oscillators, demonstrating the  
53 applicability of the wavelet bispectrum in turbulence analysis. Almost simultaneously, Rao and Indukmar [212] also  
54 introduced wavelet bispectral analysis, additionally presenting a discrete version for the investigation of discrete  
55 processes. Schack *et al.* [200] introduced a Gabor expansion for estimating the bispectrum, bicoherence and phase  
56 bicoherence, and tracked the maximal bicoherence over time in EEG signals. Jamšek *et al.* [213] used time-phase  
57 bispectral analysis to detect different types of coupling (including linear) of nonlinear oscillators. In later work,  
58 Jamšek *et al.* compared short-time-Fourier bispectral analysis with wavelet bispectral analysis [214] in the detection  
59 of couplings between oscillators with time-varying parameters. They concluded that wavelet bispectral analysis,  
60 using the Morlet wavelet, provides the best compromise for time-frequency resolution.  
61  
62

63 Jamšek *et al.* [7] also combined wavelet bispectral analysis with an information theoretic approach to study  
64 interactions among oscillators with time-varying basic frequencies.  
65

1  
2  
3 The bispectrum can be derived from the Fourier spectrum as the third-order moment  $\hat{M}(f_1, f_2)$  [189], namely  
4  
5

$$\hat{M}(f_1, f_2) = F(f_1)F(f_2)F^*(f_3), \quad (27)$$

6 where  $F$  corresponds to the Fourier transform of the time series,  $f_1, f_2$  is any pair of frequencies of interest and  
7  $f_3 = f_1 + f_2$ . (However, there are some examples in the literature of modifying  $f_3$  according to the research  
8 hypothesis, e.g.  $f_3 = 2f_1 - f_2$  [213]). In order not to overlook time-dependent effects, the signal can be partitioned  
9 into  $K$  consecutive time windows. The average bispectrum over these windows is defined as  
10  
11

$$\hat{B}(f_1, f_2) = \frac{1}{K} \sum_{k=1}^K \hat{M}_k(f_1, f_2). \quad (28)$$

12 Alternatively, time-frequency representations can be applied. Typically the short-time Fourier or wavelet transform  
13 can be used but also, less commonly, Wigner-Ville transforms [215, 216]. Here, we focus on wavelet-based analysis,  
14 since it provides the best compromise for time-frequency resolution by using an adaptive time window. We use the  
15 Morlet wavelet:  
16

$$\psi(u) = \frac{1}{\sqrt{2\pi}} \left( e^{i\omega_0 u} - e^{-\omega_0^2/2} \right) e^{-u^2/2}, \quad (29)$$

17 where  $\omega_0/(2\pi) = f_0$  is the central frequency. Then the wavelet transform of the signal  $x(t)$  is given by [217]  
18

$$W_x(s, t) = \int x(u)\psi^* \left( \frac{u-t}{s} \right) \left( \frac{1}{s} \right)^p du = \frac{1}{2\pi} \left( \frac{1}{s} \right)^{1-p} \int e^{i\xi t} \hat{x}(\xi) \hat{\psi}^*(s\xi) d\xi, \quad (30)$$

19 where a scale value  $s$  corresponds to a frequency value  $f = \omega_0/(2\pi s)$ ; here, there is a normalisation factor  $(\frac{1}{s})^p$   
20 which depends on some parameter value  $p$ , conventionally non-negative. Typically,  $p = 1/2$  is chosen, so that the  
21 square of the wavelet transform provides a suitable definition of wavelet power [217, 218]. However, choosing  $p = 1$   
22 has the significant advantage that equal-amplitude oscillations at different frequencies are represented by peaks of  
23 equal height in the wavelet transform, like they are with the Fourier or short-time Fourier transform. The peaks  
24 will also have equal spread when viewed with a logarithmic-scale frequency axis. Therefore, in our examples, we  
25 take  $p = 1$ .  
26

27 The wavelet bispectrum is then calculated as follows  
28

$$B(s_1, s_2) = \frac{1}{T} \int_0^T W(s_1, t)W(s_2, t)W^*(s_3, t) dt, \quad (31)$$

29 where  $T$  is the time length of the signal,  $W^*$  the complex conjugate of the wavelet transform,  $s_i$  are wavelet scales  
30 and  $\frac{1}{s_3} = \frac{1}{s_1} + \frac{1}{s_2}$ .  
31

32 The cross bispectrum allows for the identification of coupling between different time-series  $x(t)$  and  $y(t)$   
33

$$B_{xyy}(s_1, s_2) = \frac{1}{T} \int_0^T W_x(s_1, t)W_y(s_2, t)W_y^*(s_3, t) dt. \quad (32)$$

34 Jamšek *et al.* [214] introduced an alternative empirical correction into the wavelet function, for the sake of  
35 applying bispectral analysis to cardiovascular signals that contain oscillations spanning scales from 1 second to over  
36 100 seconds. However, the most appropriate normalisation for the wavelet bispectrum has not yet been studied or  
37 discussed from a mathematical point of view.  
38

39 Different pairs of coupled oscillations with similar types and strengths of coupling, and occupying similar regions  
40 in frequency-frequency space, could have very different amplitudes of oscillations leading to very different values  
41 of the bispectrum. Bicoherence can be used to counter the effect of different amplitudes when trying to detect  
42 couplings. However, in the case of noisy real-life signals, this normalization can be a major culprit in causing  
43 bispectrum-based investigation of the presence of couplings to have poor specificity. One possible way to overcome  
44 this problem is to apply surrogate-based statistical testing [219] when applying bispectral analysis, instead of using  
45 amplitude normalization.  
46

47 In real-world noisy signals, ascertaining the presence or absence of coupling is a great challenge. Early work  
48 on bicoherence surrogates was presented by Elgar *et al.* [220, 221], who, for Gaussian processes, found numerically  
49 the critical surrogate thresholds for testing a null hypothesis of zero bicoherence. Later, Wang *et al.* [222] pro-  
50  
51

posed surrogate testing for the null hypothesis that the original data were generated by a linear Gaussian process. For bispectra defined in terms of disjoint-window Fourier transforms, Kim *et al.* [223] proposed the procedure of randomizing the *biphase* of each time-segment while keeping the same biamplitude to test the significance of bi-coherence values. This approach was later extended to wavelet bicoherence by Li *et al.* [224], who developed a general harmonic wavelet bicoherence, which uses a phase randomization method to estimate the cross-frequency interactions. They applied it to sleep analysis. More recently, this approach was used by Scully *et al.* [225] to investigate quadratic coupling in kidney blood flow data. Siu *et al.* [219] applied the iteratively refined surrogate data technique [199] directly to the bispectrum to bypass the spurious peaks effect that are the consequence of the bicoherence normalization. They used it to investigate the couplings in renal hemodynamic data. Ge [206] analytically derived the critical threshold for wavelet bicoherence by determining the covariance structure of relevant wavelet-based moments.

In Section 9.3.3 we compare the performance of different surrogates types for the investigation of significant peaks in the bispectrum.

## 9. Applications to simulated and experimental data

### 9.1. Nonlinearity testing

#### 9.1.1. Finding nonlinearity in data using the correlation dimension

Here we present an example of one of the earliest and most important applications in surrogate data testing, confirming the presence of nonlinearity in the data. Before the introduction of surrogate data testing, the search for chaos led to many premature conclusions that it was the reason for the dynamics in many observed systems. Subsequent reviews of many of these studies failed to find even nonlinearity in the data, usually immediately ruling out the possibility of chaos. These studies serve as a cautionary tale, highlighting the importance of testing all assumptions before drawing conclusions.

One of the most popular measures used to characterise chaos is the correlation dimension,  $\nu$  (see Section 6.1). As an example of a chaotic (and thus nonlinear) system we consider the Rössler equations,

$$\begin{cases} \dot{x} = -y - z \\ \dot{y} = x + ay \\ \dot{z} = b + z(x - c), \end{cases} \quad (33)$$

with  $a = 0.165$ ,  $b = 0.2$  and  $c = 10$ . The system was integrated for 1000 seconds using a 6<sup>th</sup> order Runge-Kutta scheme with time step of 0.1 seconds. The  $x$  component was then used in the following tests for nonlinearity, with the second half (the last 500 seconds) being used in the analysis, to remove transients at the beginning of the simulation. Observational noise with NSR = 0.1 was added to the system. An example time series is shown in Figure 20(A).

If we wish to test whether the system from which this time series was measured is chaotic, we can calculate the correlation dimension,  $\nu$ . In this case, the estimated embedding dimension using the false nearest neighbours method is 3, and  $\nu = 2.08$ . The fact that this number is not an integer, and is lower than the embedding dimension, suggests that the underlying system is neither noise nor a superposition of periodic orbits [43]. This could be evidence for chaos, but we must first test whether the system is nonlinear before we can draw any conclusions from this analysis.

The surrogates discussed here for the detection of nonlinearity in data are FT, AAFT, IAAFT, WIAAFT and IDFS. Here, their performance is tested in this clear case of nonlinearity, and we should expect them all to reject the null hypothesis of a stationary linear Gaussian system, with or without measurement transformation depending on the surrogate type. 100 surrogates of each type were generated, with preprocessing performed as discussed in Section 4.3. Correlation dimensions  $\nu$  were calculated for each surrogate set, and the distribution was compared with the value for  $\nu$  in the simulated chaotic data. The embedding dimension which was estimated for the simulated data was also used in the calculation of  $\nu$  for the surrogates. As deterministic behaviour should result in a lower value for  $\nu$ , the surrogate test is one-sided, with a lower value of  $\nu$  in the real data than the 5<sup>th</sup> percentile of the surrogates considered significant. All considered surrogates were successful in rejecting the null hypothesis in this case, meaning that we can reasonably consider this system as nonlinear, as expected. Surrogate  $\nu$  distributions for the chaotic system are shown in Figure 21(A).

Next, we demonstrate how a linear system may appear to mimic some features of nonlinear systems, and demonstrate the requirement for surrogates to accurately determine their origin. High-order ARMA models can

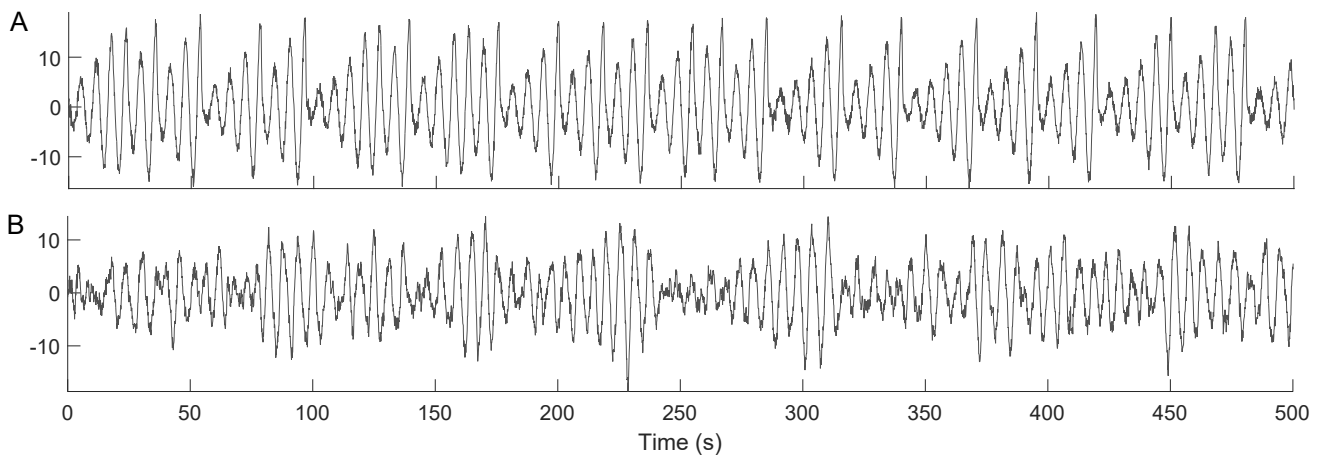


Figure 20: (A) Time series from the  $x$  component of the Rössler system described in Eqs. 33. (B) Time series from the ARMA model described in Eq. 34.

exhibit oscillations. For direct comparison with the chaotic signal, an oscillatory signal was generated using a third order ARMA model,

$$s_n = 1.625s_{n-1} + 0.284s_{n-2} + 0.355s_{n-3} + \eta_n - 0.960\eta_{n-1}, \quad (34)$$

where  $\eta_n$  follows a Gaussian distribution with variance 1. The parameters in this model were estimated from the previously used chaotic Rössler time series. An example of a linear time series generated by Eq. (34) is shown in Figure 20(B).

In this case, we naturally expect any tests for nonlinearity to fail to find it. This means that the discussed surrogates should fail to reject their null hypotheses, and there should be no significant difference between the range of  $\nu$  calculated in the surrogates, and the  $\nu$  calculated from the original data. As expected, all surrogates fail to reject the null hypothesis, as shown in Figure 21(B).

Data recorded in real systems are rarely a complete representation of the underlying system, for example it may be affected by the mechanism of measurement. This introduction of static nonlinearities may cause false rejections of the null hypothesis, or false indications of nonlinearity. It was for this case that AAFT surrogates were introduced, which account for this nonlinearity introduced into the system during measurement by ensuring that the resulting surrogates have the same amplitude distribution as the original data. This is in contrast to FT surrogates, which usually have a Gaussian distribution of values.  $\nu$  was calculated for system (34) and its surrogates, but this time with an invertible transformation  $x_n = (s_n)^3$  applied to the time series. The results, shown in Figure 21(C), demonstrate the failure of FT surrogates in this case, with them incorrectly identifying nonlinearity in the data, purely as a result of the measurement transformation. This demonstrates the benefit of the amplitude adjustment step in AAFT surrogates, but it should be noted that the condition that the data transformation should be invertible is very severe. When repeating the same test with a non-invertible transformation of the data  $x_n = (s_n)^2$ , AAFT surrogates fail, and erroneously detect nonlinearity due only to this transformation (see Figure 21(D)).

From these results IAAFT, WIAAFT and IDFS surrogates appear to be more robust to these constraints. IAAFT are the fastest of these, and thus are ideal for testing data in which both the underlying dynamics and the effects of the measurement process are unknown beforehand.

#### 9.1.2. Finding nonlinearity using Volterra polynomials

Volterra polynomials (see Section 6.3) can also be used to search for nonlinearity in data. The idea is that nonlinear signals will be better represented by nonlinear polynomials than linear signals. Therefore, the goodness of fit between the signal and polynomials of an increasing number of linear and then nonlinear terms is calculated. Again, to find the significance of the results, surrogates are required.

The performance of the surrogates developed for the detection of nonlinearity were compared using Volterra polynomials in the same four cases as in the previous section: the ARMA model presented in Eq. (34), invertible and noninvertible transformations of this data, and the  $x$  component of the Rössler system presented in Eq. (33). Volterra polynomials were calculated for the original data, and for 100 FT, AAFT, IAAFT, IDFS and WIAAFT surrogates for each case. The null hypothesis was rejected, i.e. the system was considered to be nonlinear, if the increase in the goodness of fit of the polynomial to the data following the addition of nonlinear terms increased

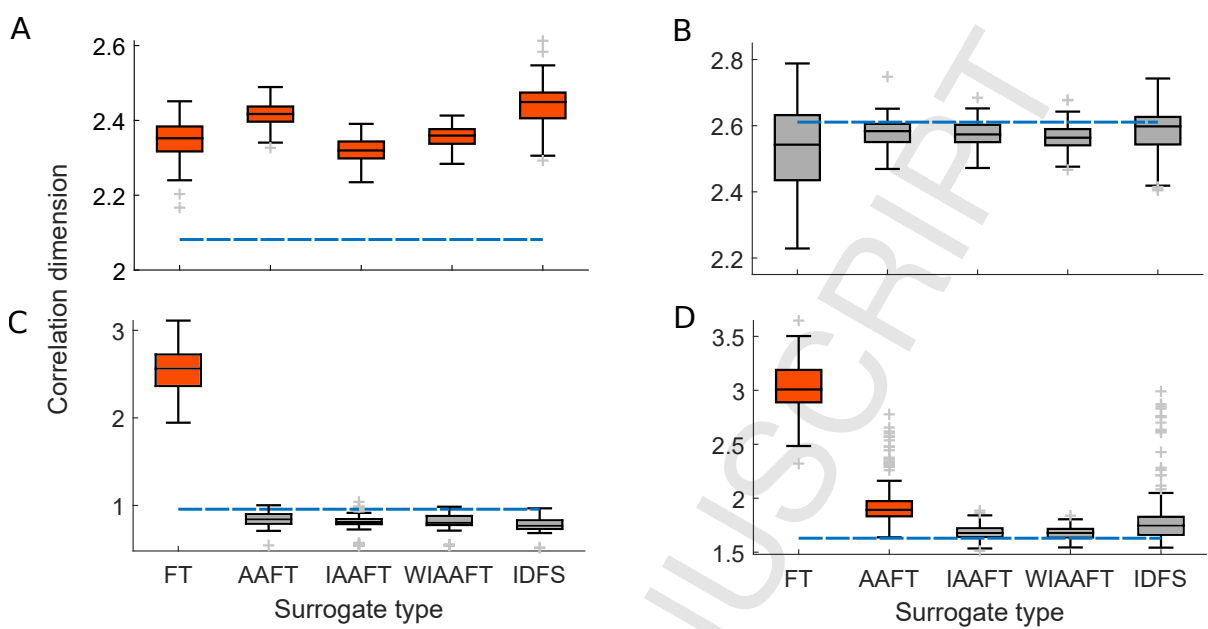


Figure 21: Comparison of the performance of different surrogates for the detection of nonlinearity using the correlation dimension,  $\nu$ . (A) For chaotic Rössler data (shown in Figure 20(A)), all surrogates reject the null hypothesis, as expected. (B) For the ARMA(3) data (shown in Figure 20(B)) all surrogates fail to reject the null hypothesis, as expected. (C) The invertibly rescaled ARMA(3) data shows the failure of the FT surrogates in this case, erroneously indicating nonlinearity in the data, purely due to the measurement transformation. (D) AAFT surrogates also reject the null hypothesis when the measurement transformation is noninvertible. The blue dashed line is  $\nu$  calculated from the original data sets, and the boxplots show the range of the calculated  $\nu$  in 100 surrogates of each type. Boxes are filled orange if nonlinearity is indicated, and filled grey if not. Significance is defined as the real  $\nu$  being below the 5<sup>th</sup> percentile of the surrogates. Estimated embedding dimensions - (A) 3, (B) 4, (C) 7, (D) 6.

above the 95<sup>th</sup> percentile of the increase in the goodness of fit of 100 surrogates.

The results are shown in Figure 22. As expected, FT surrogates only work well when there is no transformation applied to the ARMA time series. We can also see the expected behaviour of AAFT surrogates, incorrectly rejecting the null hypothesis when the measurement transformation is non-invertible. Surprisingly, they also rejected the null hypothesis when there was no measurement transformation applied. This could be due to the distortions that AAFT can introduce into the power spectrum. IAAFT2 surrogates gave the correct result in all cases, as did WIAAFT surrogates. As some of the incorrect results appear to be in the surrogates with variable power spectra, the test was repeated for IAAFT1 surrogates. The conclusions were the same as for IAAFT2 surrogates, however, the spread of the surrogate values was larger in the case of IAAFT1 surrogates. IDFS surrogates appear to perform well for all linear cases, including transformations, but fail to reject the null hypothesis for the chaotic Rössler system, which rules out their applicability in this case.

#### 9.1.3. Finding oscillations in noisy data using MCSSA

*Simulated data.* Oscillations with time varying frequencies can often be overlooked when applying frequency analysis such as the Fourier transform, due to the broadening of the spectrum. Adding noise to the situation complicates the problem even further. Figure 23 shows the results of MCSSA (see Section 6.5) on a sine wave with time-varying frequency contaminated by very strong AR(1) ( $\rho = 1, \sigma = 1$ , SNR = 0.017) noise. A small bump can be observed in the Fourier spectrum, yet without surrogates it is difficult to know whether this is the signature of a true oscillation. In this case, the wavelet transform does not show any obvious oscillations at 0.2 Hz. In contrast, the MCSSA method reveals a number of significant eigenvalues, related to the time-varying oscillation, around 0.2 Hz as expected. Embedding was performed using a 500 second window and a time delay of 1.

*Application to EEG data.* 1/f type spectra have been widely observed in neurological data, and are a result of the physical structure of neuronal networks and the limited speed of neuronal communication due to axon conduction and synaptic delays [33, 226]. Here, we apply MCSSA to an EEG signal recorded from the occipital lobe (O2 on the standard 10-20 system) of a 50 year old female sitting at rest for 30 minutes. The data were recorded at 1000 Hz, detrended by subtracting a third order polynomial and bandpass filtering within the range 0.005–20 Hz, and resampled to 40 Hz for analysis.

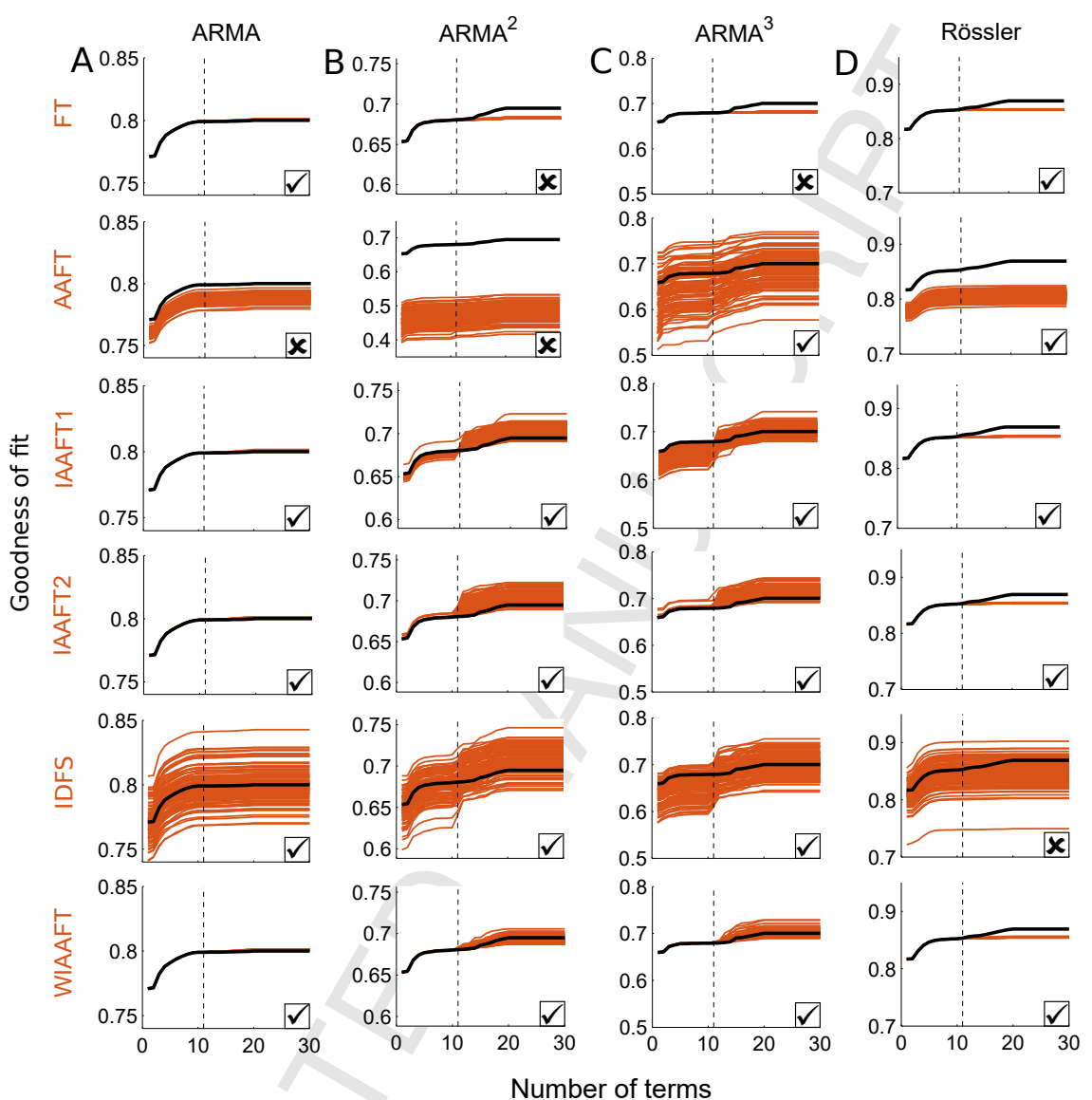


Figure 22: Volterra polynomials comparisons for the linear ARMA cases and the nonlinear chaotic Rössler system. (A) The ARMA signal  $s_n$  (Eq. (34)), (B) the same signal subject to the noninvertible transformation  $(s_n)^2$ , (C)  $s_n$  subject to the invertible transformation  $(s_n)^3$ , and (D) the  $x$  component of the chaotic Rössler system described in Eqs.(33). The results for the data are shown as black lines, and the results for 100 surrogates for each of the four different signals and five surrogate types are shown as orange lines. The point at which nonlinear terms begin to be added is marked as a black vertical dashed line. Based on the expected results, i.e. that the system be identified as linear for (A), (B) & (C), and nonlinear in (D), the success of the surrogates in reaching the correct conclusion is marked on each plot as a tick for a correct result or a cross for an incorrect result. IAAFT and WIAAFT are the only surrogates that provide the correct conclusion in all cases.

The first step was to estimate the parameters of the underlying noise model of the data, as described in Section 4.4. Due to the  $1/f^\alpha$ -like appearance of the power spectrum of the data (see Figure 24(B)) the background spectrum was calculated based on an estimation of  $\alpha$  from the time series. Detrended fluctuation analysis (DFA) was applied to the time series to obtain a DFA exponent  $d$ , which is related to  $\alpha$  by  $\alpha = 2d - 1$  [80]. Using this approach,  $\alpha$  was estimated as 1.02, very close to pink noise (for which  $\alpha = 1$ ). 1000 surrogates were then calculated with this value for  $\alpha$  and used in the analysis. Embedding was performed using a 5 second window and a time delay of 1. Significant eigenvalues were found, and their dominant frequencies investigated in Figure 24. Significant oscillations were found at around 1 Hz and at around 9–10 Hz. The former could be attributed to either the cardiac or delta brainwave activity, whilst the latter falls in the well known alpha frequency band, which from this recording location is likely to be Berger's classical posterior alpha rhythm [227] which is still the best known EEG phenomenon [228].

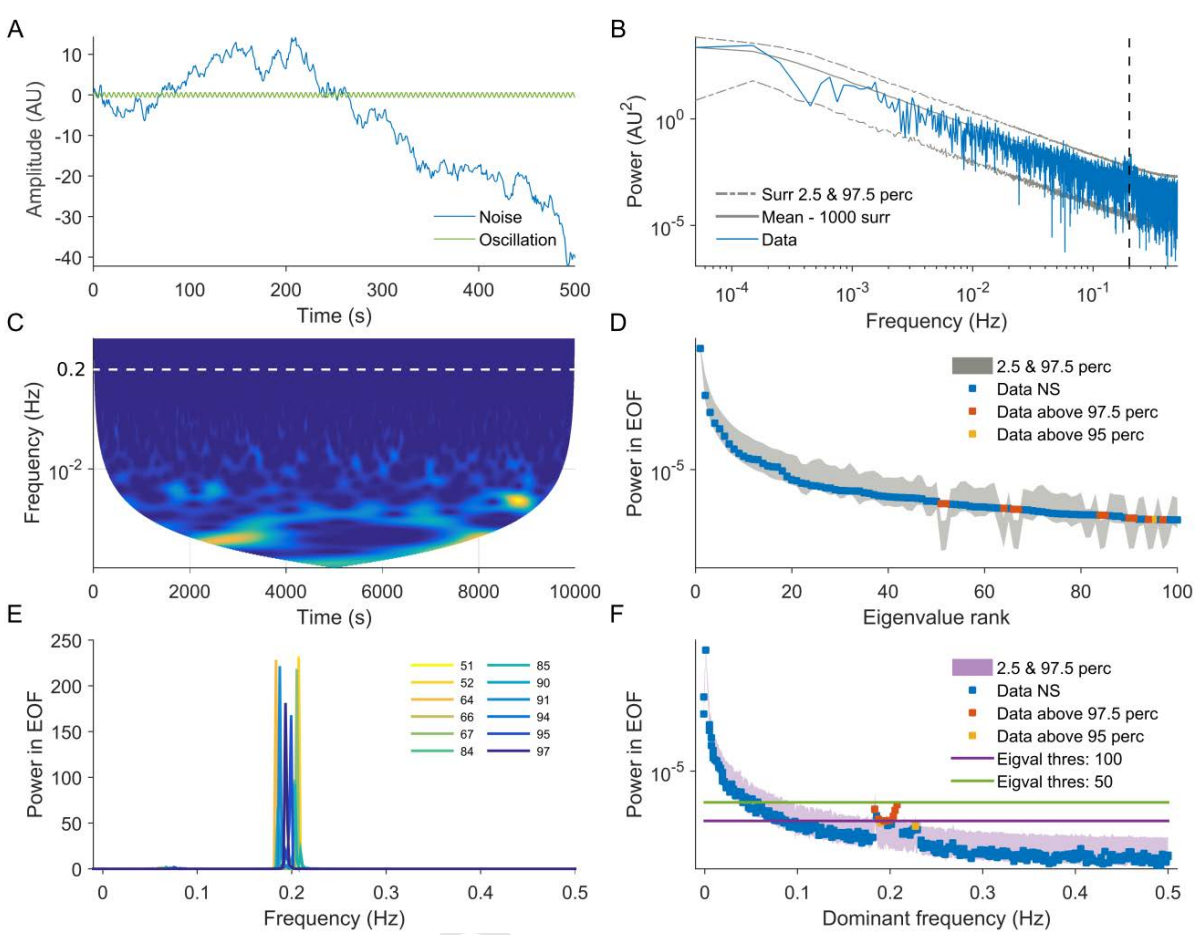


Figure 23: MCSSA analysis applied to a simulated sine wave with time-varying frequency corrupted by very strong autoregressive noise. The signal was simulated for 10,000 seconds at a sampling frequency of 1 Hz, and is comprised of an oscillatory component described by  $0.7 \sin(2\pi ft)$  where  $f = 0.2 + 0.005 \sin(2\pi f_m t)$  and the frequency of modulation  $f_m$  is 0.0001 Hz, added to an AR(1) noise component with  $\rho = 1$  and  $\sigma = 1$ . The signal-to-noise ratio is 0.017. (A) Both components before addition. (B) Fourier spectrum of the data, mean of 1000 AR(1) surrogates (estimated  $\alpha = 0.999$ ), and 2.5 and 97.5<sup>th</sup> percentiles. (C) Wavelet transform (power) of the simulated data. (D) Ranked eigenvalues compared with those from 1000 surrogates. Significant eigenvalues (above the 95<sup>th</sup> percentile of the surrogates) are marked. (E) Fourier spectra of the significant eigenvectors located in (D). (F) Eigenvalues presented in relation to their dominant frequency, as determined in (E).

### 9.2. Synchronization of two coupled oscillators

In this section we investigate the phase synchronization between two simple coupled oscillatory systems and two chaotic systems using phase coherence (see Section 8.1).

Usually, phase coherence between two signals is compared to the distribution of values obtained for the phase coherence between one of the signals (the reference signal) and a set of surrogates of the other one (the surrogated signal). In the case of synchronization testing, the null hypotheses for different surrogates are that the surrogated signal is: RP - uncorrelated noise with some distribution; FT - independent stationary linear Gaussian noise; AAFT & IAAFT - invertibly rescaled independent stationary linear Gaussian noise; PPS, TS & CPP - independent signal with no intercycle correlations and time-shifted - independent signal with intercycle behaviour preserved. Note that the FT null hypothesis is equivalent to the null hypothesis that observed synchronization is just an artifact of bias in frequency, while IAAFT is for both frequency and distribution.

Both systems were simulated using 6th order Runge-Kutta with analytical coefficients given by the first table on p. 14 in [229]. All signals produced were preprocessed as previously discussed (Section 4.3). Where embedding is required for the surrogates, the embedding dimension is estimated using false nearest neighbours, and the same embedding dimension is used for the original data and the surrogates.

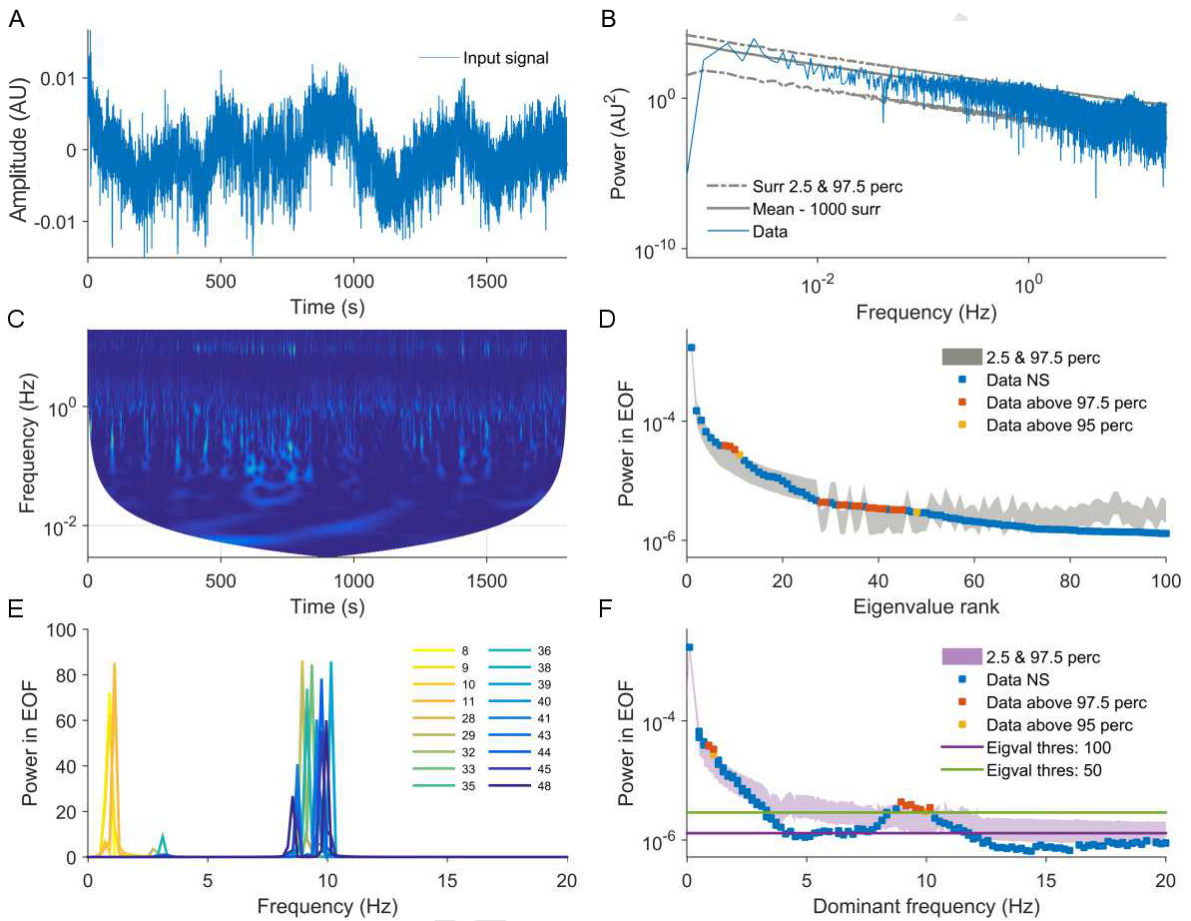


Figure 24: MCSSA analysis applied to a 30 minute EEG recording from the occipital lobe (O2) of a 50 year old female. The time series was resampled from 1000 Hz to 40 Hz. (A) Original detrended time series. (B) Fourier spectrum of the data, mean of 1000  $1/f^\alpha$  surrogates (estimated  $\alpha = 1.02$ ), and 2.5 and 97.5<sup>th</sup> percentiles. (C) Wavelet transform (power) of the experimental data. (D) Ranked eigenvalues compared with those from 1000 surrogates. Significant eigenvalues (above the 95<sup>th</sup> percentile of the surrogates) are marked. (E) Fourier spectra of the significant eigenvectors located in (D). (F) Eigenvalues presented in relation to their dominant frequency, as determined in (E). These results indicate that there are significant oscillations in the EEG around 1 Hz and around 10 Hz, corresponding to the cardiac and alpha wave intervals, respectively.

### 9.2.1. Simple oscillators

We begin with the bivariate case of two coupled oscillators. Here, we consider two coupled phase oscillators, described by the Kuramoto model (as described in detail in [230]) as follows:

$$\begin{cases} \frac{d\phi_1}{dt} = (\omega - \Delta\omega) + \epsilon \sin(\phi_2 - \phi_1) + \sigma\eta_1(t) \\ \frac{d\phi_2}{dt} = (\omega + \Delta\omega) + \epsilon \sin(\phi_1 - \phi_2) + \sigma\eta_2(t), \end{cases} \quad (35)$$

where  $\phi_{1,2}$  are phases of the respective oscillators,  $\omega$  is their common frequency,  $2\Delta\omega$  is the detuning (the difference between their frequencies),  $\epsilon$  is the coupling strength and  $\sigma$  is the noise multiplier.  $\eta_{1,2}(t)$  are two independent realisations of white Gaussian noise such that  $\langle \eta_i(t), \eta_j(\tau) \rangle = \delta(t - \tau)\delta_{ij}$ . In general, one has some functions  $f_{1,2}(\phi_1, \phi_2)$  instead of the  $\sin(\phi_{2,1} - \phi_{1,2})$  in Eqs. (35) in addition to different coupling strengths  $\epsilon_{1,2}$  and dynamical noise intensities  $\sigma_{1,2}$ , meaning that the influence of each oscillator on the other may not be equivalent and may be quite complicated. For simplicity, here we consider the case of equivalent bidirectional coupling, and equivalent noise intensities for each oscillator.

To investigate phase synchronization in this system, the relative phase difference  $\psi = \phi_2 - \phi_1$  was investigated. Subtracting the first equation from the second in Eqs. (35) gives:

$$\frac{d\psi}{dt} = 2\Delta\omega - 2\epsilon \sin \psi. \quad (36)$$

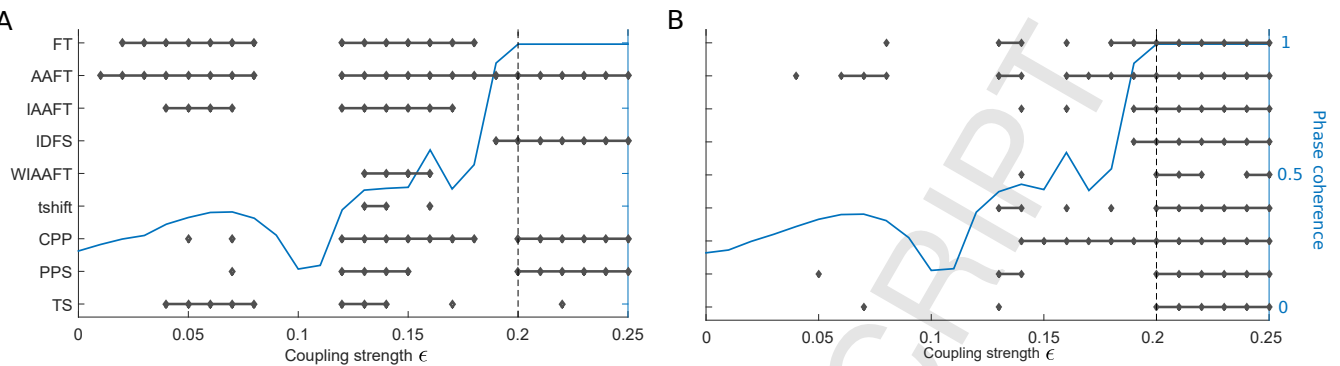


Figure 25: Surrograms for the Kuramoto system with changing coupling  $\epsilon$  for a non time-varying (A) and a time-varying case (B) (see main text for details). Synchronization occurs at  $\epsilon = 0.2$  (without noise). Blue - phase coherence of system, grey lines and diamonds indicate the values of  $\epsilon$  for which the null hypothesis is rejected based on the coherence in the data being above the 95<sup>th</sup> percentile of 100 of each type of surrogate presented.

For  $\epsilon \geq \Delta\omega$  this equation has a stable fixed point  $\psi = \arcsin \frac{\Delta\omega}{\epsilon}$ . This means that for  $\epsilon \geq \Delta\omega$  phases  $\phi_1(t)$  and  $\phi_2(t)$  are completely synchronized, although this will be slightly altered with the addition of noise. For  $0 < \epsilon < \Delta\omega$  the system is only partially synchronized, while for  $\epsilon = 0$  the phases are completely independent.

In reality, we do not directly observe the phases of oscillators, but some periodic functions of them. Thus, for the two signals arising from Eqs. (35), they can be viewed as  $f_{1,2}(\phi_{1,2}(t))$  where  $f_{1,2}$  are some periodic functions. Providing they meet the periodicity restriction  $f_{1,2}(\phi_{1,2}(t) + 2\pi) = f_{1,2}(\phi_{1,2}(t))$ , the functions could be anything, for example a sine function  $f_{1,2}(\phi_{1,2}(t)) = \sin \phi_{1,2}(t)$  or a saw-tooth function  $f_1(\phi_1(t)) = \mod(\phi_1(t))$ . This makes the analysis of phase synchronization rather nontrivial. However, methods of phase extraction (see Appendix A.3) solve this problem to a large extent.

We now compare the performance of different surrogates in the case of the underlying phase dynamics described by Eqs. (35). We consider the case for both the fixed frequency  $\omega = 2\pi$  and the variable frequency  $\omega = 2\pi + 0.25 \sin(0.2\pi t)$ ,  $\Delta\omega = 0.2$  and  $\sigma = 0.01$ . The system was integrated for 75s with 0.01s time step. The parameters were chosen such that the phase coherence will be non-zero even for zero coupling, to mimic a situation where the presence of synchronization may be falsely indicated.

The system was integrated for different coupling strengths  $\epsilon$  ranging from 0 (completely independent signals) to 0.25 (complete synchronization begins at  $\epsilon = 0.2$ ). To eliminate the transient period, we only consider the last third of the signals (25s, 2500 data points). In addition to the dynamical noise, all signals were contaminated with observational noise with noise-to-signal ratio ( $NSR = 0.1$ ). To ensure clear comparisons between simulations, the same realizations of dynamical and observational noise were added for each  $\epsilon$ .

We consider as a simple example that the signals are sine functions of the phases  $f_{1,2}(\phi_{1,2}) = \sin(\phi_{1,2})$ . The phase coherence between the oscillators and its dependence on coupling strength  $\epsilon$  is shown in Figure 25. Phase coherence was considered significant if it was above the 95<sup>th</sup> percentile of 100 surrogates of the second signal, as determined by rank ordering.

The results are shown in a form which we will refer to as a ‘surrogram’ (see Figure 25). For each coupling strength, the phase coherence (see Section 8.1) was calculated between the numerically simulated phase oscillators described in (35) with a sine function applied. 100 surrogates of the second oscillator were generated for each of the 9 surrogate types shown in Figure 25. Phase coherence was then calculated between the first phase oscillator and the surrogates of the second oscillator to give a distribution of surrogate phase coherence values. For each coupling  $\epsilon$  and each surrogate type, the real phase coherence was compared to the distribution of 100 surrogate values and deemed to be significant if the real coherence value was above the 95<sup>th</sup> percentile of the surrogate distribution. If significance was found, i.e. the null hypothesis was rejected, it was marked on the surrogram as a grey diamond. Consecutive rejections are marked as grey lines. This provides a map of the performance of each surrogate type. Within the same plot, the dependence of the phase coherence of the simulated data on the coupling strength  $\epsilon$  is plotted to show the real values of phase coherence in the system.

From Figure 25(A) it can be seen that for the non time-varying case, out of FT, AAFT and IAAFT surrogates, only AAFT indicate significance in the fully synchronous regime. This is related to the fact that when two sinusoids are completely synchronized, as they are in this case above values of  $\epsilon = 0.2$ , it is almost impossible to say whether they are really interdependent or whether they have the same frequencies by chance. The AAFT significance at this perfect coupling is simply related to the fact that AAFT surrogates do not reproduce pure harmonics, contrary to FT and IAAFT, highlighting the serious disadvantage of AAFT surrogates that they may indicate significant

1  
2  
3 synchronization even at zero coupling. In this case, IDFS surrogates only show significance for very high values of  
4  $\epsilon$ , suggesting they may not be as useful for the study of weak interdependence. It can also be seen from the figure  
5 that CPP surrogates also indicate significance in the completely synchronized regime, and also for some weaker  
6 coupling strengths. The only other surrogates to indicate significant synchronization in this case are PPS. These  
7 results show how varied and unreliable the results can be when trying to test whether perfectly coherent sinusoids  
8 are synchronized. Out of all methods, time-shifted surrogates appear to have the worst performance.  
9

10 To test a more realistic case, shown in Figure 25(B), the natural frequency  $\omega$  was allowed to vary according to  
11  $\omega = 2\pi + 0.25 \sin(0.2\pi t)$ . In this case, significant coherence is indicated by all surrogates after  $\epsilon = 0.2$ , and less  
12 overall before this threshold.

13 When using surrogates in bivariate systems, the question arises of which signal to calculate surrogates from.  
14 Consider two signals to be tested using surrogates. We name the first signal the reference signal, and the second  
15 signal the surrogated signal. It should be noted that if the reference signal was linear yet the surrogated signal were  
16 to be highly nonlinear, for example a sawtooth wave, the FT, AAFT and IAAFT methods would reject the null  
17 hypothesis even if the signals were completely independent, purely because of the nonlinearity present in the signal.  
18 Therefore we cannot conclude anything about synchronization in this case. Because of this, it is recommended that  
19 given two signals, the significance levels of phase coherence based on FT, AAFT and IAAFT surrogates should be  
20 concluded from calculating surrogates from the most linear signal of the two. This can be decided by extracting the  
21 phases of both signals, and checking which extracted phases most closely resemble their respective original signals.  
22 If both signals are highly nonlinear, these methods will not be suitable, and surrogates which include possible  
23 nonlinearity in their null hypothesis should be used. CPP, time-shifted, PPS and twin surrogates should not be  
24 affected by these issues.  
25

### 26 9.2.2. Chaotic oscillators

27 We now consider a system of chaotic oscillators. A positive Lyapunov exponent (see Section 6.6) is a condition  
28 for chaos and represents sensitivity to initial conditions. Each chaotic oscillator has at least one zero Lyapunov  
29 exponent, some number of negative ones, and at least one positive one. For simplicity, consider two three dimensional  
30 chaotic oscillators (such as the Lorenz or Rössler systems), both having one positive, one negative, and one zero  
31 Lyapunov exponent. The uncoupled system will then have two positive, two negative, and two zero exponents.  
32 Two zero Lyapunov exponents correspond to limit cycles in the oscillators and represent their oscillatory behaviour.  
33 When we couple these systems, the Lyapunov exponents of the joint system change depending on coupling strength.  
34 When increasing the coupling strength, one of the zero Lyapunov exponents of the joint system may become negative  
35 ( $\epsilon = 0.04$  for the Rössler system below, and  $\epsilon = 0.35$  for Lorenz). When this happens, it means that the two limit  
36 cycles corresponding to each chaotic oscillator are reduced to one, since there is now only one zero Lyapunov  
37 exponent. The oscillatory behaviour of the two systems becomes entrained, and they oscillate in phase, thus  
38 having a joint limit cycle, deviations from which exponentially decrease. This describes the transition to phase  
39 synchronization in chaotic systems [178].  
40

41 Increasing the coupling strength further, the remaining zero Lyapunov exponent may also become negative,  
42 while one of the positive Lyapunov exponents becomes zero ( $\epsilon = 0.12$  for the Rössler system below, and  $\epsilon = 0.75$   
43 for Lorenz), indicating a transition to so called lag synchronization [231]. In this regime, one system mimics the  
44 other, but with a time lag. Increasing the coupling strength even further reduces this lag and moves the system  
45 towards complete synchronization, which may be interrupted by regions of periodic behaviour in which the system  
46 is not chaotic.  
47

48 In this section we investigate the performance of surrogates, again combined with the phase coherence, in the  
49 well known Rössler and Lorenz systems. Phase synchronization of chaotic oscillators was discussed for the example  
50 of coupled Rössler systems in [178]. We consider the system of two bidirectionally coupled Rössler oscillators, given  
51 by the set of equations [178, 231]:  
52

$$\begin{cases} \dot{x}_{1,2} = -(\omega_{1,2})y_{1,2} - z_{1,2} + \epsilon(x_{2,1} - x_{1,2}) \\ \dot{y}_{1,2} = \omega_{1,2}x_{1,2} + ay_{1,2} \\ \dot{z}_{1,2} = b + z_{1,2}(x_{1,2} - c), \end{cases} \quad (37)$$

53 with  $a = 0.165$ ,  $b = 0.2$ ,  $c = 10$  and  $\omega_{1,2} = \omega \pm \Delta\omega$  where  $\omega = 0.97$  and  $\Delta\omega = 0.02$ , as used in [231] to establish  
54 mainly chaotic behaviour of the joint system. The system was integrated for 5000s with time step 0.1s for coupling  
55 strengths  $\epsilon$  ranging from 0 to 0.25 with a step of 0.005. An example of the Rössler oscillator system (37) and its  $x$   
56 components for zero coupling and  $\epsilon = 0.05$  is shown in Figure 26.

57 To compare surrogate performance, we consider the evolution of the system during the last 200s to discard  
58

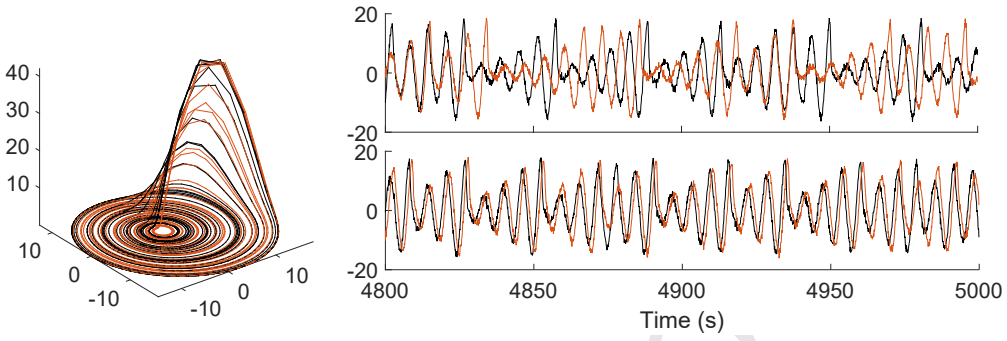


Figure 26: Rössler system. Top -  $x$  component with  $\epsilon=0$ , bottom -  $x$  component when  $\epsilon=0.05$ . Black and orange lines represent the two oscillators.

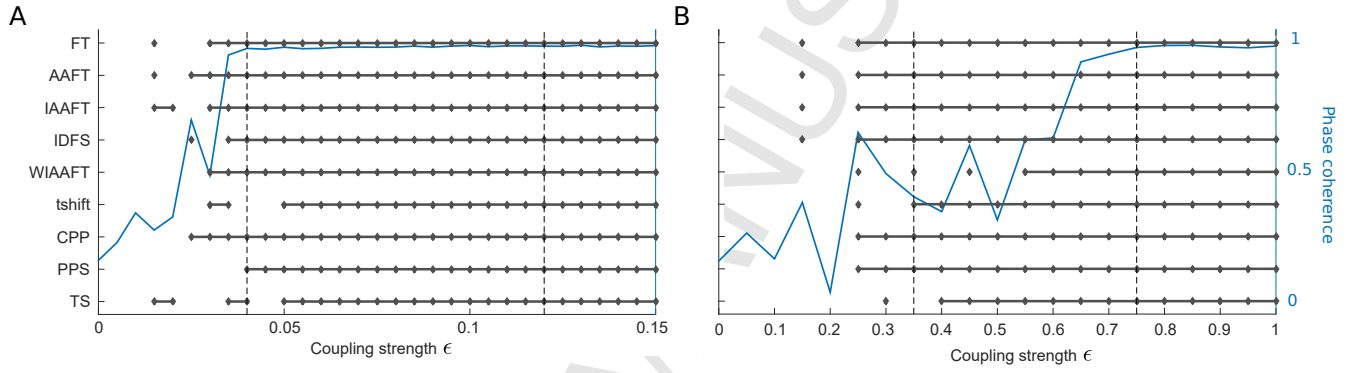


Figure 27: (A) Surrogram for the Rössler system with changing  $\epsilon$ . (B) Surrogram for the Lorenz system with changing  $\epsilon$ . Blue - phase coherence of system, grey - rejection of null hypothesis based on the coherence in the data being above the 95<sup>th</sup> percentile of 100 of each type of surrogate presented. Vertical dotted lines from left to right indicate the points of onset of phase synchronization (first) and lag synchronization (second).

transients periods and establish non-vanishing values of phase coherence at zero coupling. The signals were contaminated with 0.1 *NSR* observational noise. Phase synchronization is investigated between the  $x$  components of the system, with phases extracted using the Hilbert transform. As in the previous case, phase coherence was calculated for a range of couplings in the simulated data, and in all surrogate types. For clearer comparison, initial conditions and observational noise remained the same for all cases. Figure 27(A) compares the performance of different surrogates for this case.

This test was repeated on the coupled Lorenz system, given by:

$$\begin{cases} \dot{x}_{1,2} = \sigma(y_{1,2} - x_{1,2}) \\ \dot{y}_{1,2} = x_{1,2}(\rho - z_{1,2}) - y_{1,2} \\ \dot{z}_{1,2} = x_{1,2}y_{1,2} - (\beta_{1,2})z_{1,2} + \epsilon(z_{2,1} - z_{1,2}), \end{cases} \quad (38)$$

where  $\sigma = 10$ ,  $\rho = 28$ ,  $\beta_{1,2} = \beta \pm \Delta\beta$  where  $\beta = 8/3$  and  $\Delta\beta = 0.01$ . The system was integrated for 5000s with time step 0.01s for coupling strength  $\epsilon$  from 0 to 1.5 with a step of 0.05. To evaluate the performance of different surrogates, we consider the last 75s of the  $z$ -components of system (38), contaminated by 0.1 *NSR* noise. Phases were extracted using the Hilbert transform. Figure 27(B) compares the performance of different surrogate types for this case.

For the Rössler case and Lorenz case, all surrogates performed quite well. For the Lorenz system, contrary to the Rössler, transition to phase synchronization is not accompanied by such rapid growth of phase coherence. However, the picture almost stays the same, which proves that the surrogates do not only indicate significance for large phase coherence values, but can ‘feel’ transitions in the system dynamics. As in the simple case, it should be noted that for FT-based surrogates the nonlinearity in the signals may cause rejection of the null hypothesis even with no coupling.

Whilst all the surrogates shown in this comparison appear to be applicable to synchronization, at least when using the measure of phase coherence, it should be noted that PPS, CPP, TS and time-shifted surrogates actually

1  
2  
3 test the null hypothesis of *independence* rather than phase synchronization. Some of them do indeed indicate  
4 interdependence before the synchronization level, but in theory should indicate significance for all finite couplings.  
5 This demonstrates that they may not have very high power when searching for weak coupling.

### 6 9.2.3. Phase coherence in real biological data

7 Here, we will compare the performance of different surrogate types for the calculation of wavelet phase coherence.  
8 When using a complex wavelet such as the Morlet wavelet in the continuous wavelet transform, the resulting  
9 coefficients will also be complex, and provide both amplitude and phase information at each time and scale. The  
10 instantaneous phase information from the wavelet transforms of two signals can be extracted and used to monitor  
11 their phase difference over time, and may reveal phase relationships between them.

12 Wavelet phase coherence is calculated by first extracting the instantaneous phases  $\phi_{1k,n}$  and  $\phi_{2k,n}$  at each time  
13  $t_n$  and frequency  $f_k$  for both signals and finding their relative phase difference  $\Delta\phi_{k,n} = \phi_{2k,n} - \phi_{1k,n}$ . The sine  
14 and cosine components of the phase differences are then calculated and averaged in time, and the wavelet phase  
15 coherence defined as [46]:

$$16 C_\phi(f_k) = \sqrt{\langle \cos \Delta\phi_{k,n} \rangle^2 + \langle \sin \Delta\phi_{k,n} \rangle^2}. \quad (39)$$

17 The wavelet phase coherence  $C_\phi(f_k)$  will have a value between 0 and 1, with a value of 0 corresponding to a phase  
18 difference continuously changing in time, and a value of 1 indicating a phase relationship which remains constant  
19 in time. The phase coherence described here is the same quantity described in Section 9.2, but with a dependence  
20 on frequency. As for the phase coherence discussed previously, in reality wavelet phase coherence can have a range  
21 of values for which it is difficult to conclude interdependence without the use of surrogates. Calculation of wavelet  
22 phase coherence also highlights another issue, that the coherence between even two completely independent signals  
23 will increase at lower frequencies and tend towards 1. Thus, surrogates are also required to account for this bias.

24 *Cardiorespiratory coherence.* Respiratory sinus arrhythmia (RSA) is a well known phenomenon in which the heart  
25 rate is modulated by the breathing. Using wavelet phase coherence analysis, significant coherence was demonstrated  
26 between the instantaneous heart rate (IHR) and breathing in humans [27], and this coherence was found to decrease  
27 with age. This study [27] used intersubject surrogates, but as discussed, there is not always enough data available for  
28 this to be a viable option. Here, we compare some of the discussed surrogate types in an example cardiorespiratory  
29 system.

30 Electrocardiogram (ECG) and breathing signals were recorded for 40 minutes in a 26 year old male at a sampling  
31 frequency of 1200 Hz. ECG measures the electrical activity of the heart as it is beating, while the respiration signal  
32 can be recorded from the mechanical movement of the chest. The ECG was recorded using a 3 lead setup, and  
33 resampled to 40 Hz and the instantaneous heart rate (IHR) extracted from the wavelet transform using ridge  
34 extraction (see Appendix A.3). The IHR and respiration signals were then both resampled to 10 Hz for analysis.  
35 Their wavelet phase coherence was calculated for a frequency range between 0.005 – 2 Hz. The wavelet phase  
36 coherence between the IHR and 100 surrogates of the respiration signal were then calculated for different surrogate  
37 types, as shown in Figure 28. Significance levels were calculated as the 95<sup>th</sup> percentile of the surrogates. Intersubject  
38 surrogates were calculated from 100 mismatched IHR - respiration pairs from the same data set.

39 Figure 28 does not show large differences between the significance levels for each of the 10 compared surrogate  
40 types, except WIAAFT surrogates which indicate a higher significance level than the other surrogates at the  
41 respiration frequency, and a lower significance level at frequencies below 0.01 Hz. This may be due to the similarity  
42 of the WIAAFT surrogates to the original data not completely removing the correlations between the two signals.  
43 A number of other surrogates also show a slightly lower threshold at lower frequencies (see Figure 28).

### 44 9.3. Inferring the nature of coupling

45 When trying to extract information from bivariate data arising from two systems, care must be taken to formulate  
46 the correct null hypothesis. In the previous section, wavelet phase coherence was evaluated between time series. A  
47 significance level based on there being no coherence between data was used. However, it should be emphasised that  
48 coherence found above this level cannot provide any information about phase coupling or interactions that may or  
49 may not be present in the system, as coherence can be observed in completely independent systems if their phase  
50 difference does not change over time. Therefore, to infer this extra information from time series, the null hypothesis  
51 must be altered to reflect this.

52 Surrogate data can be applied to the problem of inferring not only that two oscillators are in sync, but also how  
53 their phases are coupled by extracting information about their coupling functions [177] over time using dynamical  
54 inference (see Section 8.4). A detailed explanation and a MatLab toolbox for the implementation of a DBI method

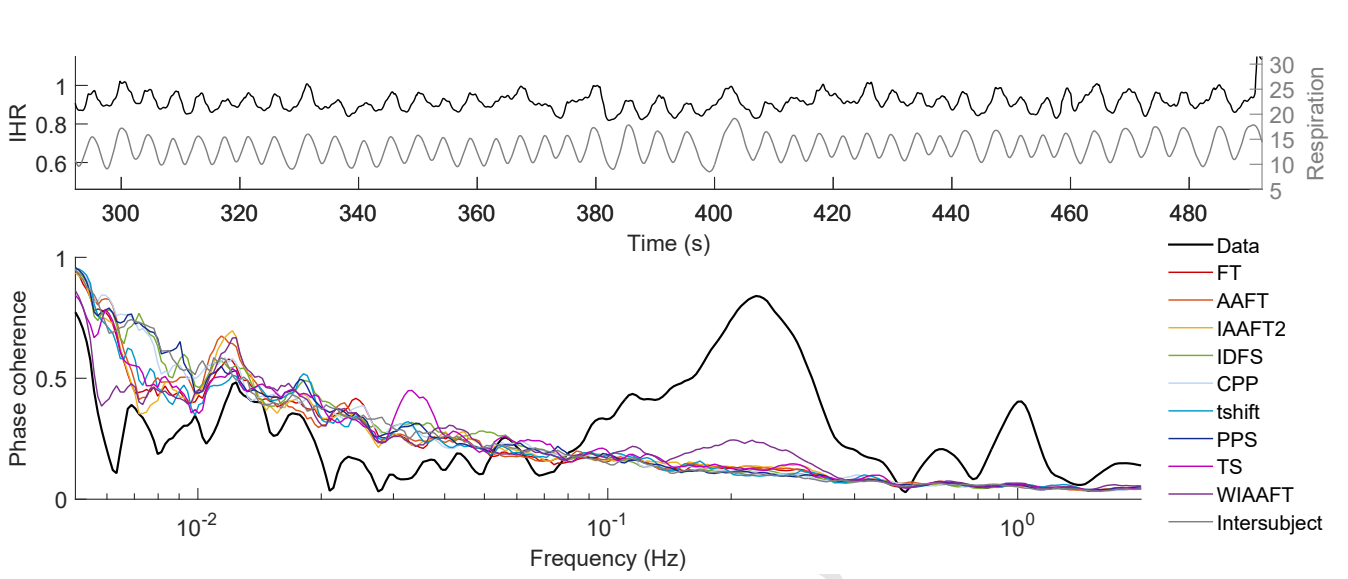


Figure 28: (A) Example segments of the instantaneous heart rate and smoothed respiration signals. (B) Wavelet phase coherence between the signals in (A) compared with the significance levels of the surrogate types shown, calculated as the 95<sup>th</sup> percentile of 100 surrogates.

can be found in [186]. This method can utilise the phase information from two or more systems to infer the coupling strength, direction of coupling, and whether the system is synchronized.

In particular, the inferred coupling strength provides a measure of the interaction between systems. Like the measures discussed previously, it is impossible to conclude whether an obtained coupling strength is significant without the use of surrogates.

### 9.3.1. Coupling in simple phase oscillators

Many biomedical signals contain more than one oscillatory mode of interest. One example of this are EEG signals, which can be separated into five different frequency bands, corresponding to different processes in the brain [33]. The characteristics of these oscillations can provide a lot of information about brain function [232]. It has also been shown that oscillations observed in the same signal may be phase coupled, i.e. the phase of one oscillator may influence the phase of the other [233]. This type of coupling can be investigated using dynamical Bayesian inference (DBI). From the time evolution of the phases of two oscillators, DBI can infer the strength and the direction of the coupling, and how it varies in time. Like many other methods that we have discussed, the absolute value of coupling strength obtained in this way may be difficult to interpret without the use of surrogates to determine a baseline value that would be obtained in the absence of coupling.

To demonstrate the use of surrogates in the calculation of coupling strength between oscillators, we begin with a pair of coupled phase oscillators,

$$\begin{cases} \dot{\phi}_1(t) = \omega_1(t) + a_1 \sin(\phi_1(t)) + a_3 \sin(\phi_2(t)) + \xi_1(t) \\ \dot{\phi}_2(t) = \omega_2(t) + a_2(t) \sin(\phi_1(t)) + a_4 \sin(\phi_2(t)) + \xi_2(t), \end{cases} \quad (40)$$

where  $\xi_1, \xi_2$  are uncorrelated white Gaussian noise such that  $\langle \xi_i(t) \xi_j(\tau) \rangle = \delta(t - \tau) \delta_{ij}$ ,  $a_n$  are coupling strength parameters, and  $\omega_1, \omega_2$  are the natural frequencies of the respective oscillators. The frequencies were set to have a ratio of 10:1, as  $\omega_1 \approx 2 = 0.32 \cdot 2\pi$  and  $\omega_2 \approx 20 = 3.2 \cdot 2\pi$ . The coupling strength parameters were set as  $a_1 = 0.2$ ,  $a_2(t) = 6 \cdot (1 + \sin(t/50))$ ,  $a_3 = 0$  and  $a_4 = 0.2$ .

This produces a system with constant weak self coupling (defined by parameters  $a_1$  and  $a_4$ ) and a unidirectional time-varying coupling (defined by  $a_2$ ) from the slower oscillator ( $\phi_1$ ) to the faster oscillator ( $\phi_2$ ). The coupling strength of the interaction  $x_1 \rightarrow x_2$  is defined as the Euclidean norm of the direct coupling and self-coupling parameters, i.e.  $\sqrt{a_2^2 + a_4^2}$ . The system (40) was integrated with a stochastic second-order Heun scheme, for 500 seconds, with a time step of 0.01s, resulting in the solutions  $\phi_1(t)$  and  $\phi_2(t)$ .

In reality, what will be measured is not the phases of the oscillations, but some function of them. Thus, more

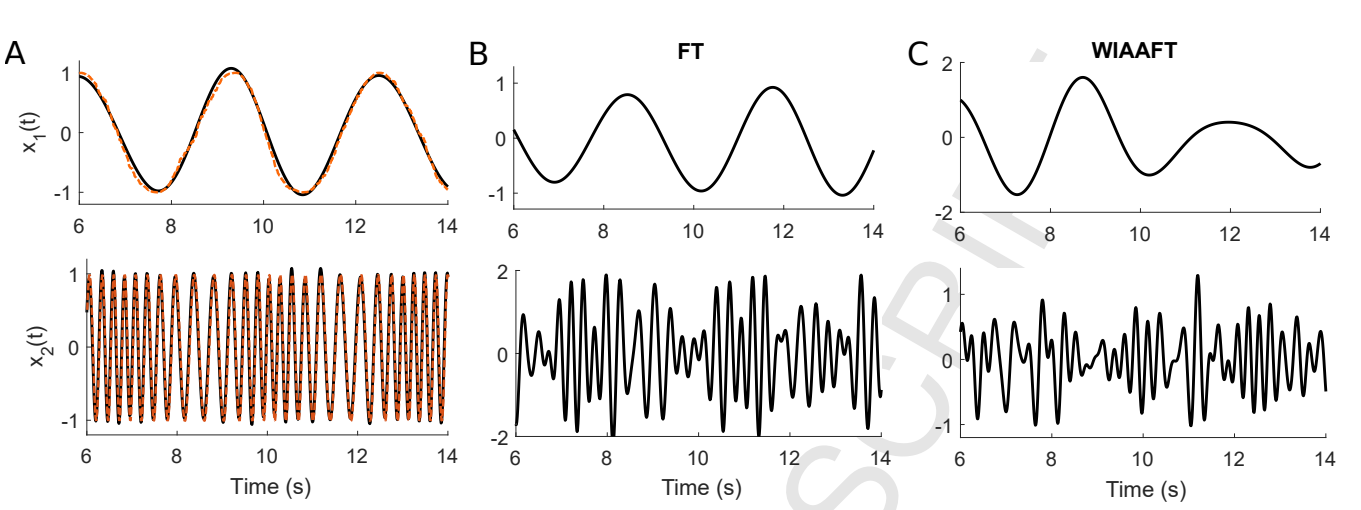


Figure 29: (A) 8 second examples of the time series of the coupled oscillators for  $x_1(t)$  (top) and  $x_2(t)$  (bottom). The original numerically generated time series (Eqs. 41) are shown as orange dashed lines. The two oscillations as filtered from  $s(t) = x_1(t) + x_2(t)$  are shown as solid black lines. (B) The two oscillations bandpass filtered from a FT surrogate of  $s(t)$  and (C) the two oscillations bandpass filtered from a WIAAFT surrogate of  $s(t)$ .

realistic signals were created by applying the cosine function to the phases,

$$\begin{aligned} x_1(t) &= \cos(\phi_1(t)), \\ x_2(t) &= \cos(\phi_2(t)). \end{aligned} \quad (41)$$

As discussed, coupled oscillators regularly manifest within the same signal, thus the final simulated time series consists of the sum of these modes,

$$s(t) = x_1(t) + x_2(t). \quad (42)$$

Considering our time series  $s(t)$ , the first step is to identify any oscillatory modes and their frequency ranges. As we already know their locations, we can bandpass filter within the range  $[\omega_i - \frac{\omega_i}{2}; \omega_i + \frac{\omega_i}{2}]$  for each oscillator. If the frequencies were not known beforehand, time-frequency analysis or nonlinear mode decomposition could be used to locate and extract them (see Appendix A.3).

Once the two separate oscillations have been extracted from the time series using Butterworth filtering, the next step is to calculate their phases in preparation for the dynamical Bayesian inference. The phases of each mode were extracted using the Hilbert transform (see Appendix A.3.1).

The two extracted phase time series were then used as input into DBI in order to evaluate its performance in inferring the time-varying coupling strength of  $a_2$ . Figure 30(A) shows the successfully inferred coupling strength of  $a_2$  compared to the numerical coupling and the coupling from the raw phases. The method not only infers a correct value of the coupling strength but can also follow its time evolution.

When the coupling strength is unknown prior to the inference, surrogates must be used to generate a level above which the coupling strength can be considered as significant. To test the null hypothesis of no coupling between oscillators, we compared the performance of three surrogate types: cyclic phase permutation (CPP), Fourier transform (FT) and wavelet iterative amplitude adjusted Fourier transform (WIAAFT) surrogates.

The most natural choice are CPP surrogates, which work directly with the phases, and remove couplings between successive cycles in the time series. FT surrogates randomize the phase information in the original data, so should also remove any phase coupling. The performance of WIAAFT was also evaluated to test whether their extra constraint of matching temporal characteristics of the data has any effect on their ability to test for phase coupling.

Surrogates were calculated from the original time series  $s(t)$  following preprocessing as discussed in Section 4.3, which reduces the available data points, and results in fewer windows for which the coupling is inferred. This explains why FT and WIAAFT (blue and pink shades) are truncated before CPP (green) in Figure 30.

FT and WIAAFT surrogates were calculated directly from  $s(t)$ , whilst CPP surrogates were calculated from the extracted phases obtained from bandpass filtering and Hilbert transforming  $s(t)$  in the frequency ranges of interest. The phases of the FT and WIAAFT surrogates were extracted in the same way as for the original time series.

Figure 29(A) shows the time series resultant from the numerically generated phases in thin dashed lines and the output of the reconstruction and filtering procedure in solid lines. It can be noted that the two almost overlap.

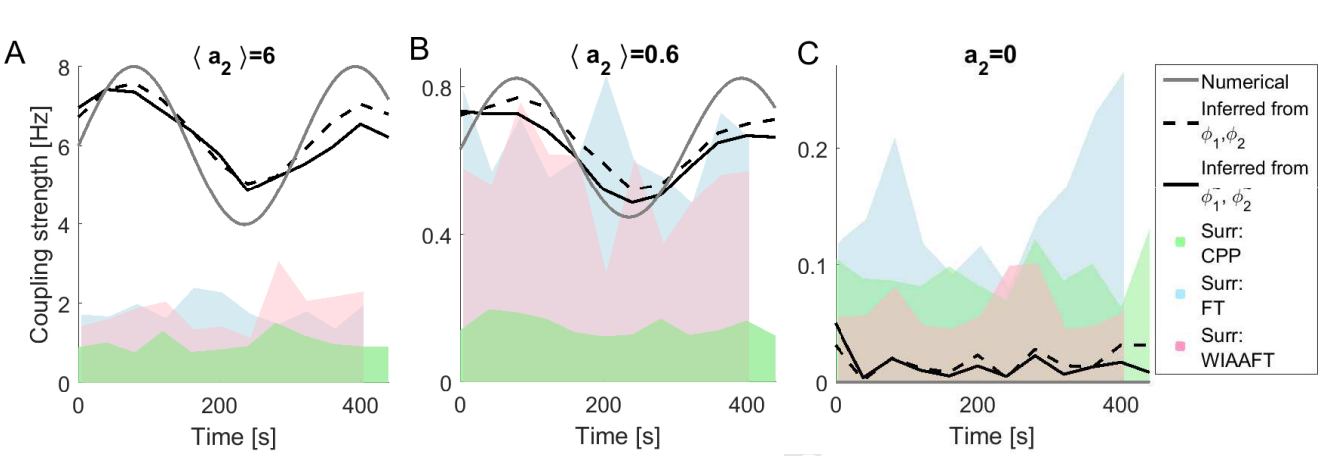


Figure 30: (A) Results of the inferred coupling strength  $a_2$  in Eqs. (40) from the dynamical Bayesian inference with finite coupling  $a_2 = 6 \cdot (1 + \sin(t/50))$ . (B) Results with finite coupling  $a_2 = 0.6 \cdot (1 + \sin(t/50))$ . (C) Results of the inferred coupling strength from the same system but with no coupling. Data shown are: the numerical time evolution of the coupling parameter (grey line), inferred coupling strength from the numerically generated phases (black dashed line) and from the reconstructed phases (black solid line). The 95<sup>th</sup> percentiles of the surrogates are shaded with transparency for CPP (green), FT (light blue) and WIAAFT (pink).

This will not be the case for more complex waveform in real data. The surrogates generated from the original time series are shown in Figure 29(B) for FT and Figure 29(C) for WIAAFT. Both methods aim to preserve the spectral content of the signal, and it can be seen in the bottom panels how the frequency modulation of  $x_2$  is, in both cases, destroyed and converted into a more complicated waveform. The resultant modulated amplitude for the two surrogates is not relevant for the aim of this computation, as the input of the dynamical Bayesian inference is the phase.

Once two sets of phases had been obtained for each surrogate type, they were used as input into DBI and the coupling strength was inferred. In the case of strong coupling ( $a_2 = 6$ ), for all surrogates the coupling strength was much lower in the surrogates than in the real coupled system, demonstrating that they were all successful in rejecting the null hypothesis of no coupling between oscillators in this case (see Figure 30(A)). The significance level was considered as the 95<sup>th</sup> percentile of the range of coupling strengths calculated for each surrogate type. CPP provided the lowest threshold, while FT and WIAAFT generated comparable average levels of surrogates.

In order to investigate this difference further, we repeated the procedure on the same system with weaker direct coupling, i.e.  $a_2 = 0.6$ . Figure 30(B) shows that CPP surrogates still provide the lowest threshold, and validates the inferred coupling strength at all times. On the contrary, both FT and WIAAFT generated a threshold comparable to the numerically set value of the coupling strength, and even higher for several time-windows. This result suggests that CPP surrogates are the most appropriate method to be used in this case.

To validate the result in the absence of coupling, the same procedure was repeated on the phases from the system with  $a_1 = a_2 = a_3 = a_4 = 0$ . From this simulation, we would expect the inferred coupling strength from the original data not to differ significantly from the coupling strength inferred in any of the surrogate types. Figure 30(C) shows that this is indeed the case.

#### 9.3.2. Cardiorespiratory coupling

The combination of dynamical Bayesian inference and surrogates for the investigation of coupling between oscillators was also applied to real experimental data. We again investigate the coupling phenomenon between the heart rate and the breathing known as respiratory sinus arrhythmia (RSA). In Section 9.2.3 we demonstrated that there is significant coherence between the instantaneous heart rate and the respiration signals in the respiration frequency range. However, as also discussed, the presence of coherence does not necessarily mean that there is coupling present in the system. Thus, here we use dynamical Bayesian inference to study this well known phenomenon.

We consider an electrocardiogram (ECG) signal as  $x_2$  and a respiration signal as  $x_1$ . Filtering was applied as in the previous section, within the frequency ranges [0.6 2] Hz for the ECG and [0.15 0.6] Hz for the respiration.

Due to the complex waveforms of the ECG and respiration signals, the filtered signals differ from the original ones (see Figure 31 (A)&(B)), and the phases are recovered consistently. Coupling strength between the filtered ECG and respiration signals was inferred using DBI for two young healthy subjects.

To find whether the obtained coupling strength is significant, surrogates were employed to test the null hypothesis of no coupling between  $x_1$  and  $x_2$ . The inferred coupling strengths and their time evolutions are shown in Figure

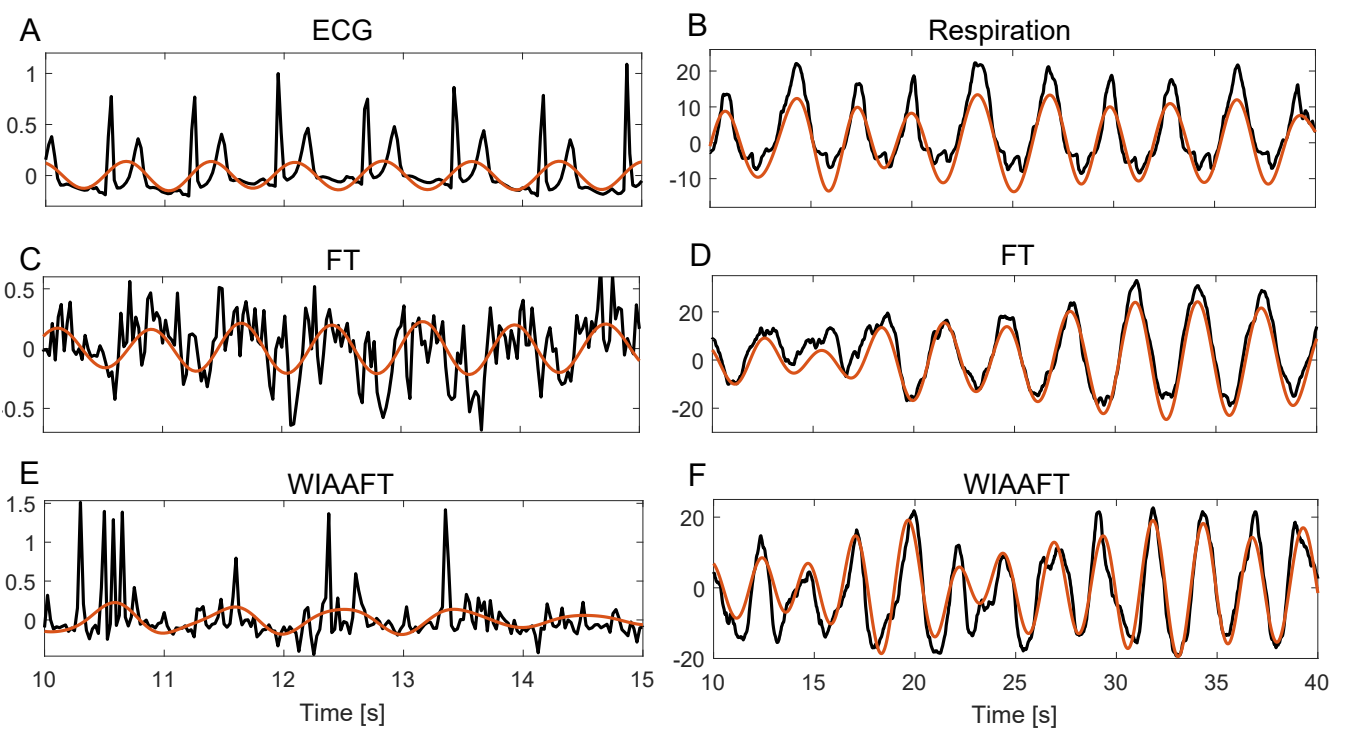


Figure 31: Time series (in black) and correspondent filtered signals (overlapped in orange) for: (A) ECG signal, (B) Respiration signal, WIAAFT surrogates applied on the time series and on the filtered signal for (C) ECG and (D) RS, FT surrogates applied on the time series and on the filtered signal for (E) ECG and (F) RS.

32.

CPP surrogates were computed from the extracted phases from each signal.

The performance of WIAAFT and FT surrogates was tested on the original data, preprocessed as discussed in Section 4.3 (Figure 31(C) to (F)).

Similarly to the numerical simulation, CPP surrogates (in green) generated the lowest threshold. FT (in blue) and WIAAFT surrogates (in pink) generated similar thresholds for both subjects, and invalidated the coupling strength for most of the time-windows. In the light of the result shown for weak numerical coupling in Figure 30(B), this result can be interpreted as FT and WIAAFT failing to fully destroy the coupling in the data, rather than CPP generating a too low threshold.

In conclusion, we showed that it is not assured that the use of WIAAFT and FT surrogates is consistent with a null hypothesis of uncoupled systems, especially for weak coupling, and it is therefore not recommended for this specific application. For validating phase-coupling between oscillators, it is crucial to generate surrogates which fit the null hypothesis of being uncoupled. Within the selections of surrogates tested in this section, CPP surrogates gave the most consistent results. The time evolution is randomised, while preserving the within-phase feature of the signals. The approach of FT surrogates seemed promising too, but by preserving the spectra there is the possibility of maintaining traces of coupling in the reconstructed surrogates. WIAAFT, which willingly mimic the time evolution of the signals, were not appropriate for this specific application, as predicted.

### 51 9.3.3. Wavelet bispectrum

52 Here, we will investigate nonlinear coupling between two time series using wavelet bispectrum analysis. As  
 53 mentioned above, surrogates should preserve all properties of the signal apart from the one that we are testing  
 54 for. We consider bispectra based on the continuous wavelet transform, therefore our wish is to destroy coupling  
 55 between wavelet coefficients at different scales, while maintaining a similar time-averaged wavelet power spectrum.  
 56 We investigate Fourier transform (FT), wavelet iterative amplitude adjusted Fourier transform (WIAAFT [76]),  
 57 wavelet time-shifted (Wtshift, as described by Breakspear [108]) and time-shifted (tshift) surrogates. A peak will  
 58 be considered as significant if its magnitude is higher than the 95<sup>th</sup> percentile of the surrogate values, obtained  
 59 using 20 surrogates. Initially, 150 surrogates were calculated, but it was found that using more than 20 did not  
 60 significantly alter the results. The optimal surrogate type would indicate the significant peaks in the precise location  
 61 corresponding to the coupling while not indicating the presence of any other spurious peaks. FT and WIAAFT  
 62

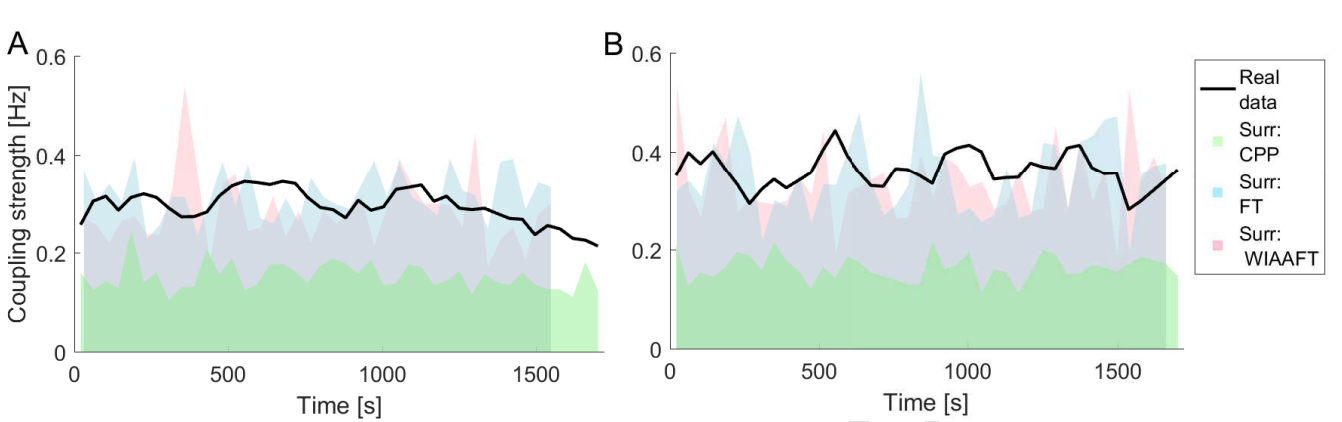


Figure 32: Results of the inferred coupling strength (black line) from the respiration to the heart, for 2 young healthy subjects (A)&(B). Surrogate thresholds are shaded with transparency for CPP (green), FT (light blue) and WIAAFT (pink).

surrogates destroy the nonlinearities within the signals, while Wtshift surrogates only disrupt correlations between wavelet coefficient levels. tshift surrogates preserve all nonlinearities.

As an example, we study a coupled pair of Poincaré oscillators described by:

$$\begin{aligned}
 \frac{dx_1}{dt} &= -q_1 x_1 - (\omega_1 + \gamma y_2) y_1 \\
 \frac{dy_1}{dt} &= (\omega_1 + \gamma y_2) x_1 - q_1 y_1 + \gamma (y_1 - y_2)^2 \\
 \frac{dx_2}{dt} &= -q_2 x_2 - \omega_2 y_2 \\
 \frac{dy_2}{dt} &= \omega_2 x_2 - q_2 y_2 \\
 q_i &= \alpha(\sqrt{x_i^2 + y_i^2} - a),
 \end{aligned} \tag{43}$$

where  $\gamma$  is a measure of nonlinear coupling strength (from system 2 to system 1),  $\omega_i = 2\pi f_i$  are the basic oscillator frequencies,  $\alpha$  is the relaxation parameter, and  $a$  is the radius of the limit cycle for the internal dynamics of each system. We investigate signals  $x_1$  and  $x_2$  with addition of 1/f noise,

$$X_i(t) = x_i(t) + \sigma \chi_i(t),$$

where  $X_1, X_2$  are the studied signals, and  $\chi_1, \chi_2$  are independent realisations of 1/f noise with standard deviation 1.

The chosen parameter values were  $f_1 = 0.86$  Hz,  $f_2 = 2.5$  Hz,  $\alpha = 1$ ,  $\gamma = 2$  and  $a = 1$ . The noise strength  $\sigma$  was varied between 0 and 1.2. The system was integrated with a Heun scheme, using a timestep of 0.1 ms. The total simulation time was  $T = 28$  s (with the initial 8 s subsequently removed) chosen to represent a minimum of 10 cycles of lower frequency ( $\sim 11$  s) but also to not overlook the possible lower harmonics.

The signals analysed were  $X_1(t)$  and  $X_2(t)$  downsampled to  $fs = 50$  Hz to allow observation of 1/10 of the cycle of the faster oscillation (25 Hz), but also to not overlook higher harmonics. Particular attention should be paid to preprocessing, as discussed in Section 4.3. The wavelet cross bispectrum  $B_{X_2 X_1 X_1}$  was computed using the Morlet wavelet with central frequency  $f_0 = 1$ .

We are primarily interested in the spectral content that appears due to the presence of nonlinear coupling. Here, there are two overlapping effects: system 2 is modulating the frequency of system 1 with strength  $\gamma$ , and at the same time is also quadratically forcing system 1. This results in the appearance of the new spectral peaks  $2f_1, 2f_2, f_1 - f_2, f_1 + f_2$  [213].

Results are shown in Figure 33, with frequencies for  $X_1$  on the horizontal axis and frequencies for  $X_2$  on the vertical axis. In each figure, the blue circle corresponds to the coupling between  $f_1$  and  $f_2$ ; the red circle, between  $f_2 - f_1$  and  $f_2$ ; and the black circle, between  $f_1$  and  $f_1$ .

The detection of nonlinear coupling using bispectra is affected by measurement noise. Figure 33(A) shows the bispectra for different values of the measurement noise intensity  $\sigma$ . The main peak is harder to detect as the level of noise is increased, and more harmonic peaks appear and form a characteristic “cross” with stronger coupling.

1  
2  
3  
4  
5  
6  
7  
8  
9  
10  
11  
12  
13  
14  
15  
16  
17  
18  
19  
20  
21  
22  
23  
24  
25  
26  
27  
28  
29  
30  
31  
32  
33  
34  
35  
36  
37  
38  
39  
40  
41  
42  
43  
44  
45  
46  
47  
48  
49  
50  
51  
52  
53  
54  
55  
56  
57  
58  
59  
60  
61  
62  
63  
64  
65

Figure 33(B-E) shows the resulting positive values after the 95th percentile of the different surrogate types is subtracted. FT surrogates (Figure 33(B)) were not capable of detecting a main peak ( $f_1, f_2$ , marked in blue). Similar results were obtained with IAAFT surrogates (data not shown). WIAAFT (Figure 33(C)) and Wtshift (Figure 33(D)) surrogates were successful in detecting the main peak when  $\sigma < 1$ . In the case where the noise level was higher, the main peak (blue) was not detected and other significant peaks appear, belonging to the harmonics, shown with red and black circles.

For all tested surrogate types, increasing the number of surrogates beyond 20 does not improve the accuracy of detection of nonlinear coupling. Although the most reliable results were obtained by WIAAFT and Wtshift surrogates, it is unlikely that any type of surrogate discussed would be reliable when the level of measurement noise becomes high ( $\sigma > 1$ ). Visual inspection of the original bispectrum (Figure 33(A),  $\sigma = 1.2$ ) in the case of a high level of measurement noise is less misleading than applying any type of surrogate.

## 10. Discussion

Surrogates, combined with appropriate discriminating statistics, provide a ‘statistical zero’, a threshold that is calculated from a range of data sets that definitely do not possess the property that is being investigated. Each surrogate has its own rules and issues, but in general we recommend that data should be preprocessed to match the ends and first derivatives (except of course in noise surrogates), significance levels should be determined using the rank method, to ensure there is no assumption of normality in the surrogate distribution, and the least nonlinear signal should be the one from which the surrogate is calculated, especially in cases where the extraction of phase is necessary.

In the first half of this work, we have reviewed many of the surrogate methods currently available for three general scenarios 1) finding dynamics in noisy data, 2) finding nonlinearity in data, and 3) investigating interactions between systems. The second part of the paper consists of original investigations into the performance of different surrogates types for these three important areas, specifically testing for nonlinearity, finding synchronization in simple and chaotic systems, and inferring coupling parameters from interacting systems.

Tests for nonlinearity revealed that not all surrogates for testing for nonlinearity are appropriate for use with all discriminating statistics. The results can be affected by nonlinear measurement transformations, and also by how well the surrogates meet the constraints of the data. The investigation into oscillations in noisy data using MCSSA demonstrated how significant oscillations can be successfully located with the method, by applying MCSSA to a numerically simulated oscillatory signal buried deep in correlated noise. The method was also applied to an EEG signal recorded from the occipital lobe of a human brain, and significant oscillations were observed.

The performance of many different surrogate types for the determination of significance levels for synchronization, as measured using phase coherence, was investigated in both simple phase oscillators, and coupled chaotic systems. The results clearly demonstrated the importance of time-variability in the phases of oscillators when trying to observe synchronization between them, with many of the surrogates failing to reject the null hypothesis of independence even when the system was fully synchronized. This is because the oscillators were almost identical over time, and thus their respective surrogates had a high level of coherence with the original data. Observing the time-varying case, we can see that the surrogates are all successful in the identification of synchronization in the synchronized system of simple sinusoidal oscillators.

Moving on to chaotic oscillators, all tested surrogates were relatively successful in indicating synchronization at the expected coupling strengths between both the coupled Rössler and Lorenz systems. It should be emphasized that none of the surrogates actually test for complete phase synchronization, but for the independence of signals, which is why they may show significance before the system is fully synchronized. Despite the apparent success of the surrogates in the demonstrated cases, for the purposes of testing for synchronization, application of FT, AAF or IAAFT surrogates may not be ideal, as they can indicate a rejection of the null hypothesis even with no synchronization, if the signal is highly nonlinear. Therefore, surrogates which allow for nonlinearity in signals are more applicable and reliable in this case. Overall, the surrogates which meet this criteria, and have some of the lowest computational costs are CPP and time-shifted surrogates. However, time-shifted surrogates may have the problem that they maintain some correlations between signals if the shift is not sufficiently large, whilst CPP surrogates can only be constructed if the phase of the oscillation can be extracted.

Wavelet phase coherence was also used as an example to test the performance of different surrogate types, using respiratory sinus arrhythmia as an example. This is a case where it is demonstrated that surrogates can be used to identify bias in methods. For the evaluation of the performance of surrogates for testing coupling strength between oscillators, FT, WIAAFT and CPP surrogates were compared in a system with known time-varying coupling strengths. The coupling strengths were extracted using dynamical Bayesian inference, with the same preprocessing

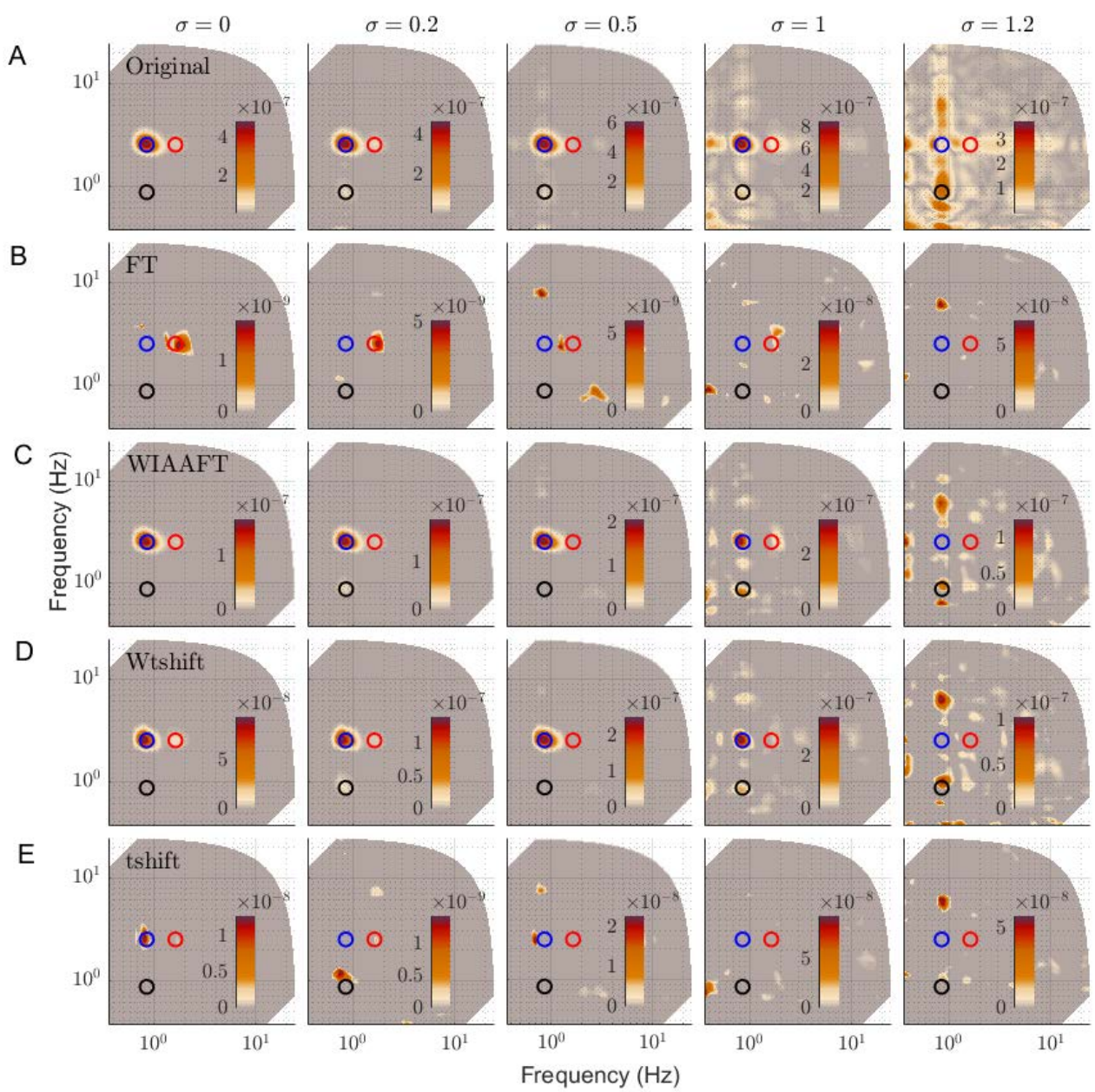


Figure 33: The effect of different measurement noise intensity ( $\sigma = 0, 0.2, 0.5, 1$  and  $1.2$ ) for different type of surrogates. Bispectra are obtained with Morlet wavelet and central frequency  $f_0 = 1$ . In each figure, the blue circle corresponds to coupling between  $f_1$  and  $f_2$ ; the red circle, between  $f_2 - f_1$  and  $f_2$ ; and the black circle, between  $f_1$  and  $f_1$ . (a) Bispectrum of the original signal, (b) FT, (c) WIAAFT, (d) Wtshift and (e) tshift surrogates. Increasing the level of noise makes detection of the main peak (blue circle:  $f_1, f_2$ ) more difficult because of more harmonic peaks (red:  $f_2 - f_1, f_2$ ; black:  $f_1, f_1$ ). As can be seen, because of detecting the main peak (blue circle:  $f_1, f_2$ ) the best performance was exhibited by WIAAFT (c) and Wtshift (d) surrogates. However reliable detection above  $\sigma = 1$  (with surrogates presented) was not possible.

and inference also applied to different surrogate types. As the only surrogate to correctly identify the significant coupling at all coupling strengths, CPP surrogates again emerged as an ideal choice. At higher coupling strengths, all surrogates were successful in rejecting the null hypothesis of independence between systems.

Application of surrogates to wavelet bispectrum analysis demonstrated that although improved performance can be obtained by using wavelet surrogates rather than FT surrogates alone, dynamics can still be very difficult to characterize when there is a high level of noise in the system, or very complex interactions. This highlights that care should be taken in the application of surrogate data testing, especially in noisy or time-dependent systems.

1  
 2  
 3 There are many other surrogate types available than those discussed here, and the field continues to expand. As  
 4 their use grows in popularity, surrogates to test increasingly specific null hypotheses are emerging, based on existing  
 5 ideas, or completely new concepts. For example, surrogates for epileptic seizure prediction were introduced by  
 6 Andrzejak and Kreuz *et al.* [234, 235] and developed further in [236]. The most general approach for the creation of  
 7 surrogates which preserve data distribution was introduced by Schreiber [237]. This method provides the possibility  
 8 of generating surrogates with any constraints, by choosing the respective cost function, the minimum of which is  
 9 equivalent to satisfying the given constraints. This minimization of the cost function is performed over a set of  
 10 all possible permutations of the data by use of a technique known as simulated annealing. However, this powerful  
 11 technique does have some drawbacks. In addition to some arbitrariness in the choice of the cost function, the  
 12 method is also very computationally expensive, with a computation time of a few days per surrogate in some cases.  
 13 There is a package available for the implementation of this and many other surrogate methods and discriminating  
 14 statistics, written in C and Fortran, known as the TISEAN package, as introduced and discussed in [4]. Another  
 15 type of surrogate known as attractor surrogates (AS) were introduced in [238], and were designed to preserve both  
 16 short time correlations and the shape of the attractor in 2D phase space, but the authors concluded that for their  
 17 purpose, the investigation of unstable periodic orbits in noisy, nonstationary data, AS did not provide any advantage  
 18 over random permutation surrogates.  
 19

20 Surrogates have also been used recently in spatial applications. Postnov *et al.* [239] used 2D surrogates to find  
 21 oscillatory patterns in laser speckle data, and Sheppard *et al.* [240] applied multivariate spatial FT surrogates of  
 22 wavelet coherence to find relationships between populations in ecology. The latter also presented an algorithm  
 23 that improves the efficiency of the calculation of wavelet coherence surrogates. Wiedermann *et al.* [241] recently  
 24 introduced spatial network surrogates which preserve either the global or local distributions of link lengths between  
 25 nodes, and used them to classify network types. Spatio-temporal propagation patterns in neuroscience and climatology  
 26 were recently investigated using a new type of surrogate named spike order surrogates [242]. Spike order  
 27 surrogates maintain the coincidence structure of spike trains, but the spike order is destroyed by swapping pairs of  
 28 spikes.  
 29

30 With applications spanning temporal and spatial domains, the powerful tool of hypothesis testing with surrogate  
 31 data should be considered not only in physics, mathematics and biology, but in any field dealing with dynamics  
 32 and interactions between systems. This approach should be an integral part of any conclusions based on statistical  
 33 measures, especially when the results may be affected by the characteristics of the data or the analysis method  
 34 itself.  
 35

36 We have provided a MatLab toolbox for the calculation of many of the discussed surrogates. As is stressed in  
 37 [4], we must also emphasize that use of our software package cannot be treated with a ‘black-box’ approach, and  
 38 any methods used should be well understood before application.  
 39

## 40 Acknowledgements

41 We are grateful to Phil Clemson, Tomislav Stankovski, Julian Newman and Milan Paluš for helpful comments  
 42 on the manuscript. We gratefully acknowledge valuable discussions with Ralph Andrzejak, Thomas Kreuz, Peter  
 43 V. E. McClintock and Lawrence Sheppard. The work was supported by the Engineering and Physical Sciences  
 44 Research Council (UK) (Grants No. EP/M006298/1 and No EP/100999X1), Action Medical Research UK (Grant  
 45 No. GN1963), the Innovative Training Network COSMOS program (funded by the EU Horizon 2020 research and  
 46 innovation program under the Marie Skłodowska-Curie Grant Agreement No. 642563), the Slovenian Research  
 47 Agency (Program No. P20232) and the Lancaster University Department of Physics.  
 48

## 49 A. Further details

### 50 A.1. MatLab toolbox

51 Matlab codes for the implementation of many of the surrogates discussed in this paper are available at <http://pybiomedical.lancs.ac.uk/>  
 52

### 53 A.2. Computational cost

54 When choosing the optimal surrogate method for a particular application, one consideration will inevitably be  
 55 the amount of time they take to calculate. While computational cost should not decide the null hypothesis, it may  
 56 influence the decision if multiple surrogate methods are suitable, and one is much faster. To demonstrate the speed  
 57 of computation, surrogates were calculated using each of the methods shown in Figure 34. The surrogates were  
 58 calculated from a time-varying noisy sinusoid described by  $\sin(2\pi(t + 0.5\sin(2\pi t/10))/3)$  with additive Gaussian  
 59 noise. The computation times for each of the methods are shown in Table 1. The computation times for the  
 60 surrogates were calculated using the TISEAN package [4] and the spike order surrogates were calculated using  
 61 the MatLab toolbox [242]. The computation times for the attractor surrogates were calculated using the  
 62 MatLab toolbox [242]. The computation times for the 2D surrogates were calculated using the MatLab  
 63 toolbox [242]. The computation times for the 3D surrogates were calculated using the MatLab  
 64 toolbox [242]. The computation times for the 4D surrogates were calculated using the MatLab  
 65 toolbox [242].

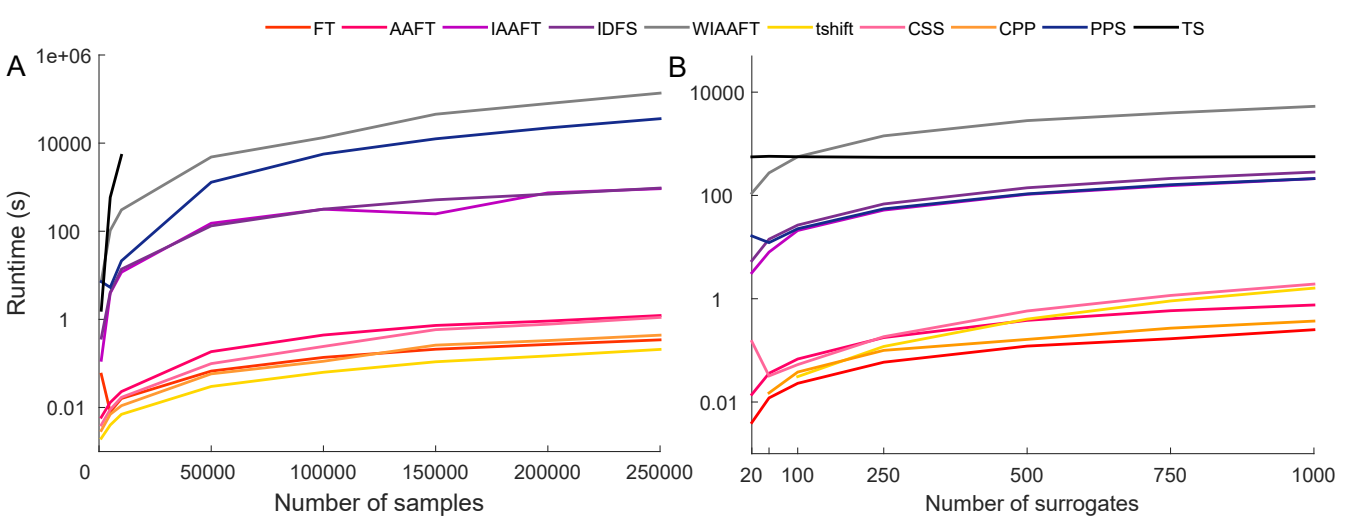


Figure 34: Computation time (in seconds) for the generation of surrogates of a 50 s noisy sinusoid with time-varying period  $\sin(2\pi(t + 0.5\sin(2\pi t/10))/3)$  of (A) 20 surrogates of time series of varying lengths [1000 5000 10000 50000 100000 150000 200000 250000] and (B) a time series of 5000 points in length for varying number of surrogates [20 50 100 250 500 750 1000]. Note the logarithmic y-scale, due to some surrogates being several orders of magnitude slower to calculate.

white noise with  $NSR = 0.1$ , with sampling frequency 100 Hz. Figure 34(A) shows the dependence of computation time on the length of the signal in points,  $L$ , and (B) shows the dependence on the number of surrogates. Calculations were performed using MatLab 2015a on Windows 10 (64-bit, 3.4GHz Intel Core i7). Generally, increasing signal length and surrogate number will increase the computation time. Twin surrogates are an exception to this rule, as their long computation time is due to the initial finding of twins, which only needs to be performed once, after which the surrogates can be calculated quickly, meaning that the computational speed is almost independent of the number of surrogates (see Figure 34(B)). However, as can be seen in Figure 34(A), for large data sets, the calculation of twin surrogates is not possible, due to the large amount of memory required.

The computation time of WIAAFT surrogates may be improved by finding a more efficient matching algorithm for each scale, or applying the updated PWIAAFT algorithm discussed in [76].

### A.3. Phase extraction

The phase of a signal containing only one oscillation can be extracted using the Hilbert transform (see below). For more complex signals, time-frequency analysis (see Appendix A.5) can be used for the separation of oscillatory modes, and to extract their instantaneous phase using either ridge extraction [243, 244, 245] or nonlinear mode decomposition [21]. For phase construction to be meaningful, it is important that the time series is oscillatory [78].

#### A.3.1. The Hilbert transform

The Hilbert transform, devised by the mathematician David Hilbert, converts a real signal into a complex signal known as its analytic representation, and takes the form [29]:

$$H(t) = \frac{1}{\pi} \int_{-\infty}^{\infty} \frac{f(u)}{u - t} du, \quad (44)$$

which is equivalent to the convolution of the time series  $f(t)$  with  $\frac{1}{\pi t}$ .

The analytic signal recovered using the Hilbert transform can be expressed as:

$$x_a(t) = x_m(t)e^{j\phi(t)}, \quad (45)$$

where the instantaneous amplitude  $x_m(t)$  and phase  $\phi(t)$  can be extracted as the modulus and the argument (polar angle) of  $x_a$ , respectively.

This representation specifies the amplitude and phase of the signal as a function of time [246]. Information obtained via the Hilbert transform retains the same sampling frequency as the original data. The Hilbert transform does not perform well in cases in which there are many oscillations present in the data, or when the data are highly nonstationary. Thus, many applications employ bandpass filtering before applying the Hilbert transform.

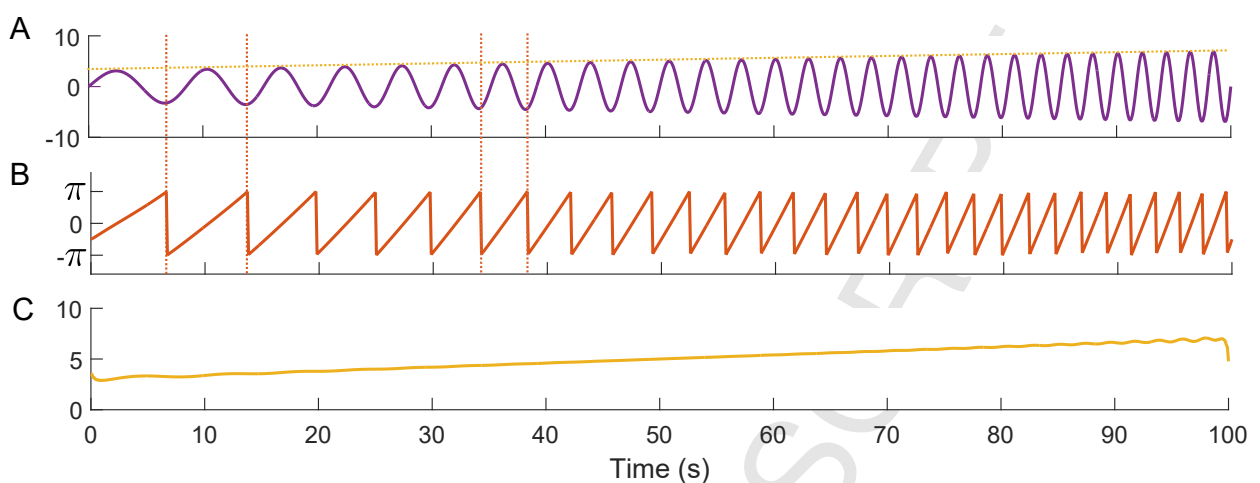


Figure 35: Example amplitude and phase information separation from the Hilbert transform of a sine wave with increasing amplitude and frequency. (A) The original time series. The dotted lines show the amplitude (yellow) and two example full phase cycles (orange). (B) The phase extracted using the Hilbert transform. (C) The amplitude extracted from the Hilbert transform. The original signal A can be reconstructed as  $A = C \cos(B)$ .

An example of the separation of the amplitude and phase of a signal using the Hilbert transform for a simple oscillatory signal is shown in Figure 35.

#### A.3.2. Phase vs. protophase

Throughout the text, when referring to the phase of oscillators, we assume that it is growing uniformly, and gains  $2\pi$  with each cycle, as it would during simple harmonic motion. This means that the system rotates on a limit cycle at a constant speed. However, this assumption is not always valid, especially in the case of nonlinear oscillators, for which the phase generally does not increase uniformly. In these cases, extracted phases may differ depending on the method used, and may in fact provide the *protophase* rather than the phase. The protophase still gains  $2\pi$  with each cycle, but does not necessarily grow uniformly, preserving more complex intra-cycle phase evolutions. In order to obtain an invariant phase of nonlinear systems, a protophase-to-phase conversion should be applied [247, 248]. An exception to this rule is when estimating conditional mutual information as introduced by Paluš (see Section 6.7), which is invariant with respect to monotonous data transformation [private communication, 2017].

#### A.3.3. Nonlinear mode decomposition

Nonlinear mode decomposition (NMD) is a recently developed technique for the extraction of nonlinear modes from time series [21]. It combines many different techniques in order to accurately reconstruct nonlinear waveforms. It uses time-frequency analysis methods to extract the fundamental oscillation and its harmonics, and surrogate data to identify whether these harmonics are real. The oscillation can then be reconstructed and subtracted from the original time series, and the process repeated until all oscillatory modes have been located.

#### A.4. Filtering

As discussed above, the Hilbert transform only has clear meaning for narrow band signals [249], and this is used as justification for filtering in the frequency interval of interest before trying to obtain instantaneous amplitude and phase from a signal. Hilbert phase only completely represents the actual phase for a pure sinusoid. In other cases, additional components may distort the extracted phase in some way, but generally the variation in period will be preserved. Le Van Quyen *et al.* concluded that the Hilbert transform is equivalent to the wavelet transform for the extraction of instantaneous phase from time series [249], but bandpass filtering was applied before the application of both methods.

Filtering increases the risk of information loss, especially in systems with time-varying dynamics or harmonics, so should be avoided whenever possible. Instantaneous phase, frequency and amplitude information can be extracted directly from clear modes in the wavelet transform using ridge extraction [243, 244, 245] or nonlinear mode decomposition [21].

Naturally, if filtering is to be used for hypothesis testing using surrogates, the exact same procedures must be applied both to the original data and to every realization of surrogate data [250], and surrogates should always be calculated before filtering to ensure that any differences are not merely as a result of the filtering.

1  
2  
3 *A.5. Time-frequency analysis*4 *A.5.1. Windowed Fourier transform*

5 When assessing the frequency content of a signal, the first method to be applied is usually the Fourier transform.  
 6 However, for signals arising from many real systems, the assumption of stationary of the data does not hold. If  
 7 the data contain oscillations with frequencies which vary in time, the Fourier transform will provide no information  
 8 about when in the recording these variations occurred, and will instead provide one ‘blurred’ peak. In order to  
 9 address this problem, the windowed Fourier transform (WFT) was developed. The WFT separates the signal into  
 10 windows, and calculates the Fourier transform in each [218]. The multiple frequency spectra are then lined up in  
 11 sequence, and a 3D picture is built of the frequency variations over time. However, this approach is not without its  
 12 drawbacks, mostly related to the variations in time and frequency resolution based on the choice of the window size.  
 13 For example, it is hard to choose an optimal window size, as in many real situations the properties of oscillations  
 14 and typical frequency differences between the neighbouring ones depend on their frequencies, while the windowed  
 15 Fourier transform has the same resolution at all frequencies.

17 *A.5.2. The continuous wavelet transform*

18 Whilst it is impossible to have excellent time and frequency resolution simultaneously, the continuous wavelet  
 19 transform (CWT) provides a more universal and applicable choice of time-frequency resolution structure than the  
 20 WFT. It is especially useful in the analysis of data which contain low frequency oscillations, due to its logarithmic  
 21 frequency scale [251, 252]. This means that multiple low frequency oscillatory modes can be more easily distinguished  
 22 in data. In the CWT, a mother wavelet is stretched and compressed while being translated along a signal in order  
 23 to find information about the local frequency content of the signal.

26 *A.5.3. The discrete wavelet transform*

27 The discrete wavelet transform decomposes a time series into different scales. The time series is repeatedly  
 28 convolved with a wavelet and a scaling function, which change in scale as the finer detail is separated out from the  
 29 signal. Usually, the highest frequency detail (up to the Nyquist frequency) is extracted first, and then the time  
 30 series is downsampled by a factor of two to extract the next level of coefficients. This is repeated until the length  
 31 of the time series becomes a single data point [29].

32 This loss of data points at each level of wavelet coefficients is problematic for the creation of wavelet surrogates,  
 33 where we wish to retain the time information for each scale. Therefore, the maximum overlap discrete wavelet  
 34 transform (MODWT) is used instead, as it gives coefficients sets which are the same length as the time series [107].  
 35

37 *A.6. Embedding*

38 Embedding is the process of transforming a time series into phase space and was developed by Takens [253] and  
 39 Māñe [136]. A  $d$ -dimensional phase space representation of the time series is created by generating multiple delayed  
 40 versions of the original time series [29]:

$$42 \quad 43 \quad 44 \quad 45 \quad 46 \quad 47 \quad \mathbf{X}(t_i) = \begin{bmatrix} x(t_i) \\ x(t_i + \tau) \\ \vdots \\ x(t_i + (d - 1)\tau) \end{bmatrix}$$

48 where  $\tau$  is the delay time and  $x(t_i)$  is the original signal. An example phase reconstruction on the  $x$  component of  
 49 the Lorenz system,

$$50 \quad 51 \quad 52 \quad 53 \quad \begin{cases} \dot{x} = \sigma(y - x) \\ \dot{y} = x(\rho - z) - y \\ \dot{z} = xy - \beta z, \end{cases} \quad (46)$$

54 with  $\sigma = 10$ ,  $\rho = 28$  and  $\beta = 8/3$  and time step 0.01 is shown in Figure 36.

55 When embedding time series with phase space representations which are less distinctive than the Lorenz system,  
 56 it can be difficult to choose the optimum values for the parameters  $\tau$  and  $d$ . It is also possible that the system  
 57 will be higher than 3 dimensional, and thus can no longer be visualised through plotting. Many attempts have  
 58 been made to solve this problem. It should also be noted that time-delay embedding removes all time-dependent  
 59 information. Further discussion can be found in [29]. Here we discuss only how the parameters were obtained for  
 60 the examples presented in this paper.

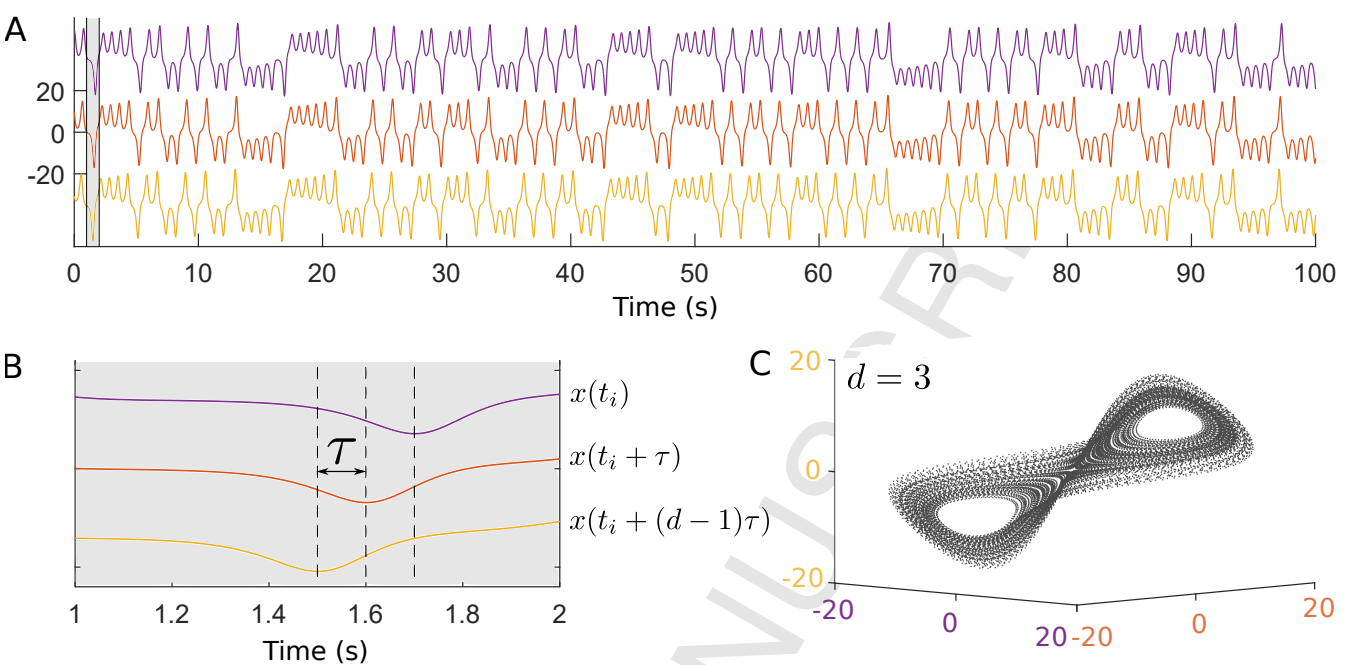


Figure 36: Example time delay embedding of the  $x$  component of the Lorenz system. (A) Following embedding, a series of delayed time series are obtained. Here the embedding dimension  $d$  is 3, and thus three time series are produced. Time series amplitude is offset for clarity. (B) Zoomed in view of the grey area shown in (A), to demonstrate the time delay  $\tau = 0.1$  s. (C) Reconstruction of the attractor in phase space is obtained by plotting the embedded signals on the same plot.

#### A.6.1. Estimation of time delay $\tau$

The time delay  $\tau$  should maximise the spread of the data in phase space [29]. In order to find time delays for which the correlation between time points is minimal, and thus ensuring a greater spread of points, the autocorrelation was calculated as [29]:

$$r(l) = \frac{\sum_{n=1}^{L-l} (x(t_n + l\Delta t) - \bar{x})(x(t_n) - \bar{x})}{\sum_{n=1}^{L-l} (x(t_n) - \bar{x})^2}, \quad (47)$$

where  $\bar{x} = \frac{1}{L-l} \sum x(t_n)$  is the mean [254], and  $\tau = l\Delta t$ . The first point up to a certain threshold where the autocorrelation reaches zero (or if it does not, where it reaches its minimum value) determines  $\tau$ .

#### A.6.2. Estimation of embedding dimension $d$

The most widely used technique for the estimation of the embedding dimension is the false nearest neighbours method [118] and is the method used in this paper, both in the generation of pseudo-periodic and twin surrogates, and in the calculation of the correlation dimension.

The false nearest neighbours technique examines how close points from the two closest neighbouring embedding vectors remain in phase space as the dimension is increased. When the dimension is low, and not sufficient to represent all of the system dynamics, close points in phase space are more likely to be ‘false’ neighbours, and will reduce in number as the embedding dimension is increased. The first dimension for which the number of false nearest neighbours goes below a threshold (usually  $< 1\%$  [29]) provides the estimated embedding dimension.

- 1  
2  
3 [1] B. Efron, Computers and the theory of statistics: thinking the unthinkable, SIAM Rev. 21 (4) (1979) 460–480.  
4  
5 [2] B. Efron, R. J. Tibshirani, An introduction to the bootstrap, CRC press, 1994.  
6  
7 [3] J. Theiler, S. Eubank, A. Longtin, B. Galdrikian, J. Farmer, Testing for nonlinearity in time series: The  
8 method of surrogate data, Physica D 58 (1–4) (1992) 77–94.  
9  
10 [4] T. Schreiber, A. Schmitz, Surrogate time series, Physica D 142 (3-4) (2000) 346–382.  
11  
12 [5] M. Small, D. Yu, R. G. Harrison, Surrogate test for pseudoperiodic time series data, Phys. Rev. Lett. 87 (18)  
13 (2001) 188101.  
14  
15 [6] M. Paluš, D. Hoyer, Detecting nonlinearity and phase synchronization with surrogate data, IEEE Eng. Med.  
16 Biol. 17 (6) (1998) 40–45.  
17  
18 [7] J. Jamšek, M. Paluš, A. Stefanovska, Detecting couplings between interacting oscillators with time-varying  
19 basic frequencies: Instantaneous wavelet bispectrum and information theoretic approach, Phys. Rev. E 81 (3)  
20 (2010) 036207.  
21  
22 [8] M. R. Allen, L. A. Smith, Monte Carlo SSA: Detecting irregular oscillations in the presence of colored noise,  
23 J. Climate 9 (12) (1996) 3373–3404.  
24  
25 [9] K. M. Leighly, A comprehensive spectral and variability study of narrow-line Seyfert 1 galaxies observed by  
26 ASCA. I. observations and time series analysis, Astrophys. J. Suppl. S. 125 (2) (1999) 297.  
27  
28 [10] M. Gan, Y. Huang, M. Ding, X. Dong, J. Peng, Testing for nonlinearity in solar radiation time series by a  
29 fast surrogate data test method, Solar Energy 86 (9) (2012) 2893–2896.  
30  
31 [11] M. Mannattil, H. Gupta, S. Chakraborty, Revisiting evidence of chaos in x-ray light curves: The case of GRS  
32 1915+ 105, Astrophys. J. 833 (2) (2016) 208.  
33  
34 [12] A. Grinsted, J. C. Moore, S. Jevrejeva, Application of the cross wavelet transform and wavelet coherence to  
35 geophysical time series, Nonlin. Process Geophys. 11 (5-6) (2004) 561–566.  
36  
37 [13] D. Chakraborty, T. K. Roy, Generation and prediction of self-similar processes by surrogates, Fractals 14 (01)  
38 (2006) 17–26.  
39  
40 [14] J. M. Nichols, K. D. Murphy, Modeling and Estimation of Structural Damage, Wiley, 2016.  
41  
42 [15] M. Ghil, M. R. Allen, M. D. Dettinger, K. . Ide, D. Kondrashov, M. E. Mann, A. W. Robertson, A. Saunders,  
43 Y. Tian, F. Varadi, P. Yiou, Advanced spectral methods for climatic time series, Rev. Geophys. 40 (1) (2002)  
44 3–1–3–41.  
45  
46 [16] M. Schulz, M. Mudelsee, REDFIT: Estimating red-noise spectra directly from unevenly spaced paleoclimatic  
47 time series, Computers & Geosciences 28 (3) (2002) 421–426.  
48  
49 [17] B. Cazelles, M. Chavez, D. Bertrand, F. Ménard, J. O. Vik, S. Jenouvrier, N. C. Stenseth, Wavelet analysis  
50 of ecological time series, Oecologia 156 (2) (2008) 287–304.  
51  
52 [18] L. W. Sheppard, J. R. Bell, R. Harrington, D. C. Reuman, Changes in large-scale climate alter spatial  
53 synchrony of aphid pests, Nat. Clim. Change 6 (2015) 610–613.  
54  
55 [19] M. Small, C. K. Tse, Applying the method of surrogate data to cyclic time series, Physica D 164 (3) (2002)  
56 187–201.  
57  
58 [20] M. Xu, P. Shang, J. Huang, Modified generalized sample entropy and surrogate data analysis for stock markets,  
59 Commun. Nonlin. Sci. 35 (2016) 17–24.  
60  
61 [21] D. Iatsenko, P. V. E. McClintock, A. Stefanovska, Nonlinear mode decomposition: A noise-robust, adaptive  
62 decomposition method, Phys. Rev. E 92 (2015) 032916.  
63  
64 [22] M. Paluš, Nonlinearity in normal human EEG: cycles, temporal asymmetry, nonstationarity and randomness,  
65 not chaos, Biol. Cybern. 75 (5) (1996) 389–396.

- [23] B. Musizza, A. Stefanovska, P. V. E. McClintock, M. Paluš, J. Petrovčič, S. Ribarič, F. F. Bajrović, Interactions between cardiac, respiratory, and EEG- $\delta$  oscillations in rats during anaesthesia, *J. Physiol.* 580 (1) (2007) 315–326.
- [24] K. Lehnertz, S. Bialonski, M.-T. Horstmann, D. Krug, A. Rothkegel, M. Staniek, T. Wagner, Synchronization phenomena in human epileptic brain networks, *J. Neurosci. Methods* 183 (1) (2009) 42–48.
- [25] L. Faes, G. D. Pinna, A. Porta, R. Maestri, G. I. Nollo, Surrogate data analysis for assessing the significance of the coherence function, *IEEE Trans. Biomed. Eng.* 51 (7) (2004) 1156–1166.
- [26] Y. Shiogai, A. Stefanovska, P. V. E. McClintock, Nonlinear dynamics of cardiovascular ageing, *Phys. Rep.* 488 (2010) 51–110.
- [27] D. Iatsenko, A. Bernjak, T. Stankovski, Y. Shiogai, P. J. Owen-Lynch, P. B. M. Clarkson, P. V. E. McClintock, A. Stefanovska, Evolution of cardiorespiratory interactions with age, *Phil. Trans. R. Soc. A* 371 (2013) 20110622.
- [28] V. von Tscharner, P. Zandiyeh, Multi-scale transitions of fuzzy sample entropy of RR-intervals and their phase-randomized surrogates: A possibility to diagnose congestive heart failure, *Biomed. Signal Process. Control* 31 (2017) 350–356.
- [29] P. T. Clemson, A. Stefanovska, Discerning non-autonomous dynamics., *Phys. Rep.* 542 (4) (2014) 297–368.
- [30] P. Clemson, G. Lancaster, A. Stefanovska, Reconstructing time-dependent dynamics, *Proc. IEEE* 104 (2) (2016) 223–241.
- [31] C. Schäfer, M. G. Rosenblum, H.-H. Abel, J. Kurths, Synchronization in the human cardiorespiratory system, *Phys. Rev. E* 60 (1) (1999) 857.
- [32] A. Stefanovska, M. Bračić, Physics of the human cardiovascular system, *Contemp. Phys.* 40 (1) (1999) 31–55.
- [33] G. Buzsáki, A. Draguhn, Neuronal oscillations in cortical networks, *Science* 304 (2004) 1926–1929.
- [34] A. Stefanovska, Coupled oscillators: Complex but not complicated cardiovascular and brain interactions, *IEEE Eng. Med. Biol. Mag.* 26 (6) (2007) 25–29.
- [35] C. J. Stam, B. Jelles, H. A. M. Achtereekte, S. A. R. B. Rombouts, J. P. J. Slaets, R. W. M. Keunen, Investigation of EEG non-linearity in dementia and Parkinson’s disease, *Electroencephalogr. Clin. Neurophysiol.* 95 (5) (1995) 309–317.
- [36] R. G. Andrzejak, D. Chicharro, K. Lehnertz, F. Mormann, Using bivariate signal analysis to characterize the epileptic focus: The benefit of surrogates, *Phys. Rev. E* 83 (4) (2011) 046203.
- [37] T. Stankovski, V. Ticcinelli, P. V. E. McClintock, A. Stefanovska, Neural cross-frequency coupling functions, *Front. Syst. Neurosci.* 11 (2017) 33.
- [38] D. A. Kenwright, A. Bernjak, T. Draegni, S. Dzeroski, M. Entwistle, M. Horvat, P. Kvandal, S. A. Landsverk, P. V. E. McClintock, B. Musizza, J. Petrovčič, J. Raeder, L. W. Sheppard, A. F. Smith, T. Stankovski, A. Stefanovska, The discriminatory value of cardiorespiratory interactions in distinguishing awake from anaesthetised states: A randomised observational study, *Anaesthesia* 70 (12) (2015) 1356–1368.
- [39] T. Stankovski, W. H. Cooke, L. Rudas, A. Stefanovska, D. L. Eckberg, Time-frequency methods and voluntary ramped-frequency breathing: A powerful combination for exploration of human neurophysiological mechanisms, *J. Appl. Physiol.* 115 (12) (2013) 1806–1821.
- [40] P. Grassberger, I. Procaccia, Measuring the strangeness of strange attractors, *Physica D* 9 (1983) 189–208.
- [41] J. P. Eckmann, D. Ruelle, Ergodic theory of chaos and strange attractors, *Rev. Mod. Phys.* 57 (3) (1983) 617–656.
- [42] J. Theiler, D. Prichard, Constrained-realization Monte-Carlo method for hypothesis testing, *Physica D* 94 (4) (1996) 221–235.

- [43] M. Small, Applied Nonlinear Time Series Analysis: Applications in Physics, Physiology and Finance, World Scientific Series on Nonlinear Science Series A, 2005.
- [44] M. Paluš, Testing for nonlinearity using redundancies: Quantitative and qualitative aspects, *Physica D*. 80 (1) (1995) 186–205.
- [45] M. Paluš, From nonlinearity to causality: statistical testing and inference of physical mechanisms underlying complex dynamics, *Contemp. Phys.* 48 (6) (2007) 307–348.
- [46] A. Bandrivskyy, A. Bernjak, P. V. E. McClintock, A. Stefanovska, Wavelet phase coherence analysis: Application to skin temperature and blood flow, *Cardiovasc. Eng.* 4 (1) (2004) 89–93.
- [47] J. P. Lachaux, E. Rodriguez, J. Martinerie, F. J. Varela, Measuring phase synchrony in brain signals, *Human Brain Mapping* 8 (4) (1999) 194–208.
- [48] D. A. Kenwright, A. Bahraminasab, A. Stefanovska, P. V. E. McClintock, The effect of low-frequency oscillations on cardio-respiratory synchronization, *Eur. Phys. J. B*. 65 (3) (2008) 425–433.
- [49] E. Koscielny-Bunde, A. Bunde, S. Havlin, H. E. Roman, Y. Goldreich, H. Schellnhuber, Indication of a universal persistence law governing atmospheric variability, *Phys. Rev. Lett.* 81 (3) (1998) 729.
- [50] G. E. Uhlenbeck, L. S. Ornstein, On the theory of Brownian motion, *Phys. Rev.* 36 (1930) 823–841.
- [51] K. Dolan, M. L. Spano, F. Moss, Detecting unstable periodic orbits in biological systems, *Handbook of Biological Physics* 4 (2001) 131–153.
- [52] P. C. Ivanov, L. A. N. Amaral, A. L. Goldberger, S. Havlin, M. G. Rosenblum, H. E. Stanley, Z. R. Struzik, From 1/f noise to multifractal cascades in heartbeat dynamics, *Chaos* 11 (3) (2001) 641–652.
- [53] Y. F. Suprunenko, P. T. Clemson, A. Stefanovska, Chronotaxic systems: a new class of self-sustained nonautonomous oscillators, *Phys. Rev. Lett.* 111 (2) (2013) 024101.
- [54] Y. F. Suprunenko, P. T. Clemson, A. Stefanovska, Chronotaxic systems with separable amplitude and phase dynamics, *Phys. Rev. E* 89 (1) (2014) 012922.
- [55] P. T. Clemson, Y. F. Suprunenko, T. Stankovski, A. Stefanovska, Inverse approach to chronotaxic systems for single-variable time series, *Phys. Rev. E* 89 (3) (2014) 032904.
- [56] G. Lancaster, P. T. Clemson, Y. F. Suprunenko, T. Stankovski, A. Stefanovska, Detecting chronotaxic systems from single-variable time series with separable amplitude and phase, *Entropy* 17 (6) (2015) 4413–4438.
- [57] H. Kantz, T. Schreiber, *Nonlinear Time Series Analysis*, Cambridge Univ. Press, 2003.
- [58] N. Wiener, Generalized harmonic analysis, *Acta Math.* 55 (1) (1930) 117–258.
- [59] J. Theiler, P. S. Lindsay, D. M. Rubin, Detecting nonlinearity in data with long coherence times, in: N. A. G. A. S. Weigend (Ed.), *Time Series Prediction: Forecasting the Future and Understanding the Past*, Santa Fe Institute Studies in the Science of Complexity, Proc. Vol. XV, Addison-Wesley, 1992, pp. 429–455.
- [60] D. Prichard, J. Theiler, Generating surrogate data for time series with several simultaneously measured variables, *Phys. Rev. Lett.* 73 (7) (1994) 951–954.
- [61] T. Schreiber, A. Schmitz, Improved surrogate data for nonlinearity tests, *Phys. Rev. Lett.* 77 (4) (1996) 635–638.
- [62] K. T. Dolan, M. L. Spano, Surrogate for nonlinear time series analysis, *Phys. Rev. E* 64 (4) (2001) 046128.
- [63] K. T. Dolan, A. Neiman, Surrogate analysis of coherent multichannel data, *Phys. Rev. E* 65 (2) (2002) 026108.
- [64] W. S. Pritchard, C. J. Stam, Nonlinearity in human resting, eyes-closed EEG: an in-depth case study., *Acta Neurobiol. Exp.* 60 (1) (2000) 109–121.
- [65] J. Theiler, On the evidence for low-dimensional chaos in an epileptic electroencephalogram, *Phys. Lett. A* 196 (1) (1995) 335–341.

- [66] P. E. Rapp, Chaos in the neurosciences: Cautionary tales from the frontier, *Biologist* 40 (2) (1993) 89–94.
- [67] R. G. Andrzejak, F. Mormann, G. Widman, T. Kreuz, C. E. Elger, K. Lehnertz, Improved spatial characterization of the epileptic brain by focusing on nonlinearity, *Epilepsy Res.* 69 (1) (2006) 30–44.
- [68] C. J. Stam, J. P. M. Pijn, W. S. Pritchard, Reliable detection of nonlinearity in experimental time series with strong periodic components, *Physica D* 112 (3) (1998) 361–380.
- [69] X. Luo, T. Nakamura, M. Small, Surrogate test to distinguish between chaotic and pseudoperiodic time series, *Phys. Rev. E* 71 (2) (2005) 026230.
- [70] G. E. P. Box, G. M. Jenkins, G. C. Reinsel, G. M. Ljung, *Time series analysis: forecasting and control*, John Wiley & Sons, 2015.
- [71] J. Timmer, Power of surrogate data testing with respect to nonstationarity, *Phys. Rev. E* 58 (4) (1998) 5153.
- [72] P. Borgnat, P. Flandrin, Stationarization via surrogates, *J. Stat. Mech. Theor. Exp.* 2009 (01) (2009) P01001.
- [73] J. H. Lucio, R. Valdés, L. R. Rodríguez, Improvements to surrogate data methods for nonstationary time series, *Phys. Rev. E* 85 (5) (2012) 056202.
- [74] T. Nakamura, M. Small, Y. Hirata, Testing for nonlinearity in irregular fluctuations with long-term trends, *Phys. Rev. E* 74 (2) (2006) 026205.
- [75] C. J. Keylock, Constrained surrogate time series with preservation of the mean and variance structure, *Phys. Rev. E* 73 (3) (2006) 036707.
- [76] C. J. Keylock, A wavelet-based method for surrogate data generation, *Physica D* 225 (2) (2007) 219–228.
- [77] M. McCullough, A. Kareem, Testing stationarity with wavelet-based surrogates, *J. Eng. Mech.* 139 (2) (2013) 200–209.
- [78] J. M. Hurtado, L. L. Rubchinsky, K. A. Sigvardt, Statistical method for detection of phase-locking episodes in neural oscillations, *J. Neurophysiol.* 91 (4) (2004) 1883–1898.
- [79] M. S. Keshner,  $1/f$  noise, *Proc. IEEE* 70 (3) (1982) 212–218.
- [80] B. Pilgram, D. T. Kaplan, A comparison of estimators for  $1/f$  noise, *Physica D* 114 (1) (1998) 108–122.
- [81] D. Piper, K. Schiecke, L. Leistritz, B. Pester, F. Benninger, M. Feucht, M. Ungureanu, R. Strungaru, H. Witte, Synchronization analysis between heart rate variability and EEG activity before, during, and after epileptic seizure, *Biomed. Tech.* 59 (4) (2014) 343–355.
- [82] Y. Yamamoto, R. L. Hughson, J. R. Sutton, C. S. Houston, A. Cymerman, E. L. Fallen, M. V. Kamath, Operation Everest II: An indication of deterministic chaos in human heart rate variability at simulated extreme altitude, *Biol. Cybern.* 69 (3) (1993) 205–212.
- [83] S. A. R. B. Rombouts, R. W. M. Keunen, C. J. Stam, Investigation of nonlinear structure in multichannel EEG, *Phys. Lett. A* 202 (5) (1995) 352–358.
- [84] M. Breakspear, J. R. Terry, Detection and description of non-linear interdependence in normal multichannel human EEG data, *Clin. Neurophysiol.* 113 (5) (2002) 735–753.
- [85] P. E. Rapp, A. M. Albano, I. D. Zimmerman, M. A. Jimenez-Montano, Phase-randomized surrogates can produce spurious identifications of nonrandom structure, *Phys. Lett. A* 192 (1) (1994) 27–33.
- [86] M. Paluš, D. Novotna, Sunspot cycle: a driven nonlinear oscillator?, *Phys. Rev. Lett.* 83 (17) (1999) 3406.
- [87] D. Kugiumtzis, Test your surrogate data before you test for nonlinearity, *Phys. Rev. E* 60 (3) (1999) 2808.
- [88] A. Bernjak, P. V. E. McClintock, A. Stefanovska, P. J. Owen-Lynch, P. B. M. Clarkson, Coherence of fluctuations in blood flow with those in tissue oxygen saturation, *Fluct. Noise Lett.* 11 (1) (2012) 1240013.

- 1  
2  
3 [89] A. Bernjak, J. Cui, S. Iwase, T. Mano, A. Stefanovska, D. L. Eckberg, Human sympathetic outflows to skin  
4 and muscle target organs fluctuate concordantly over a wide range of time-varying frequencies, *J. Physiol.*  
5 590 (2) (2012) 363–375.  
6  
7 [90] B. Musizza, F. F. Bajrović, J. Petrovčić, A. Stefanovska, S. Ribarić, Fluctuations and interactions between  
8 brain waves during deep and shallow anesthesia, *Fluct. Noise Lett.* 11 (01) (2012) 1240018.  
9  
10 [91] M. Paluš, A. Stefanovska, Direction of coupling from phases of interacting oscillators: An information-theoretic  
11 approach, *Phys. Rev. E* 67 (2003) 055201(R).  
12  
13 [92] P. Kvandal, L. Sheppard, S. A. Landsverk, A. Stefanovska, K. A. Kirkeboen, Impaired cerebrovascular reactivity  
14 after acute traumatic brain injury can be detected by wavelet phase coherence analysis of the intracranial  
15 and arterial blood pressure signals, *J. Clin. Monit. Comput.* 27 (4) (2013) 375–383.  
16  
17 [93] L. W. Sheppard, A. Stefanovska, P. V. E. McClintock, Testing for time-localised coherence in bivariate data,  
18 *Phys. Rev. E* 85 (2012) 046205.  
19  
20 [94] C. L. Ehlers, J. Havstad, D. Prichard, J. Theiler, Low doses of ethanol reduce evidence for nonlinear structure  
21 in brain activity, *J. Neurosci.* 18 (18) (1998) 7474–7486.  
22  
23 [95] C. Räth, M. Gligozzi, I. E. Papadakis, W. Brinkmann, Revisiting algorithms for generating surrogate time  
24 series, *Phys. Rev. Lett.* 109 (14) (2012) 144101.  
25  
26 [96] C. J. Stam, J. P. M. Pijn, P. Suffczynski, F. H. L. Da Silva, Dynamics of the human alpha rhythm: evidence  
27 for non-linearity?, *Clin. Neurophysiol.* 110 (10) (1999) 1801–1813.  
28  
29 [97] R. G. Andrzejak, K. Lehnertz, F. Mormann, C. Rieke, P. David, C. E. Elger, Indications of nonlinear deter-  
30 ministic and finite-dimensional structures in time series of brain electrical activity: Dependence on recording  
31 region and brain state, *Phys. Rev. E* 64 (6) (2001) 061907.  
32  
33 [98] W. H. Press, Numerical Recipes 3rd Edition: The Art of Scientific Computing, Cambridge University Press,  
34 2007.  
35  
36 [99] M. Small, K. Judd, Detecting nonlinearity in experimental data, *Int. J. Bifurcat. Chaos* 8 (06) (1998) 1231–  
37 1244.  
38  
39 [100] D. Kugiumtzis, Surrogate data test on time series, in: Modelling and Forecasting Financial Data, Springer,  
40 2002, pp. 267–282.  
41  
42 [101] A. Porta, S. Guzzetti, R. Furlan, T. Gnechi-Ruscone, N. Montano, A. Malliani, Complexity and nonlinearity  
43 in short-term heart period variability: comparison of methods based on local nonlinear prediction, *IEEE  
44 Trans. Biomed. Eng.* 54 (1) (2007) 94–106.  
45  
46 [102] T. Maiwald, E. Mammen, S. Nandi, J. Timmer, Surrogate data – a qualitative and quantitative analysis, in:  
47 Mathematical Methods in Signal Processing and Digital Image Analysis, Springer, 2008, pp. 41–74.  
48  
49 [103] D. Kugiumtzis, On the reliability of the surrogate data test for nonlinearity in the analysis of noisy time  
50 series, *Int. J. Bifurcat. Chaos* 11 (07) (2001) 1881–1896.  
51  
52 [104] D. Kugiumtzis, Surrogate data test for nonlinearity including nonmonotonic transforms, *Phys. Rev. E* 62 (1)  
53 (2000) R25.  
54  
55 [105] D. Kugiumtzis, Evaluation of surrogate and bootstrap tests for nonlinearity in time series, *Stud. Nonlinear  
56 Dyn. Econometrics* 12 (1) (2008) 1–26.  
57  
58 [106] C. J. Keylock, Discussion of “Testing stationarity with wavelet-based surrogates” by Megan McCullough and  
59 Ahsan Kareem, *J. Eng. Mech.* 140 (4) (2014) 200–209.  
60  
61 [107] D. B. Percival, A. T. Walden, Wavelet Methods for Time Series Analysis, Vol. 4, Cambridge University Press,  
62 2006.  
63  
64 [108] M. Breakspear, M. Brammer, P. A. Robinson, Construction of multivariate surrogate sets from nonlinear data  
65 using the wavelet transform, *Physica D* 182 (1) (2003) 1–22.

- 1  
2  
3 [109] E. Bullmore, C. Long, J. Suckling, J. Fadili, G. Calvert, F. Zelaya, T. A. Carpenter, M. Brammer, Colored  
4 noise and computational inference in neurophysiological (fMRI) time series analysis: Resampling methods in  
5 time and wavelet domains, *Hum. Brain Mapp.* 12 (2) (2001) 61–78.  
6  
7 [110] C. J. Keylock, Characterizing the structure of nonlinear systems using gradual wavelet reconstruction, *Nonlin.*  
8 *Proc. Geophys.* 17 (6) (2010) 615.  
9  
10 [111] C. J. Keylock, R. Stresing, J. Peinke, Gradual wavelet reconstruction of the velocity increments for turbulent  
11 wakes, *Phys. Fluids* 27 (2) (2015) 025104.  
12  
13 [112] S. Gur, T. Danielson, Q. Xiong, C. Hin, S. Pannala, G. Frantziskonis, A. Savara, C. S. Daw, Wavelet-based  
14 surrogate time series for multiscale simulation of heterogeneous catalysis, *Chem. Eng. Sci.* 144 (2016) 165–175.  
15  
16 [113] M. Paluš, Bootstrapping multifractals: Surrogate data from random cascades on wavelet dyadic trees, *Phys.*  
17 *Rev. Lett.* 101 (13) (2008) 134101.  
18  
19 [114] C. J. Keylock, Multifractal surrogate-data generation algorithm that preserves pointwise Hölder regularity  
20 structure, with initial applications to turbulence, *Phys. Rev. E* 95 (3) (2017) 032123.  
21  
22 [115] M. Paluš, Multiscale atmospheric dynamics: cross-frequency phase-amplitude coupling in the air temperature,  
23 *Phys. Rev. Lett.* 112 (7) (2014) 078702.  
24  
25 [116] G. W. Frank, T. Lookman, M. A. H. Nerenberg, C. Essex, J. Lemieux, W. Blume, Chaotic time series analyses  
26 of epileptic seizures, *Physica D* 46 (3) (1990) 427–438.  
27  
28 [117] P. C. Ivanov, L. A. N. Amaral, A. L. Goldberger, S. Havlin, M. G. Rosenblum, Z. R. Struzik, H. E. Stanley,  
29 Multifractality in human heartbeat dynamics, *Nature* 399 (6735) (1999) 461–465.  
30  
31 [118] M. B. Kennel, R. Brown, H. D. I. Abarbanel, Determining embedding dimension for phase-space reconstruction  
32 using a geometrical construction, *Phys. Rev. A* 45 (6) (1992) 3403–3411.  
33  
34 [119] M. Small, K. Judd, Correlation dimension: A pivotal statistic for non-constrained realizations of composite  
35 hypotheses in surrogate data analysis, *Physica D* 120 (3) (1998) 386–400.  
36  
37 [120] J. Zhang, X. Luo, M. Small, Detecting chaos in pseudoperiodic time series without embedding, *Phys. Rev. E*  
38 73 (1) (2006) 016216.  
39  
40 [121] M. Shiro, Y. Hirata, K. Aihara, Failure of pseudo-periodic surrogates, *Artif. Life Robotics* 15 (4) (2010)  
41 496–499.  
42  
43 [122] Y. Zhao, T. Weng, M. Small, Response of the parameters of a neural network to pseudoperiodic time series,  
44 *Physica D* 268 (2014) 79–90.  
45  
46 [123] M. Thiel, M. C. Romano, J. Kurths, M. Rolfs, R. Kliegl, Twin surrogates to test for complex synchronisation,  
47 *Europhys. Lett.* 75 (4) (2006) 535.  
48  
49 [124] C. J. Keylock, Identifying linear and non-linear behaviour in reduced complexity modelling output using  
50 surrogate data methods, *Geomorphology* 90 (3) (2007) 356–366.  
51  
52 [125] R. Moeckel, B. Murray, Measuring the distance between time series, *Physica D* 102 (3) (1997) 187–194.  
53  
54 [126] R. Hegger, H. Kantz, T. Schreiber, Practical implementation of nonlinear time series methods: The TISEAN  
55 package, *Chaos* 9 (2) (1999) 413–435.  
56  
57 [127] F. Takens, On the numerical determination of the dimension of an attractor, in: B. H. W. Braaksma, B. L. J.,  
58 F. Takens (Eds.), *Dynamical Systems and Bifurcations*, Lecture notes in mathematics, Springer, Berlin, 1985,  
59 pp. 99–106.  
60  
61 [128] J. Theiler, Lacunarity in a best estimator of fractal dimension, *Phys. Lett. A* 133 (4) (1988) 195–200.  
62  
63 [129] J. Theiler, Efficient algorithm for estimating the correlation dimension from a set of discrete points, *Phys.*  
64 *Rev. A* 36 (9) (1987) 4456.  
65

- 1  
2  
3 [130] T. Schreiber, A. Schmitz, Discrimination power of measures for nonlinearity in a time series, Phys. Rev. E  
4 55 (5) (1997) 5443.
- 5  
6 [131] M. Barahona, C.-S. Poon, Detection of nonlinear dynamics in short, noisy time series, Nature 381 (6579)  
7 (1996) 215–217.
- 8  
9 [132] M. Paluš, D. Novotna, Detecting modes with nontrivial dynamics embedded in colored noise: Enhanced  
10 Monte Carlo SSA and the case of climate oscillations, Phys. Lett. A 248 (1998) 191–202.
- 11  
12 [133] M. Paluš, D. Novotná, Quasi-biennial oscillations extracted from the monthly NAO index and temperature  
13 records are phase-synchronized, Nonlin. Processes in Geophys. 13 (3) (2006) 287–296.
- 14  
15 [134] M. Vejmelka, M. Paluš, Detecting nonlinear oscillations in broadband signals, Chaos 19 (1) (2009) 015114.
- 16  
17 [135] M. Vejmelka, M. Paluš, K. Šušmáková, Identification of nonlinear oscillatory activity embedded in broadband  
18 neural signals, Int. J. Neural Syst. 20 (02) (2010) 117–128.
- 19  
20 [136] R. Mañé, On the dimension of the compact invariant sets of certain non-linear maps, in: D. A. Rand, L. S.  
21 Young (Eds.), Lecture notes in Mathematics, Vol. 898, Springer, New York, 1981.
- 22  
23 [137] K. Karhunen, Zur spektraltheorie stochastischer prozesse, Ann. Acad. Sci. Fenn. A1, Math. Phys. 37.
- 24  
25 [138] M. Loèvre, Fonctions aleatoires de second ordre, C. R. Acad. Sci.
- 26  
27 [139] M. Hožič, A. Stefanovska, Karhunen – Loèvre decomposition of peripheral blood flow, Physica A 281 (2000)  
28 587–601.
- 29  
30 [140] A. M. Lyapunov, The general problem of the stability of motion (Translated into English by A. T. Fuller),  
31 Int. J. Control 55 (3) (1992) 531–773.
- 32  
33 [141] M. Sano, Y. Sawada, Measurement of the Lyapunov spectrum from a chaotic time series, Phys. Rev. Lett.  
34 55 (10) (1985) 1082.
- 35  
36 [142] J.-P. Eckmann, S. O. Kamphorst, D. Ruelle, S. Ciliberto, Liapunov exponents from time series, Phys. Rev.  
37 A 34 (6) (1986) 4971.
- 38  
39 [143] M. Paluš, V. Albrecht, I. Dvořák, Information theoretic test for nonlinearity in time series, Phys. Lett. A  
40 175 (3-4) (1993) 203–209.
- 41  
42 [144] M. Paluš, Detecting nonlinearity in multivariate time series, Phys. Lett. A 213 (3) (1996) 138–147.
- 43  
44 [145] L. W. Sheppard, A. Stefanovska, P. V. E. McClintock, Detecting the harmonics of oscillations with time-  
45 variable frequencies, Phys. Rev. E 83 (2011) 016206.
- 46  
47 [146] T. Rouyer, J.-M. Fromentin, N. C. Stenseth, B. Cazelles, Analysing multiple time series and extending  
48 significance testing in wavelet analysis, Mar. Ecol. Prog. Ser. 359 (2008) 11–23.
- 49  
50 [147] C. J. Stam, B. W. Van Dijk, Synchronization likelihood: an unbiased measure of generalized synchronization  
51 in multivariate data sets, Physica D 163 (3) (2002) 236–251.
- 52  
53 [148] E. Pereda, R. Q. Quiroga, J. Bhattacharya, Nonlinear multivariate analysis of neurophysiological signals,  
54 Prog. Neurobiol. 77 (1) (2005) 1–37.
- 55  
56 [149] A. Pikovsky, M. Rosenblum, J. Kurths, Synchronization – A Universal Concept in Nonlinear Sciences, Cam-  
57 bridge University Press, Cambridge, 2001.
- 58  
59 [150] P. Tass, M. G. Rosenblum, J. Weule, J. Kurths, A. Pikovsky, J. Volkmann, A. Schnitzler, H.-J. Freund,  
60 Detection of  $n:m$  phase locking from noisy data: Application to magnetoencephalography, Phys. Rev. Lett.  
61 81 (15) (1998) 3291–3294.
- 62  
63 [151] M. Paluš, Detecting phase synchronization in noisy systems, Phys. Lett. A 235 (1997) 341–351.
- 64  
65 [152] T. Stankovski, P. V. E. McClintock, A. Stefanovska, Dynamical inference: Where phase synchronization and  
66 generalized synchronization meet, Phys. Rev. E 89 (6) (2014) 062909.

- 1  
2  
3 [153] M. G. Rosenblum, A. S. Pikovsky, Detecting direction of coupling in interacting oscillators, *Phys. Rev. E.*  
4 64 (4) (2001) 045202.  
5  
6 [154] J. Sun, X. Hong, S. Tong, Phase synchronization analysis of EEG signals: An evaluation based on surrogate  
7 tests, *IEEE Trans. Biomed. Eng.* 59 (8) (2012) 2254–2263.  
8  
9 [155] K. Mezeiová, M. Paluš, Comparison of coherence and phase synchronization of the human sleep electroen-  
10 cephalogram, *Clin. Neurophysiol.* 123 (9) (2012) 1821–1830.  
11  
12 [156] M. C. Romano, M. Thiel, J. Kurths, K. Mergenthaler, R. Engbert, Hypothesis test for synchronization: Twin  
13 surrogates revisited, *Chaos* 19 (1) (2009) 015108.  
14  
15 [157] L. W. Sheppard, V. Vuksanović, P. V. E. McClintock, A. Stefanovska, Oscillatory dynamics of vasoconstriction  
16 and vasodilation identified by time-localized phase coherence, *Phys. Med. Biol.* 56 (2011) 3583–3601.  
17  
18 [158] E. Toledo, S. Akselrod, I. Pinhas, D. Aravot, Does synchronization reflect a true interaction in the cardiores-  
19 piratory system?, *Med. Eng. & Phys.* 24 (1) (2002) 45–52.  
20  
21 [159] P. Van Leeuwen, D. Geue, S. Lange, D. Cysarz, H. Bettermann, D. H. W. Grönemeyer, Is there evidence of  
22 fetal-maternal heart rate synchronization?, *BMC Physiol.* 3 (1) (2003) 2.  
23  
24 [160] V. Ticcinelli, T. Stankovski, D. Iatsenko, A. Bernjak, A. E. Bradbury, A. R. Gallagher, P. Clarkson, P. V. E.  
25 McClintock, A. Stefanovska, Coherence and coupling functions reveal microvascular impairment in treated  
hypertension, *Front. Physiol.* 8 (2017) 749.  
26  
27 [161] T. Stankovski, S. Petkoski, J. Raeder, A. F. Smith, P. V. E. McClintock, A. Stefanovska, Alterations in the  
28 coupling functions between cortical and cardio-respiratory oscillations due to anaesthesia with propofol and  
29 sevoflurane, *Phil. Trans. R. Soc. A* 374 (2067) (2016) 20150186.  
30  
31 [162] R. Donner, M. Thiel, Scale-resolved phase coherence analysis of hemispheric sunspot activity: A new look at  
32 the north-south asymmetry, *Astron. Astrophys.* 475 (3) (2007) L33–L36.  
33  
34 [163] M. Vejmelka, M. Paluš, Inferring the directionality of coupling with conditional mutual information, *Phys.*  
35 *Rev. E.* 77 (2) (2008) 026214.  
36  
37 [164] M. Thiel, M. C. Romano, J. Kurths, M. Rolfs, R. Kliegl, Generating surrogates from recurrences, *Phil. Trans.*  
38 *R. Soc. A* 366 (1865) (2008) 545–557.  
39  
40 [165] N. Marwan, M. C. Romano, M. Thiel, J. Kurths, Recurrence plots for the analysis of complex systems, *Phys.*  
41 *Rep.* 438 (5) (2007) 237–329.  
42  
43 [166] M. Thiel, M. C. Romano, J. Kurths, How much information is contained in a recurrence plot?, *Phys. Lett. A*  
44 330 (5) (2004) 343–349.  
45  
46 [167] J. F. Donges, Y. Zou, N. Marwan, J. Kurths, The backbone of the climate network, *EPL* 87 (4) (2009) 48007.  
47  
48 [168] M. C. Romano, M. Thiel, J. Kurths, C. Grebogi, Estimation of the direction of the coupling by conditional  
probabilities of recurrence, *Phys. Rev. E* 76 (3) (2007) 036211.  
49  
50 [169] P. Van Leeuwen, D. Geue, M. Thiel, D. Cysarz, S. Lange, M. C. Romano, N. Wessel, J. Kurths, D. H.  
51 Grönemeyer, Influence of paced maternal breathing on fetal–maternal heart rate coordination, *PNAS* 106 (33)  
52 (2009) 13661–13666.  
53  
54 [170] R. Q. Quiroga, A. Kraskov, T. Kreuz, P. Grassberger, Performance of different synchronization measures in  
real data: A case study on electroencephalographic signals, *Phys. Rev. E* 65 (4) (2002) 041903.  
55  
56 [171] R. G. Andrzejak, A. Kraskov, H. Stogbauer, F. Mormann, T. Kreuz, Bivariate surrogate techniques: Necessity,  
57 strengths, and caveats, *Phys. Rev. E* 68 (6) (2003) 066202.  
58  
59 [172] R. T. Canolty, E. Edwards, S. S. Dalal, M. Soltani, S. S. Nagarajan, H. E. Kirsch, M. S. Berger, N. M.  
60 Barbaro, R. T. Knight, High gamma power is phase-locked to theta oscillations in human neocortex, *Science*  
61 313 (5793) (2006) 1626–1628.

- 1  
2  
3 [173] A. M. Petrock, D. L. Donnelly, M. L. Rosenberg, Quantifying cardio-pulmonary correlations using the cross-  
4 wavelet transform: Validating a correlative method, in: EMBS 2008. 30th Annual International Conference  
5 of the IEEE, IEEE, 2008, pp. 2940–2943.  
6  
7 [174] T. I. Netoff, S. J. Schiff, Decreased neuronal synchronization during experimental seizures, *J. Neurosci.* 22 (16)  
8 (2002) 7297–7307.  
9  
10 [175] L. Faes, A. Porta, G. Nollo, Mutual nonlinear prediction as a tool to evaluate coupling strength and direc-  
11 tionality in bivariate time series: Comparison among different strategies based on  $k$  nearest neighbors, *Phys.*  
12 *Rev. E* 78 (2) (2008) 026201.  
13  
14 [176] I. Vlachos, D. Kugiumtzis, Nonuniform state-space reconstruction and coupling detection, *Phys. Rev. E* 82 (1)  
15 (2010) 016207.  
16  
17 [177] T. Stankovski, T. Pereira, P. V. E. McClintock, A. Stefanovska, Coupling functions: universal insights into  
18 dynamical interaction mechanisms, *Rev. Mod. Phys.* 89 (2017) 045001.  
19  
20 [178] M. G. Rosenblum, A. S. Pikovsky, J. Kurths, Phase synchronization of chaotic oscillators, *Phys. Rev. Lett.*  
21 76 (11) (1996) 1804–1807.  
22  
23 [179] B. Kralemann, M. Fröhwirth, A. Pikovsky, M. Rosenblum, T. Kenner, J. Schaefer, M. Moser, In vivo cardiac  
24 phase response curve elucidates human respiratory heart rate variability, *Nat. Commun.* 4 (2013) 2418.  
25  
26 [180] T. Stankovski, A. Duggento, P. V. E. McClintock, A. Stefanovska, Inference of time-evolving coupled dynam-  
27 ical systems in the presence of noise, *Phys. Rev. Lett.* 109 (2012) 024101.  
28  
29 [181] I. T. Tokuda, S. Jain, I. Z. Kiss, J. L. Hudson, Inferring phase equations from multivariate time series, *Phys.*  
30 *Rev. Lett.* 99 (2007) 064101.  
31  
32 [182] Z. Levnajić, A. Pikovsky, Network reconstruction from random phase resetting, *Phys. Rev. Lett.* 107 (2011)  
33 034101.  
34  
35 [183] M. Timme, Revealing network connectivity from response dynamics, *Phys. Rev. Lett.* 98 (22) (2007) 224101.  
36  
37 [184] A. Duggento, T. Stankovski, P. V. E. McClintock, A. Stefanovska, Dynamical Bayesian inference of time-  
38 evolving interactions: From a pair of coupled oscillators to networks of oscillators, *Phys. Rev. E* 86 (6) (2012)  
39 061126.  
40  
41 [185] V. N. Smelyanskiy, D. G. Luchinsky, A. Stefanovska, P. V. E. McClintock, Inference of a nonlinear stochastic  
42 model of the cardiorespiratory interaction, *Phys. Rev. Lett.* 94 (9) (2005) 098101.  
43  
44 [186] T. Stankovski, A. Duggento, P. V. E. McClintock, A. Stefanovska, A tutorial on time-evolving dynamical  
45 Bayesian inference, *Eur. Phys. J. Special Topics* 223 (13) (2014) 2685–2703.  
46  
47 [187] M. Paluš, M. Vejmelka, Directionality of coupling from bivariate time series: How to avoid false causalities  
48 and missed connections, *Phys. Rev. E* 75 (5) (2007) 056211.  
49  
50 [188] B. Jelfs, R. H. M. Chan, Directionality indices: Testing information transfer with surrogate correction, *Phys.*  
51 *Rev. E* 96 (5) (2017) 052220.  
52  
53 [189] C. L. Nikias, J. M. Mendel, Signal processing with higher-order spectra, *IEEE Signal Process. Mag.* 10 (3)  
54 (1993) 10–37.  
55  
56 [190] A. Swami, G. B. Giannakis, G. Zhou, Bibliography on higher-order statistics, *Signal Process.* 60 (1) (1997)  
57 65–126.  
58  
59 [191] E. Komatsu, D. N. Spergel, Acoustic signatures in the primary microwave background bispectrum, *Phys. Rev.*  
60 *D* 63 (6) (2001) 063002.  
61  
62 [192] P. Huber, B. Kleiner, T. Gasser, G. Dumermuth, Statistical methods for investigating phase relations in  
63 stationary stochastic processes, *IEEE Trans. Audio Electroacoust.* 19 (1971) 78–86.  
64  
65 [193] K. Hasselmann, W. Munk, G. MacDonald, Bispectra of ocean waves, New York: Wiley, 1963.

- 1  
2  
3 [194] N.-C. Yao, S. Neshyba, H. Crew, Rotary cross-bispectra and energy transfer functions between non-gaussian  
4 vector processes I. development and example, *J. Phys. Oceanogr.* 5 (1974) 164–172.  
5  
6 [195] T. P. Barnett, L. C. Johnson, P. Naitoh, N. Hicks, C. Nute, Bispectrum analysis of electroencephalogram  
7 signals during waking and sleeping, *Science* 172 (3981) (1971) 401–402.  
8  
9 [196] G. Dumermuth, P. J. Huber, B. Kleiner, T. Gasser, Analysis of the interrelations between frequency bands  
10 of the EEG by means of the bispectrum a preliminary study, *Clin. Neurophysiol.* 31 (2) (1971) 137–148.  
11  
12 [197] T. Ning, J. D. Bronzino, Bispectral analysis of the rat eeg during various vigilance states, *IEEE Trans.*  
13 *Biomed. Eng.* 36 (1989) 497–499.  
14  
15 [198] J. C. Sigl, N. G. Chamoun, An introduction to bispectral analysis for the electroencephalogram, *J. Clin.*  
16 *Monit.* 10 (6) (1994) 392–404.  
17  
18 [199] G. Widman, T. Schreiber, B. Rehberg, A. Hoeft, C. E. Elger, Quantification of depth of anesthesia by nonlinear  
19 time series analysis of brain electrical activity, *Phys. Rev. E* 62 (4) (2000) 4898.  
20  
21 [200] B. Schack, H. Witte, M. Helbig, C. Schelenz, M. Specht, Time-variant non-linear phase-coupling analysis of  
22 EEG burst patterns in sedated patients during electroencephalic burst suppression period, *Clin. Neurophysiol.*  
23 112 (8) (2001) 1388–1399.  
24  
25 [201] J. Jamšek, A. Stefanovska, P. V. E. McClintock, Nonlinear cardio-respiratory interactions resolved by time-  
26 phase bispectral analysis, *Phys. Med. Biol.* 49 (18) (2004) 4407–4425.  
27  
28 [202] S. A. Taplidou, L. J. Hadjileontiadis, Nonlinear analysis of wheezes using wavelet bicoherence, *Comput. Biol.*  
29 *Med.* 37 (4) (2007) 563–570.  
30  
31 [203] A. Spicher, W. J. Miloch, L. B. N. Clausen, J. I. Moen, Plasma turbulence and coherent structures in the  
32 polar cap observed by the ici-2 sounding rocket, *J. Geophys. Res. A* 120 (12).  
33  
34 [204] T. Dudok de Wit, V. V. Krasnosel'skikh, Wavelet bicoherence analysis of strong plasma turbulence at the  
35 Earth's quasiparallel bow shock, *Phys. Plasmas* 2 (11) (1995) 4307–4311.  
36  
37 [205] B. P. van Milligen, E. Sanchez, T. Estrada, C. Hidalgo, B. Branas, B. Carreras, L. Garcia, Wavelet bicoherence  
38 – a new turbulence analysis tool, *Phys. Plasmas* 2 (8) (1995) 3017–3032.  
39  
40 [206] Z. Ge, Significance testing for wavelet bicoherence and its application in analyzing nonlinearity in turbulent  
41 shear flows, *Phys. Rev. E* 81 (5) (2010) 056311.  
42  
43 [207] D. Raju, O. Sauter, J. B. Lister, Study of nonlinear mode coupling during neoclassical tearing modes using  
44 bispectrum analysis, *Plasma Phys. Controlled Fusion* 45 (4) (2003) 369.  
45  
46 [208] T. W. S. Chow, G. Fei, Three phase induction machines asymmetrical faults identification using bispectrum,  
47 *IEEE Trans. Energy Convers.* 10 (1995) 688–693.  
48  
49 [209] M. D. Godfrey, An exploratory study of the bi-spectrum of economic time series, *J. R. Stat. Soc. Ser. C Appl.*  
50 *Stat.* 14 (1965) 48–69.  
51  
52 [210] T. Matsuoka, J. Ulrych, Phase estimation using the bispectrum, *Proc. IEEE* 72.  
53  
54 [211] B. P. van Milligen, C. Hidalgo, E. Sánchez, Nonlinear phenomena and intermittency in plasma turbulence,  
55 *Phys. Rev. Lett.* 74 (1995) 395–398.  
56  
57 [212] T. S. Rao, K. C. Indukumar, Spectral and wavelet methods for the analysis of nonlinear and nonstationary  
58 time series, *J. Franklin Inst.* 333 (3) (1996) 425–452.  
59  
60 [213] J. Jamšek, A. Stefanovska, P. V. E. McClintock, I. A. Khovanov, Time-phase bispectral analysis, *Phys. Rev.*  
61 *E* 68 (1) (2003) 016201.  
62  
63 [214] J. Jamšek, A. Stefanovska, P. V. E. McClintock, Wavelet bispectral analysis for the study of interactions  
64 among oscillators whose basic frequencies are significantly time variable, *Phys. Rev. E* 76 (2007) 046221.  
65

- 1  
2  
3 [215] J. R. Fonollosa, C. T. Nikias, Wigner higher order moment spectra: definition, properties, computation and  
4 application to transient signal analysis, *IEEE Trans. Signal Process.* 41 (1) (1993) 245.  
5  
6 [216] B. Boashash, B. Ristic, Polynomial time-frequency distributions and time-varying higher order spectra: ap-  
7 plication to the analysis of multicomponent fm signals and to the treatment of multiplicative noise, *Signal  
8 Process.* 67 (1) (1998) 1–23.  
9  
10 [217] G. Kaiser, *A Friendly Guide to Wavelets*, Birkhäuser, Boston, 1994.  
11  
12 [218] D. Iatsenko, P. V. E. McClintock, A. Stefanovska, Linear and synchrosqueezed time-frequency representations  
13 revisited: Overview, standards of use, resolution, reconstruction, concentration, and algorithms, *Digit. Signal  
14 Process.* 42 (2015) 1–26.  
15  
16 [219] K. L. Siu, J. M. Ahn, K. Ju, M. Lee, K. Shin, K. H. Chon, Statistical approach to quantify the presence of  
17 phase coupling using the bispectrum, *IEEE Trans. Biomed. Eng.* 55 (5) (2008) 1512–1520.  
18  
19 [220] S. Elgar, R. T. Guza, Statistics of bicoherence, *IEEE Trans. Acoust., Speech, Signal Process.* 36 (10) (1988)  
20 1667–1668.  
21  
22 [221] S. Elgar, G. Sebert, Statistics of bicoherence and biphasic, *J. Geophys. Res. Oceans* 94 (C8) (1989) 10993–  
23 10998.  
24  
25 [222] X. Wang, Y. Chen, M. Ding, Testing for statistical significance in bispectra: A surrogate data approach and  
26 application to neuroscience, *IEEE Trans. Biomed. Eng.* 54 (11) (2007) 1974–1982.  
27  
28 [223] T. Kim, E. J. Powers, W. M. Grady, A. Arapostathis, A novel QPC detector for the health monitoring of  
29 rotating machines, in: IMTC 2007, IEEE, 2007, pp. 1–6.  
30  
31 [224] X. Li, D. Li, L. J. Voss, J. W. Sleigh, The comodulation measure of neuronal oscillations with general harmonic  
32 wavelet bicoherence and application to sleep analysis, *NeuroImage* 48 (3) (2009) 501–514.  
33  
34 [225] C. G. Scully, N. Mitrou, B. Braam, W. A. Cupples, K. H. Chon, Detecting interactions between the renal  
35 autoregulation mechanisms in time and space, *IEEE Trans. Biomed. Eng.* 64 (3) (2017) 690–698.  
36  
37 [226] C. Demanuele, C. J. James, E. J. S. Sonuga-Barke, Distinguishing low frequency oscillations within the 1/f  
38 spectral behaviour of electromagnetic brain signals, *Behav. Brain Funct.* 3 (1) (2007) 1.  
39  
40 [227] H. Berger, Über das Elektroenzephalogramm des Menschen, *Arch. Psychiatr. Nervenkr.* 87 (1929) 527–570.  
41  
42 [228] E. Niedermeyer, Alpha rhythms as physiological and abnormal phenomena, *Int. J. Psychophysiol.* 26 (1)  
43 (1997) 31–49.  
44  
45 [229] J. C. Butcher, On Runge-Kutta processes of high order, *J. Austral. Math. Soc.* 4 (02) (1964) 179–194.  
46  
47 [230] Y. Kuramoto, *Chemical Oscillations, Waves, and Turbulence*, Springer-Verlag, Berlin, 1984.  
48  
49 [231] M. G. Rosenblum, A. S. Pikovsky, J. Kurths, From phase to lag synchronization in coupled chaotic oscillators,  
50 *Phys. Rev. Lett.* 78 (22) (1997) 4193–4196.  
51  
52 [232] G. Buzsáki, *Rhythms of the Brain*, Oxford University Press, Oxford, 2006.  
53  
54 [233] O. Jensen, L. L. Colgin, Cross-frequency coupling between neuronal oscillations, *Trends Cognit. Sci.* 11 (7)  
55 (2007) 267–269.  
56  
57 [234] R. G. Andrzejak, F. Mormann, T. Kreuz, C. Rieke, A. Kraskov, C. E. Elger, K. Lehnertz, Testing the null  
58 hypothesis of the nonexistence of a preseizure state, *Phys. Rev. E* 67 (1) (2003) 010901.  
59  
60 [235] T. Kreuz, R. G. Andrzejak, F. Mormann, A. Kraskov, H. Stögbauer, C. E. Elger, K. Lehnertz, P. Grassberger,  
61 Measure profile surrogates: a method to validate the performance of epileptic seizure prediction algorithms,  
62 *Phys. Rev. E* 69 (6) (2004) 061915.  
63  
64 [236] R. G. Andrzejak, D. Chicharro, C. E. Elger, F. Mormann, Seizure prediction: any better than chance?, *Clin.  
65 Neurophysiol.* 120 (8) (2009) 1465–1478.

- 1  
2  
3 [237] T. Schreiber, Constrained randomization of time series data, *Phys. Rev. Lett.* 80 (10) (1998) 2105.  
4  
5 [238] K. Dolan, A. Witt, M. L. Spano, A. Neiman, F. Moss, Surrogates for finding unstable periodic orbits in noisy  
6 data sets, *Phys. Rev. E* 59 (5) (1999) 5235.  
7  
8 [239] D. E. Postnov, A. Y. Neganova, D. D. Postnov, A. R. Brazhe, Monitoring of rhythms in laser speckle data,  
9 *J. Innov. Opt. Health Sci.* 7 (03) (2014) 1450015.  
10  
11 [240] L. W. Sheppard, P. C. Reid, D. C. Reuman, Rapid surrogate testing of wavelet coherences, *EPJ Nonlin. Biomed. Phys.* 5 (1) (2017) 9.  
12  
13 [241] M. Wiedermann, J. F. Donges, J. Kurths, R. V. Donner, Spatial network surrogates for disentangling complex  
14 system structure from spatial embedding of nodes, *Phys. Rev. E* 93 (4) (2016) 042308.  
15  
16 [242] T. Kreuz, E. Satuvuori, M. Pofahl, M. Mulansky, Leaders and followers: Quantifying consistency in spatio-  
17 temporal propagation patterns, *New J. Phys.* 19 (4) (2017) 043028.  
18  
19 [243] N. Delprat, B. Escudie, P. Guillemain, R. Kronland-Martinet, P. Tchamitchian, B. Torrésani, Asymptotic  
20 wavelet and Gabor analysis: Extraction of instantaneous frequencies, *IEEE Trans. Inf. Theory* 38 (2) (1992)  
21 644–664.  
22  
23 [244] R. A. Carmona, W. L. Hwang, B. Torrésani, Characterization of signals by the ridges of their wavelet trans-  
24 forms, *IEEE Trans. Sig. Proc.* 45 (10) (1997) 2586–2590.  
25  
26 [245] D. Iatsenko, P. V. E. McClintock, A. Stefanovska, Extraction of instantaneous frequencies from ridges in  
27 time-frequency representations of signals, *Signal Process.* 125 (2016) 290–303.  
28  
29 [246] A. Bruns, Fourier-, Hilbert- and wavelet-based signal analysis: are they really different approaches?, *J. Neurosci. Methods* 137 (2) (2004) 321–332.  
30  
31 [247] B. Kralemann, L. Cimponeriu, M. Rosenblum, A. Pikovsky, R. Mrowka, Uncovering interaction of coupled  
32 oscillators from data, *Phys. Rev. E* 76 (5) (2007) 055201.  
33  
34 [248] B. Kralemann, L. Cimponeriu, M. Rosenblum, A. Pikovsky, R. Mrowka, Phase dynamics of coupled oscillators  
35 reconstructed from data, *Phys. Rev. E* 77 (6, Part 2) (2008) 066205.  
36  
37 [249] M. Le Van Quyen, J. Foucher, J. P. Lachaux, E. Rodriguez, A. Lutz, J. Martinerie, F. J. Varela, Comparison  
38 of Hilbert transform and wavelet methods for the analysis of neuronal synchrony, *J. Neurosci. Methods* 111 (2)  
39 (2001) 83–98.  
40  
41 [250] D. Prichard, The correlation dimension of differenced data, *Phys. Lett. A* 191 (3) (1994) 245–250.  
42  
43 [251] M. Bračić, A. Stefanovska, Wavelet based analysis of human blood flow dynamics, *Bull. Math. Biol.* 60 (5)  
44 (1998) 919–935.  
45  
46 [252] A. Stefanovska, M. Bračić, H. D. Kvernmo, Wavelet analysis of oscillations in the peripheral blood circulation  
47 measured by laser Doppler technique, *IEEE Trans. Bio. Med. Eng.* 46 (10) (1999) 1230–1239.  
48  
49 [253] F. Takens, Detecting strange attractors in turbulence, in: D. A. Rand, L. S. Young (Eds.), *Lecture notes in Mathematics*, Vol. 898, Springer, New York, 1981.  
50  
51 [254] R. N. Bracewell, *The Fourier transform and its applications*, McGraw-Hill New York, 1986.  
52  
53  
54  
55  
56  
57  
58  
59  
60  
61  
62  
63  
64  
65